Vav guanine nucleotide exchange factors control B cell antigen receptor-induced Ca^{2+}-signaling

Dissertation

for the award of the degree

“Doctor rerum naturalium”

of the Georg-August-Universität Göttingen

within the doctoral program Molecular Biology

of the Georg-August University School of Science (GAUSS)

submitted by

Christoffer Hitzing

from

Göttingen, Germany

Göttingen 2015

This thesis was conducted in the Institute of Cellular and Molecular Immunology at the Georg-August University in Göttingen from May 2012 until October 2015 under the supervision of Dr. Niklas Engels in the group of Prof. Dr. Jürgen Wienands.

Thesis Committee

Prof. Dr. Jürgen Wienands, Institute of Cellular and Molecular Immunology, University Medical Center, Göttingen

Prof. Dr. Lutz Walter, Department of Primate Genetics, German Primate Center, Göttingen

Prof. Dr. Andreas Wodarz, Department of Anatomy and Cell Biology, Georg-August University, Göttingen

Members of the Examination Board

Referee: Prof. Dr. Jürgen Wienands, Institute of Cellular and Molecular Immunology, University Medical Center, Göttingen

2nd Referee: Prof. Dr. Lutz Walter, Department of Primate Genetics, German Primate Center, Göttingen

Further members of the Examination Board

Prof. Dr. Matthias Dobbelstein, Institute of Molecular Oncology, University Medical Center, Göttingen

Prof. Dr. Blanche Schwappach, Department of Molecular Biology, University Medical Center, Göttingen

Prof. Dr. Steven Johnsen, Clinic for General, Visceral and Pediatric Surgery, University Medical Center, Göttingen

Date of oral examination: 21st of December 2015

Affidavit

Herewith, I declare that I prepared the doctoral thesis “Vav guanine nucleotide exchange factors control B cell antigen receptor-induced Ca^{2+}-signaling” on my own and with no other sources and aids than quoted.

Göttingen, 30th of October 2015

Christoffer Hitzing

Acknowledgement

At first, I want to express my gratitude to Prof. Wienands for giving me the opportunity to conduct my PhD project in his institute, so that I could join the wonderful world of B cell biology.

Thank you, Niklas! Thanks for supervising me, for the interesting project, for motivating discussions in hard times, for guidance, but also for the freedom to follow my own ideas. I learned so much during the last years.

In addition, I want to thank Prof. Lutz Walter and Prof. Andreas Wodarz for support as members of my thesis committee and for helpful advices during thesis committee meetings.

Next, I would like to thank Dr. Steffen Burkhardt and Kerstin Grüninger from the Molecular Biology program coordination office for their great support at any time of the day or night during my PhD years. Thanks to the GGNB for supporting my PhD project with financial funding by the GGNB excellence stipend.

I am very, very thankful to Ines Heine for paramount technical assistance. You can call me, whenever you need more ‘Eichsfelder Mettwurst’! I also want to thank Gabriele Sonntag for answering technical question, whenever I needed quick help. Special thanks to the charming team of the secretary office Ingrid Teuteberg and Anika Schindler, for being helpful with all organizational matters. I also want to thank my lab rotation students Insa, Lena, Lisa and Tina.

I am very thankful to Kathrin, Caren, Henrike, Kanika and especially Niklas for proofreading my thesis. If anyone detects mistakes, it is their fault. Special thanks to Sebastian, who was my technical support in the lab over the last years.

Thanks to all current and former members of the Institute of Cellular and Molecular Immunology. Especially, I want to thank the coffee group for good times and nice discussions about everything one can think of. Special thanks to Kathrin, Caren, Henrike, Kai, Wiebke, Sona, Kanika, Niklas, Johannes, Michael and Julius for amazing activities outside the lab, like lab dinners, grill sessions, watching volleyball matches and many more.

Moreover, I want to thank all the people from the lab and from the LA Cool Runnings, who joined me in amazing running events in Göttingen, Hamburg, Kassel, Vienna and many more.

In addition, thanks to my cousin and flat mate Jan, for nice cooking evenings, sport activities and being there, whenever I needed some help. Furthermore, I want to thank Jonas, Kai, Ariane, Michael and Eva-Maria for their friendship and for distracting me from work with extracurricular activities!

Special thanks to my parents and my sister. I cannot thank you enough for the support that I got during my lifetime. You made this possible. In addition, I also want to thank the rest of my family for the huge team spirit that we have.

In the end, I want to thank Kathrin for ‘running’ with me the last three years, does not matter if up or down. We reached the final of the PhD marathon and I think the next marathon in life is waiting already!

Table of Contents

Affidavit I

Acknowledgement II

Table of Contents IV

1 Abstract 1

2 Introduction 2

2.1 The immune system at a glance 2

2.2 The B cell antigen receptor - How to become a functional B cell 3

2.3 Initiation of BCR signaling 4

2.4 Beyond the Ca^{2+}-initiation complex 6

2.5 Vav - guanine nucleotide exchange factors of Rho family G-proteins 8

2.5.1 Vav1 - a multi-domain protein with diverse functions 9

2.6 Aim of this thesis 14

3 Materials and Methods 15

3.1 Materials 15

3.1.1 Chemicals and reagents 15

3.1.2 Consumables 15

3.1.3 Enzymes 16

3.1.4 Reaction systems (kits) 16

3.1.5 Synthetic DNA oligonucleotides 17

3.1.6 Vectors and Plasmids 25

3.1.7 Antibodies 28

3.1.8 Synthetic peptides 29

3.1.9 Instruments 30

3.1.10 Software 31

3.1.11 Data base 31

3.2 Methods 32

3.2.1 Molecular biology 32

3.2.1.1 Bacteria strains 32

3.2.1.2 Media for bacteria....33
3.2.1.3 Agar plates....33
3.2.1.4 Sterilisation procedure....33
3.2.1.5 Isolation and purification of nucleic acids....33
3.2.1.5.1 Isolation of genomic DNA....33
3.2.1.5.2 Isolation of plasmid DNA (Mini-preparation)....34
3.2.1.5.3 Isolation of plasmid DNA (Midi-preparation)....34
3.2.1.5.4 Measurement of nucleic acid concentration....34
3.2.1.6 Cloning techniques....34
3.2.1.6.1 Restriction of DNA using endonucleases....34
3.2.1.6.2 DNA gel extraction....35
3.2.1.6.3 Sub-cloning of PCR products....35
3.2.1.6.4 Ligation of DNA fragments....35
3.2.1.6.5 Transformation of competent bacteria....35
3.2.1.7 Gel electrophoresis....36
3.2.1.8 Polymerase chain reaction (PCR)....36
3.2.1.8.1 Standard PCR....36
3.2.1.8.2 Overlap PCR....37
3.2.1.8.3 Sequencing PCR....37
3.2.2 Biochemistry....37
3.2.2.1 Preparation of cleared cellular lysate....37
3.2.2.2 Stimulation of B cells....38
3.2.2.3 Expression of recombinant GST-fusion proteins....38
3.2.2.4 Preparation of recombinant GST-fusion proteins....39
3.2.2.5 Elution of GST-fusion proteins....39
3.2.2.6 Affinity purification (AP)....40
3.2.2.7 SDS-Polyacrylamide Gel Electrophoresis (SDS-PAGE)....40
3.2.2.8 Western blot analysis....41
3.2.2.9 Immunostaining....41
3.2.3 Cell biology....42

3.2.3.1 Media for cell culture 42
3.2.3.2 Cell lines....42
3.2.3.3 Cell culture of none-adherent cells 44
3.2.3.4 Cell culture of adherent cells 44
3.2.3.5 Long-term storage of cells 44
3.2.3.6 Revitalization of cells 44
3.2.3.7 Isolation of primary human B cells 44
3.2.3.8 Transfection methods 45
3.2.3.8.1 Transfection via nucleofection 45
3.2.3.8.2 Retroviral transfection/infection 46
3.2.3.9 Flow cytometry 46
3.2.3.9.1 Expression analysis of surface receptors 46
3.2.3.9.2 Expression analysis of ectopic expressed fluorophore-tagged proteins....47
3.2.3.9.3 Cell sorting....47
3.2.3.9.4 Analysis of Ca^{2+}-mobilization....47
3.2.3.10 Confocal microscopy 48
3.2.4 Gene targeting methods....48
3.2.4.1 Transcription Activator-like Effector Nucleases - TALEN 48
3.2.4.2 CRISPR/Cas 50
4 Results....52
4.1 The guanine nucleotide exchange factor Vav1 is a key regulator of BCR-proximal signaling in human B cells 52
4.1.1 Establishment of the TALEN method to generate a Vav1-deficient sub-line of DG75 52
4.1.2 Vav1 is essential for BCR-induced Ca^{2+}-mobilization 56
4.1.3 Vav1 and Vav3 control Ca^{2+}-mobilization upon BCR stimulation in DG75 B cells 58
4.1.4 Loss of Vav1 does not influence the assembly of the Ca^{2+}-initiation complex...61
4.1.5 Vav1 influences Akt activation upon BCR stimulation 63

4.2 Recruitment of Vav1 to phosphorylated BCR ITAMs enables Ca^{2+}-mobilization 64

4.2.1 The Vav1 SH2-domain can directly bind to the BCR ITAMs and is essential for Ca^{2+}-mobilization upon BCR stimulation 64

4.2.2 The Vav1 SH2-domain can be functionally replaced by SH2-domains of other Igα/Igβ interacting proteins.....68

4.3 The interaction between Vav1 and SLP-65 permits BCR-induced Ca^{2+}-mobilization 72

4.3.1 Generation of a SLP-65-deficient DG75 sub-line.....72

4.3.2 SLP-65 is essential for BCR-induced Ca^{2+}-mobilization in DG75 cells 74

4.3.3 SLP-65 tyrosines 72, 84 and 119 are important for its function in BCR-induced Ca^{2+}-mobilization 75

4.3.4 Recruitment of Vav1 to SLP-65 enables BCR-induced Ca^{2+}-mobilization.....78

4.3.5 CD19-mediated Vav1 recruitment is not involved in BCR-induced Ca^{2+}-mobilization.....80

4.4 The structural integrity of the DH-PH-ZF-domain unit of Vav1 is essential for BCR-induced Ca^{2+}-mobilization.....81

4.4.1 The Vav1 DH-domain is critical for Vav1 function in the context of BCR-induced Ca^{2+}-mobilization 81

4.4.2 The DH-domain is not involved in plasma membrane recruitment of Vav1.....82

4.4.3 DH-domain surrounding regions of Vav1 influence its Ca^{2+}-promoting function84

4.4.4 Do Rac family proteins influence BCR-induced Ca^{2+}-mobilization? - Generation of a Rac2-deficient DG75 sub-line 86

4.4.5 Rac2-deficient DG75 cells are capable to mobilize Ca^{2+} upon BCR stimulation 88

4.5 Analysis of the Vav1 CH-domain 88

4.5.1 The Vav1 CH-domain is critical for BCR-induced Ca^{2+}-signaling.....88

4.5.2 Actin-binding CH-domains cannot functionally replace the Vav1 CH-domain ...90

4.5.3 The CH-domain of Vav1 functions independently of its intramolecular localization.....91

4.5.4 The CH-domain of Vav1 is not involved in plasma membrane recruitment.....92

4.6 Phosphatidyl-inositol-4-phosphate 5-kinase in BCR-induced Ca^{2+}-mobilization.....94

5 Discussion 97

5.1 Vav proteins constitute a major signaling knot in BCR-induced Ca^{2+}-mobilization ..98

5.2 BCR-proximal localization of Vav1 enables efficient Ca^{2+}-mobilization 99

5.3 The structural integrity of the Vav1 DH-PH-ZF-domain unit is an essential prerequisite for BCR-signaling.....101

5.4 The Vav1 CH-domain is an indispensable regulator region of Vav1 activities.....103

5.5 Does Vav1 influence the generation of PIP_2 in BCR-induced Ca^{2+}-signaling? 105

6 Conclusion.....107

7 References 109

8 Appendix.....122

8.1 List of Figures.....122

8.2 List of Tables.....123

8.3 Abbreviations 123

9 Curriculum Vitae 130

1 Abstract

Differentiation of B cells into antibody secreting plasma cells is an indispensable step to cope with pathogens. Antigen binding to the B cell antigen receptor (BCR) initiates signaling cascades leading in combination with co-stimulatory signals to the differentiation of B cells. A hallmark of early B cell activation is the mobilization of Ca^{2+} from internal and external sources into the cytosol. Several proteins are reported to orchestrate Ca^{2+}-mobilization downstream of the BCR including the adaptor protein SLP-65 that forms together with key signaling enzymes the central signaling complex in that context. Components of that multi-protein complex are members of the Vav protein guanine nucleotide exchange factor (GEF) family consisting of Vav1, Vav2 and Vav3, which based on genetic mouse models are predicted to fulfill important tasks in BCR signaling. However, the operating principle by which the Vav GEF family acts in BCR-induced Ca^{2+}-mobilization is poorly understood. In my PhD project, I showed that Vav proteins constitute crucial signaling elements, controlling Ca^{2+}-mobilization after BCR stimulation in B cells. For my investigations, I used the TALEN and CRISPR/Cas gene targeting technologies to generate new genetic model systems in a human B cell line. I found that especially Vav1 and Vav3, but not Vav2, are potent signaling factors in human B cells that enable BCR-induced Ca^{2+}-mobilization. Genetic and biochemical approaches showed, that the functionality of Vav1 strictly depends on interactions mediated by its SH2-domain. In that context, I characterized a so far undiscovered interaction of Vav1 with the BCR. Furthermore, I showed that Vav1 localization within the BCR signalosome is not restricted to a specific signaling complex, since both exclusive binding to the BCR or the well-known Vav interaction partner SLP-65 enabled BCR-induced Ca^{2+}-flux. In addition, I showed by mutational analysis that the functionality of Vav1 in BCR-induced Ca^{2+}-mobilization strictly depends on two mechanisms carried out by different protein domains, the CH-domain and the DH-PH-ZF-domain unit. The DH-PH-ZF-domain unit is reported to be exclusively responsible for the binding and activation of Rho family G-proteins such as Rac1/2 and RhoA. In connection to that, I found that the structural integrity of the DH-PH-ZF-domain unit is a prerequisite for the functionality of Vav1 in BCR-induced Ca^{2+}-mobilization, highlighting a potential role of small G-proteins in this process. The generation of a Rac2-deficient DG75 B cell line, however, showed no alteration of Ca^{2+}-mobilization, so that other small G-proteins might be more important. The CH-domain supports the function of the DH-PH-ZF-domain unit probably by recruiting additional signaling factors, which need to be identified in future experiments. Collectively, my results demonstrate the paramount function of the Vav protein family in controlling the BCR-induced Ca^{2+}-signaling cascade most likely by binding and activating of small Rho family G-proteins.

2 Introduction

2.1 The immune system at a glance

The immune system of mammals is a complex composition of individual cell types and molecules that in contrast to other organs is distributed over the complete body. In general, it can be divided into two different sections, the innate and the adaptive immune system. The innate immune system constitutes the first barrier of host defense against pathogens. Here, granulocytes, macrophages and dendritic cells encounter invading pathogens that were able to cross physical barriers such as mucosal or epithelial layers. To recognize pathogens efficiently and fast, cells of the innate immune system are equipped with specific pattern recognition receptors on their surface that are able to detect widespread molecular patterns found on many microorganisms. After detection, pathogens are cleared primarily by phagocytosis (Janeway and Medzhitov, 2002; Iwasaki and Medzhitov, 2015).

Despite the elaborate organization of the innate immune system, it shows certain disadvantages in the context of adaptation to newly arising or changing pathogens, which are not efficiently detected by pattern recognition receptors. In addition, the innate immune system cannot mount a stronger response against pathogens that have been encountered before, as opposed to the adaptive immune system (Medzhitov and Janeway Jr., 1997; Parkin and Cohen, 2001; Flajnik and Kasahara, 2010).

The adaptive immune system consists of two branches, a cell-mediated and a humoral immune system. The former is carried out by antigen specific T cells responsible for detection and elimination of intracellular pathogens. This is accompanied most commonly by the release of cytokines, which in turn activate further effector cells of the adaptive as well as the innate immune system. In contrast, humoral immunity is mediated by B cell produced antibodies that have a broad variety of functions. These range from neutralization of bacterial toxins and virus particles to opsonization of pathogens, followed by activation of the complement system or phagocytes to promote the elimination of the pathogen (Flajnik and Kasahara, 2010; Cooper, 2015).

On primary encounter with a pathogen, innate immune cells control the first days of infection. The differentiation of B cells into either antibody secreting, short-lived plasma cells or long-lived memory B cells takes a couple of days. Short-lived plasma cells dominate the primary immune response, which is rather moderate concerning velocity and specificity. A faster and more specific immune response is initiated upon the secondary encounter with a pathogen by memory B cells. B cell responses are initiated following

recognition of a specific antigen by the B cell antigen receptor (BCR) expressed on the cell surface (LeBien and Tedder, 2008; Cooper, 2015; Kurosaki et al., 2015).

2.2 The B cell antigen receptor - How to become a functional B cell

Arrangement of a functional BCR is a crucial step in each B cell's life, since it controls B cell development. Each B cell expresses a BCR with a unique specificity on its surface that stepwise underwent structural rearrangements during B cell development (Pleiman et al., 1994; Kraus et al., 2004). The BCR is a multi-protein complex consisting of a membrane-bound immunoglobulin (mIg) responsible for the detection of the antigen and a heterodimer consisting of the two transmembrane proteins Igα and Igβ constituting the signaling unit of the complex (Reth and Wienands, 1997). Noteworthy, antibodies that are ultimately secreted by a B cell possess the same specificity as the mIg of the BCR. Evolutional pressure generated a sophisticated system to achieve an adequate antigen receptor repertoire for the detection of an almost unlimited number of potential antigens without extremely increasing the size of a cell's genome. In other words, the approximately 20000 genes of the human genome (Pertea and Salzberg, 2010) are far too few to provide as many distinct BCRs that would be necessary to cover all potential antigens (Flajnik and Kasahara, 2010). B cells undergo a process called somatic recombination in which Ig encoding genes are rearranged during B cell development. In detail, gene segments of Ig heavy chain (H) genes are present in segmented form in many copies and are named V_H, D_H and J_H segments. These segments are rearranged to code together with the C_H loci for a complete Ig heavy chain, whereas light chain (L) gene segments, V_L and J_L, are rearranged to code with the C_L loci for a complete Ig light chain. This somatic recombination is a random process in which one gene segment from many copies is randomly chosen in each developing B cell (Schatz and Ji, 2011). In total, two identical Ig heavy chains as well as two light chains assemble together to form the mIg that constitutes the antigen-recognition element of the BCR. Although the function of the BCR stands and falls with antigen recognition, association of mIg with the Igα/Igβ heterodimer is an absolute requirement for BCR expression, since Igα/Igβ contain not only the signaling capacity of the BCR complex, but are also responsible to guide the mIg to the cell surface (Kraus et al., 2004). While disulfide bonds covalently link the Igα/Igβ heterodimer, the association of the mIg and Igα/Igβ occurs non-covalently. Having a completely assembled BCR on its surface, a B cell is basically qualified for its life time

functions: Antigen recognition and antibody secretion (Kraus et al., 2004; Siegers et al., 2006).

After the first encounter with their specific antigen, B cells can undergo two differentiation fates. They can either develop into a plasma cell secreting low affinity IgM antibodies or enter specialized regions of secondary lymphoid organs, namely germinal centers, in which optimization of BCRs takes place (Kurosaki et al., 2015). Here, processes like somatic hypermutation of V gene regions and Ig class-switch recombination increase their antigen affinity and equip the BCR as well as the secreted antibodies with a different constant domain and thus new traits (Odegard and Schatz, 2006; Stavnezer et al., 2008). In the process of Ig class-switch recombination, the C_H gene segment encoding the constant region of the BCR heavy chain is rearranged leading to antibody isotype switching. In the end, B cells can generate one of five different antibody classes, which can be of IgM, IgD, IgA, IgG or IgE type (Xu et al., 2012). While IgM antibodies are predominantly produced during the first pathogen encounter, IgG antibodies account for approximately 70% of circulating antibodies and are produced during memory responses. By contrast, IgA and especially IgE are found in lower amounts. While IgA antibodies are the only ones that can pass epithelia and therefore fulfill important functions in the gut and the lung, IgE antibodies mediate allergic reactions by the binding of mast cells. IgD is found as membrane bound form as well as in low amounts in the blood serum, its exact function is not well understood (Schroeder and Cavacini, 2010).

Until the point of antibody secretion, various signaling processes have to be carried out, starting with activation of the BCR. In cooperation with activating co-receptors like CD19 and CD40 or inhibiting co-receptors like CD22, BCR-derived signals are integrated and dictate the B cell fate. For that reason, signals from the BCR and its co-receptors have to be tightly regulated, since they are responsible to keep the balance between proliferation and apoptosis to prevent B cell responses that might lead to autoimmunity (Marshall et al., 2000; Niiro and Clark, 2002).

2.3 Initiation of BCR signaling

Nowadays, two opposing activation models describing the initiation of BCR signaling are discussed. According to the generally accepted text book model, antigen binding leads to clustering of a vast number of monomeric BCRs that associate with membrane microdomains known as lipid rafts (Cheng et al., 1999; Harwood and Batista, 2010; Pierce and Liu, 2010). In contrast, a new model in which BCRs are in a pre-clustered state in the absence of antigen results in inhibition of signaling processes. In that model, the presence

of antigen leads to the dissociation of pre-clustered BCRs, which allows signaling activation in defined membrane areas (Yang and Reth, 2010). Both models have in common that BCRs locate into specific membrane microdomains. Here, Src family kinases (SFK) like Lyn and Fyn are enriched due to their N-terminal myrestoylation. Subsequently, immunoreceptor tyrosine-based activation motifs (ITAMs) of the Igα/Igβ heterodimer become phosphorylated by SFKs (Campbell and Sefton, 1992; Yamanashi et al., 1992; Casey, 1995). Each of the Igα or Igβ chains contain one ITAM sequence in their cytoplasmic tail that is in charge of transmitting signals to the cell interior (Sanchez et al., 1993). ITAMs are widely spread among immune receptors found in various cell types of the adaptive as well as the innate immune system (Humphrey et al., 2005). The ITAM consensus sequence is Yxx(I/L)x6-8Yxx(I/L) (single letter code for amino acids, x can be any amino acid) and constitutes a binding site for the tandem Src-homology 2 (SH2)-domains of the Spleen tyrosine kinase (Syk) (Reth, 1989; Kurosaki et al., 1995; Fütterer et al., 1998). Upon Syk-ITAM interaction, autoinhibition of Syk is relieved. In addition, structural rearrangements lead to the exposure of Syk regions that were previously masked by its own tandem SH2-domains. Transphosphorylation as well as autophosphorylation of several conserved tyrosine residues in Syk finally lead to its activation (Kurosaki et al., 1995). Active Syk can also phosphorylate ITAM tyrosine residues and thereby support its own activation process in a feed-forward loop (Rolli et al., 2002).

While Syk is recruited to phosphorylated ITAMs, a phosphorylated non-ITAM tyrosine residue (pY204) that is exclusively found in Igα recruits the SH2-domain-containing leukocyte adaptor protein of 65 kDa (SLP-65, also named BLNK or BASH) (Fu et al., 1998; Goitsuka et al., 1998; Wienands et al., 1998; Engels et al., 2001). Upon SLP-65 recruitment to pY204, ITAM-bound Syk phosphorylates SLP-65 on various tyrosine residues that function as docking sites for further SH2-domain containing proteins (Fu et al., 1998). In addition, several proline-rich interaction motifs in SLP-65 mediate further contacts with Src-homology 3 (SH3)-domain containing proteins (Grabbe and Wienands, 2006; Oellerich et al., 2011). In that sense, SLP-65 represents the main signaling platform in BCR signaling, influencing several downstream signaling pathways (Oellerich et al., 2009). This model is supported by the phenotype of SLP-65-deficient mice showing reduced numbers of B cells as well as defective Ca^{2+}-signaling and proliferation responses (Jumaa et al., 1999). Assistance receives SLP-65 from its constitutive interaction partner Cbl-interacting protein of 85 kDa (CIN85) that serves as crucial factor in SLP-65 plasma membrane recruitment (Oellerich et al., 2011). At the plasma membrane, SLP-65 nucleates the so-called Ca^{2+}-initiation complex. Besides SLP-65, it consists of Bruton's tyrosine kinase (Btk) and phospholipase C (PLC) γ2, which both bind

phospho-tyrosine residues in SLP-65 by virtue of their SH2-domains (Engelke et al., 2007; Scharenberg et al., 2007). The formation is supported by the Pleckstrin-homology (PH)-domains of both Btk and PLCγ2 that mediate binding to phosphatidyl-inositol-3,4,5-trisphosphate (PIP_3) in the plasma membrane (Salim et al., 1996; Falasca et al., 1998). Following recruitment of Btk to SLP-65, Btk gets phosphorylated and activated, which allows the activated Btk to phosphorylate and thereby activate PLCγ2. (Hashimoto et al., 1999; Engelke et al., 2007). Activated PLCγ2 in turn hydrolyzes its substrate phosphatidyl-inositol-4,5-bisphosphate (PIP_2) into the second messengers diacylglycerol (DAG) and inositol-1,4,5-triphosphate (IP_3), which is the starting point for diversification of BCR signals (Reth and Wienands, 1997).

2.4 Beyond the Ca^{2+}-initiation complex

The soluble second messenger IP_3 diffuses in the cytoplasm and binds to IP_3-receptors, which are ligand-gated Ca^{2+}-channels located in the membrane of the endoplasmic reticulum (ER). Receptor binding by IP_3 induces channel opening leading to a Ca^{2+}-flux following the Ca^{2+}-concentration gradient from the ER into the cytoplasm. Sarcoplasmic/endoplasmic Ca^{2+}-ATPases, which are constantly active, accomplish restoration of the ER Ca^{2+}-depot (Kurosaki, 1999). Once the ER Ca^{2+}-depot is exhausted, store-operated Ca^{2+}-channels (SOCs) in the plasma membrane are opened leading to a sustained Ca^{2+}-influx from the extracellular milieu into the activated B cell. This is achieved by the interaction of two different types of proteins, namely the stromal interaction protein (STIM) and the Ca^{2+} release-activated Ca^{2+}-channel (CRAC) ORAI (Cahalan, 2009). STIM is located in the membrane of the ER and contains a Ca^{2+}-binding EF-hand-domain at the ER-luminally located N-terminus to monitor Ca^{2+}-levels within the ER lumen (Zhang et al., 2005). Binding of Ca^{2+} to STIM causes its dimerization. Following Ca^{2+}-depletion from the ER, STIM starts to oligomerize, which leads to formation of aggregates migrating along tubulovesicular structures to juxtamembrane regions of the cell periphery (Zhang et al., 2005). Here, STIM-cluster can directly interact with ORAI enabling its complete assembly and activation (Park et al., 2009). As a result, Ca^{2+} is able to pass the CRAC-channel leading to a sustained Ca^{2+}-influx. From here, BCR signals start to diversify into many downstream signaling pathways, that are regulated by the second messenger Ca^{2+} and DAG (Kurosaki et al., 2010).

For example, the activation of transcription factors of the NFAT (nuclear factor of activated T cells) family is regulated in a Ca^{2+}-dependent manner. Increasing cytosolic Ca^{2+} levels activate the serine/threonine phosphatase calcineurin, which subsequently

dephosphorylates NFAT proteins and thus enables their translocation into the nucleus for gene regulation (Kawasaki et al., 1998; Crabtree and Olson, 2002).

In contrast to IP_3, DAG remains within the plasma membrane and recruits the serine/threonine protein kinase C (PKC) family member PKC-β, which also depends on Ca^{2+}-binding for complete activation (Takai et al., 1979). This is the starting point of the canonical NF-κB (Nuclear factor of κ light polypeptide gene enhancer in B cells) pathway resulting in the translocation of NF-κB into the nucleus, where it can fulfill its transcription factor role (Guo et al., 2004; Sen, 2006). One further example for DAG dependent signaling is the recruitment of Ras guanine nucleotide release proteins (RasGRP) to the plasma membrane. These are guanine nucleotide exchange factors for G-proteins of the Ras family that in lymphocytes control the Erk/MAP kinase pathway leading to lymphocyte proliferation (Oh-hora et al., 2003).

Besides the previously described BCR-induced formation of the Ca^{2+}-initiation complex and its downstream effects, BCR engagement induces also membrane recruitment of phosphoinositide 3'-kinase (PI3K) family members, which phosphorylate the PLCγ2 substrate PIP_2 to generate PIP_3. PIP_3 constitutes a docking site for proteins with PH-domains such as Btk and PLCγ2, supporting the membrane recruitment of the Ca^{2+}-initiation complex (Salim et al., 1996; Falasca et al., 1998). Furthermore, Akt (also named protein kinase B, PKB) is recruited to the membrane anchor PIP_3 (Mee et al., 2010; Hersa et al., 2011), which subsequently leads to its phosphorylation and activation by PDK1 (phosphoinositide-dependent kinase-1). Activated Akt in turn phosphorylates several downstream factors, which influence lymphocyte survival and proliferation (Okkenhaug and Vanhaesebroeck, 2003; Hersa et al., 2011).

The functionality of BCR signaling is of tremendous importance, since the absence or dysfunction of single components can lead to severe B cell deficiencies. For example, mutations in Btk result in X-linked agammaglobulinemia (XLA) in humans and X-linked immunodeficiency (Xid) in mice that are characterized by a complete lack of antibodies (Satterthwaite et al., 1998). Collectively, BCR-induced signaling pathways have critical impacts on the fate of a B cell. However, unexplored factors remain, so that BCR-induced signaling is not entirely understood. One of these less-well characterized factors in the BCR signaling cascade is the Vav guanine nucleotide exchange factor family that represents the major subject of my PhD project.

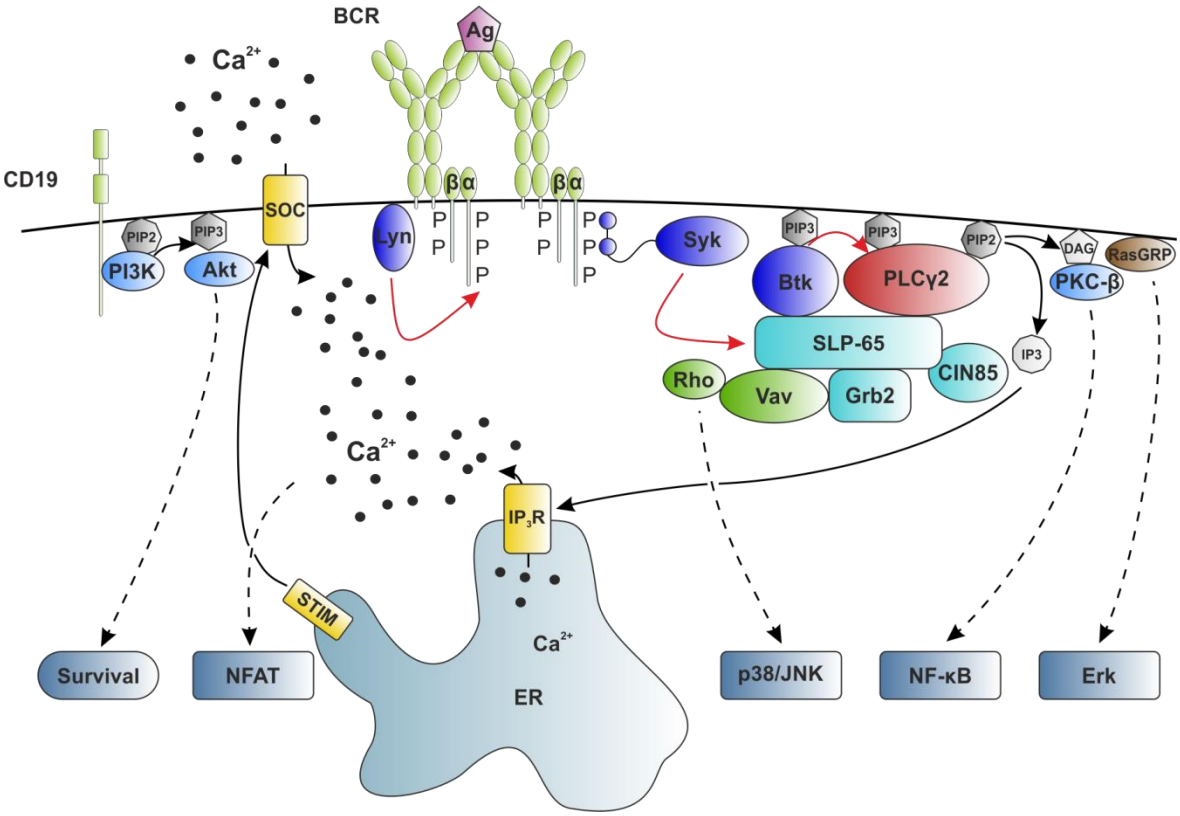

Figure 2.1: Schematic drawing of BCR-proximal signaling events. BCR cross-linking by antigens leads to phosphorylation of ITAMs within the Igα/Igβ heterodimer by Src family kinases like Lyn. Subsequently, Syk is recruited to phosphorylated ITAMs leading to the phosphorylation of SLP-65, followed by the assembly of the 'core' Ca^{2+}-initiation complex on the key adaptor protein SLP-65. In addition, further signaling factors are gathered on this platform like CIN85, Grb2 and Vav1. From that point, several downstream signaling pathways are triggered (see text for details). Red arrows indicate phosphorylation processes, solid arrows indicate translocation processes, dashed arrows indicate multistep signaling pathways, Ca^{2+} is indicated by black dots. Color-code: IgM-BCR and CD19 are depicted in light green, antigen in dark pink, tyrosine kinases in dark purple, other kinases in blue, adaptor proteins in turquoise, second messengers in light grey, membrane phospholipids in dark grey, small G-protein Rho (family) and the guanine nucleotide exchange factor Vav (family) in green, RasGRP in brown, IP_3R, STIM and Soc in yellow.

2.5 Vav - guanine nucleotide exchange factors of Rho family G-proteins

Since signals emanating from the BCR are responsible for cell fate decisions of each B cell, they have to be tightly controlled. BCR signaling is an interplay of enzymes and adaptors. The latter ones orchestrate the assembly and disassembly of activating as well as inhibitory signaling complexes. A small group of proteins that can combine both, enzymatic as well as adaptor functions is the family of Vav guanine nucleotide exchange factors for small G-proteins of the Rho family, which I will describe in detail in the following chapter.

Vav1 was discovered in gene transfer assays determining the presence of transforming genes in human esophageal carcinomas in 1989 (Katzav et al., 1989). Since *VAV1* was the sixth transforming gene discovered in the laboratory of Prof. Barbacid, it was named according to the sixth letter of the Hebrew alphabet, as the native language of its discoverer was Hebrew (Katzav et al., 1989). In the following years, the Vav family was stocked up by the discovery of the further members Vav2 and Vav3 (Henske et al., 1995; Movilla and Bustelo, 1999), which share a high degree of similarity regarding domain architecture and amino acid sequence homology (50-60 %). Despite their homology, individual Vav protein family members are adjusted to their specific signaling pathway, which is reflected by their different expression profiles. While the Vav2 and Vav3 expression pattern includes almost any cell type in mice, Vav1 expression is rigorously restricted to the hematopoietic cell lineage (Schuebel et al., 1996; Ogilvy et al., 1998; Movilla and Bustelo, 1999). Nevertheless, experiments in mice revealed a certain redundancy between Vav family members, as Vav1-deficient mice show a normal T and B cell development. In contrast, Vav1/Vav2 double-deficient mice revealed a block of B and T cell development at early developmental stages. In accordance with defects of lymphocyte populations, B and T cell antigen receptor signaling is impaired in Vav1/Vav2 double-deficient mice including Ca^{2+}-mobilization (Tedford et al., 2001). Furthermore, Vav1/Vav2/Vav3 triple-deficient mice support these findings and show more pronounced defects compared to Vav1/Vav2 double- or Vav1-deficient animals (Fujikawa et al., 2003). Collectively, mouse experiments pushed the Vav family members to the focus of attention, since they represent a central signaling knot in B and T cells regulating the cellular fate of both lineages. Nevertheless, despite intensive investigations over the last decades, the exact mechanisms by which Vav proteins control these processes are only partially understood.

2.5.1 Vav1 - a multi-domain protein with diverse functions

Vav1 is a multi-domain protein with an approximate molecular weight of 100 kDa consisting of several protein domains (figure 2.2). In principle, Vav1 can be divided into two segments. The N-terminal segment contains five different protein domains or regions including a Calponin- (CH), a Dbl- (DH), a PH-, a Zinc-finger (ZF)-domain and an acidic stretch. These regions act in concert for efficient activation of small Rho family G-proteins by catalyzing the exchange of GDP to GTP and therefore comprise the enzymatic function of Vav1. In contrast, the C-terminal segment contains an adaptor region including an SH2-domain flanked by two SH3-domains. However, the exact role of N- and C-terminal Vav1

segments in the context of BCR-induced Ca^{2+}-mobilization remains poorly understood. (Bustelo, 2001; Tybulewicz, 2005)

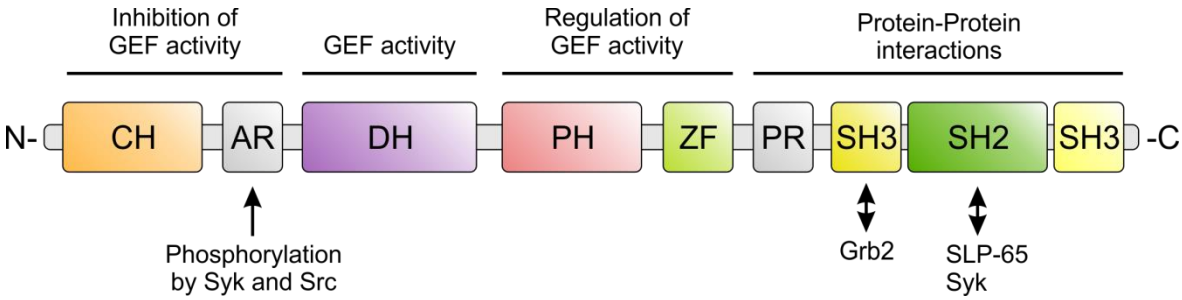

Figure 2.2: Domain architecture of Vav1. Individual protein domains are depicted and their respective functions are indicated. Phosphorylation of the acidic region is done by Syk and Src family kinases. Grb2 interacts with N-terminal SH3 domain, whereas SLP-65 and Syk are binding partners for the SH2-domain. (CH: Calponin-homology-domain, AR: Acidic region, DH: Dbl-homology-domain, PH: Pleckstrin-homology-domain, ZF: Zinc finger-domain, PR: Proline rich region, SH3: Src-homology 3-domain, SH2: Src-homology 2-domain)

The DH-PH-ZF-domain unit

The DH-, PH-, ZF-domains form a functional unit that mediates the enzymatic GEF activity of Vav1. In that context, the DH-domain is responsible for the exchange of GDP with GTP in Rho family poteins (Hoffman and Cerione, 2002). The spectrum of Vav1-activated G-proteins is not completely defined, since Vav1-mediated G-protein activation might depend on cell type and signaling pathways. Furthermore, *in vitro* and *in vivo* experimental conditions might influence Vav1's catalytic specificity towards small G-proteins. In fact, two coupled events, binding and subsequent enzymatic reaction, are critical for efficient and specific Vav1-mediated G-protein activation. Both depend on the interaction with two separate regions of Rho proteins (Movilla et al., 2001). In B-cells, Vav1 has been shown to activate several G-proteins including Rac1, Rac2, RhoA and RhoG (Saci and Carpenter, 2005; Brezski and Monroe, 2007; Arana et al., 2008; Malhotra et al., 2009). The Vav1-activated G-proteins mediate downstream effects like rearrangement of the cytoskeleton, cell proliferation and survival (Bustelo, 2001; Zugaza et al., 2002).

The activity of the Vav1 DH-domain is regulated by several mechanisms. First, the adjacent PH domain makes intramolecular contacts with the DH-domain and thus stabilizes its 3D structure (Hoffman and Cerione, 2002). Second, the PH-domain influences the catalytic activity of the DH-domain depending on the PIP-species it binds to. Binding of PIP_2 to the PH-domain decreases DH-domain activity, whereas binding of PIP_3 increases its activity (Das et al., 2000). Third, the DH-domain proximal acidic region

contains three tyrosine residues that block the active center of the DH-domain, thereby acting as inhibitory loop (Zugaza et al., 2002) that is strengthened through a further internal interaction between the CH- and ZF-domains. Phosphorylation of tyrosines within the acidic stretch leads to opening of inhibitory structures and enhanced DH-domain-mediated GEF activity (Zugaza et al., 2002). Fourth, also the ZF-domain might act as structural DH-domain stabilizer, since mutations in the ZF-domain diminish Vav1 GEF activity (Zugaza et al., 2002). Taken together, the Vav1 GEF activity is tightly regulated in a stepwise process to prevent unintended G-protein activation.

The relationship between Vav1's GEF activity and antigen receptor-mediated Ca^{2+}-signaling in lymphocytes was investigated in mice focusing primarily on T cell activation. Mice expressing Vav1 with an inactive DH-domain showed no altered Ca^{2+}-mobilization upon TCR stimulation (Saveliev et al., 2009). In contrast, mutations affecting the GEF activity of Vav1 that are located away from the active center of the DH-domain, lead to a dramatic defect in TCR-induced Ca^{2+}-mobilization (Ksionda et al., 2012). These mutations probably influence the structural integrity of the DH-domain causing a loss of GEF-dependent functions. In B cells, little is known about the relation between the Vav1 DH-domain function and BCR-induced Ca^{2+}-mobilization. However, loss of Vav3 in the chicken B cell line DT40 leads to reduced Ca^{2+}-mobilization upon BCR stimulation, which might be caused by impaired Rac1 activation (Inabe et al., 2002). Further investigations focused on the role of Vav1-mediated activation of Rac1 and Rac2 for B cell development, proliferation and survival (Walmsley et al., 2003). In addition, Vav1-mediated Rac activation leads to cytoskeletal rearrangements and promotes BCR endocytosis (Arana et al., 2008; Malhotra et al., 2009). The connection between BCR-induced Ca^{2+}-mobilization and the function of the Vav1 DH-domain, however, remains unclear.

The CH-domain

CH-domains comprise roughly 100 amino acids and occur in five different types. Originally, type 1 and 2 CH-domains, when arranged in tandem, were shown to form an Actin-binding domain (ABD) that binds to the Actin cytoskeleton. Based on amino acid sequence analysis, each ABD contains three different stretches of conserved residues characterized as Actin-binding sites (ABS) that mediate the direct contact to the Actin cytoskeleton. However, only type 1 and type 2 CH-domains contain the conserved ABS, whereas type 3, 4 and 5 CH-domains lost these residues during evolution. Therefore, possible functions of type 3, 4 and 5 CH-domains are still under debate (Gimona et al., 2002).

Regarding type 3 CH-domains, it is currently assumed that the exact task of each domain is strongly connected to the individual protein function (Gimona et al., 2002). The Vav1 type 3 CH-domain was shown to be a crucial regulator of Vav1 GEF activity, since its deletion leads to an increased transforming potential, which is reflected by an enhanced Vav1 GEF activity towards Rho family G-proteins (Katzav et al., 1991; Zugaza et al., 2002). Based on these results, the Vav1 CH-domain fulfills an inhibitory function in the context of Vav1 GEF activity. Structural investigations further support this hypothesis, since they show formation of an inhibitory loop that is stabilized by a direct contact between the CH-domain and the central DH-PH-ZF-domain unit (Zugaza et al., 2002; Yu et al., 2010). Furthermore, the Vav1 CH-domain is essential for TCR-induced Ca^{2+}-mobilization, since its deletion leads to a dramatic Ca^{2+}-mobilization defect (Li et al., 2013). The reason for this defect in Ca^{2+}-mobilization might be based on the loss of protein-protein interaction. Only a few binding partners of the Vav1 CH-domain have been described including the ubiquitous Ca^{2+}-sensor protein calmodulin and a Rho GDP dissociation inhibitor named Ly-GDI (Groysman et al., 2000; Li et al., 2013). However, their function in Vav1-mediated Ca^{2+}-mobilization is vague. In B cells, little is known about the function of the CH-domain, except its operating principle in the context of G-protein activation. A putative function with regard to BCR-induced Ca^{2+}-mobilization remains unknown.

The adaptor part of Vav1

The C-terminal Vav1 adaptor region consists of three protein binding domains in an SH3-SH2-SH3-domain arrangement (figure 2.2). SH2-domains interact with phosphorylated tyrosine-containing motifs in active signaling complexes, whereas SH3-domains most commonly mediate rather constitutive protein-protein interactions by binding to proline-rich motifs (Alexandropoulos et al., 1995; Birge et al., 1996). Hence, Vav1 can localize to active signaling spots via its SH2-domain and integrate additional proteins via SH3-domain-mediated interactions.

The N-terminally located SH3-domain of Vav1 (hereafter referred to as N-SH3) binds the adaptor protein Grb2 (Kim et al., 1998; Jang et al., 2009). This interaction is mediated by an unusual face to face interaction between the C-terminal Grb2 SH3-domain and the N-SH3-domain of Vav1 (Kim et al., 1998; Nishida et al., 2001). Canonical binding of the N-SH3-domain to a proline-rich motif is not possible due to a binding pocket blockage by an intramolecular proline-rich motif and missing prerequisites for correct proline-rich peptide recognition (Nishida et al., 2001). The functional relevance of the Vav1-Grb2 interaction is

not completely defined. However, Grb2 mediates in concert with SLP-65 membrane recruitment of Vav3 in chicken DT40 B cells leading to an efficient activation of Rac1 (Kim et al., 1998; Salojin, 2000; Johmura et al., 2003). Further interaction partners have not been described until today. Nevertheless, other Grb2 family members might be able to interact with the Vav1 N-SH3-domain as well.

In contrast, the C-terminal SH3 domain (hereafter referred to as C-SH3) of Vav1 binds to proline-rich motifs in a common manner. Deletion of the C-SH3-domain leads to a loss of Vav1 GEF activity (Zugaza et al., 2002). In fact, various binding partners of the C-SH3-domain were identified however, a functional connection of the interaction partners with the GEF activity of Vav1 was not reported. The identified interaction partners include nuclear proteins involved in DNA-repair (Ku-70) and mRNA processing (hnRNP-K, hnRNP-C) as well as the focal contact protein zyxin (Hobert et al., 1996; Romero et al., 1996; Romero et al., 1998). The functional relevance of theses interactions is not known.

In addition to the C-SH3-domain, the centrally located SH2-domain of the Vav1 adaptor region is of primary importance, since it guides Vav1 to active signaling regions. It preferentially binds phosphorylated YxEP motifs that can be found in essential proteins of the BCR as well as TCR signaling cascade including Syk, ZAP70 (70 kDa zeta-chain associated protein), SLP-65 and SLP-76 (SH2 domain-containing leukocyte phosphoprotein of 76 kDa) (Songyang et al., 1994; Deckert et al., 1996; Wu J. et al., 1996; Wu J. et al., 1997; Wienands et al., 1998), indicating that Vav1 is part of the signaling platform formed by the key adaptor SLP-65. Based on in vitro peptide affinity purification experiments, the Vav1 SH2-domain was shown to exclusively bind to the phosphorylated tyrosine 91 (pY91) of chicken SLP-65 (Chiu et al., 2002). Nevertheless, it remains unclear whether the SLP-65-Vav1 interaction has any functional consequences in B cells. Inactivation of the SH2-domain leads to a complete loss of GEF activity as well as to defects in Ca^{2+}-mobilization and TCR microcluster formation in T cells (Zugaza et al., 2002; Sylvain et al., 2011). In B cells, the Vav1 SH2-domain binds to the phosphorylated tyrosine residues Y341 and Y345 of Syk upon BCR stimulation. In turn, Syk phosphorylates tyrosines in the acidic region and thereby activates Vav1's GEF function (Deckert et al., 1996; Lopez-Lago et al., 2000). In addition, Vav1's GEF activity is fine-tuned by the activating and inhibiting co-receptors CD19 and CD22, respectively (Sato et al., 1997). Phosphorylation of the intracellular tail of CD19 leads to the recruitment of Vav1 and the Src-kinase Lyn, which also results in Vav1 phosphorylation and activation in addition to BCR-induced Vav1 activation (Weng et al., 1994; Sato et al., 1997; Fujimoto et al., 1999). In contrast, recruitment of the tyrosine-protein phosphatase non-receptor type 6

(PTPN6) to CD22 inhibits Vav1 activity via dephosphorylation of tyrosine residues (Sato et al., 1997).

Taken together, the Vav1 adaptor region fulfills essential tasks that are mainly correlated with the Vav1 GEF activity. Investigations concerning antigen receptor signaling focused primarily on TCR-induced Ca^{2+}-mobilization and showed a critical role of the Vav1 adaptor region in that context. Yet, whether or not the Vav adaptor region has a similar function in BCR-induced signaling events remains unclear.

2.6 Aim of this thesis

The Vav guanine nucleotide exchange factor family has been shown to be a crucial factor for adaptive immunity, where it influences the antigen receptor signaling capacity in mature and developing lymphocytes and the maturation of lymphocytes starting from early developmental stages (Tedford et al., 2001; Fujikawa et al., 2003). Nevertheless, how Vav1 exerts its function in B cell antigen receptor signaling remains poorly understood. Therefore, the goal of my thesis was to elucidate the mechanisms by which Vav1 controls signaling processes emanating from the BCR.

During my PhD project, I focused on the following issues:

1. Generation of a Vav1-deficient human B cell line to study the role of Vav family members in BCR-proximal Ca^{2+}-signaling.
2. How is Vav1 connected to the BCR signalosome? Which protein-protein interactions are important in that process?
3. Is the guanine nucleotide exchange activity of Vav1 involved in BCR-induced Ca^{2+}-mobilization? Which other Vav1 domains might be important in Ca^{2+}-mobilization?
4. Are small G-proteins of the Rho family involved in BCR-proximal Ca^{2+}-signaling?

3 Materials and Methods

3.1 Materials

3.1.1 Chemicals and reagents

Chemicals and reagents were purchased from Invitrogen, Merck, Roth or Sigma, unless it is not directly indicated in the following materials and methods chapters.

3.1.2 Consumables

Table 3.1: Consumables used in this study.

Consumables	Company
Blotting Paper Whatman™	Sartorius Stedim
Cell culture equipment (pipettes, tubes, culture dishes)	Greiner Bio-one
Cuvettes	Roth
DNA-ladder	Fermentas
6x DNA-loading buffer	NEB
dNTPs	NEB
FCS	PAA
Ficoll-Paque Plus	Amersham Bioscience
Filtropur filters	Sarstedt
Glutathione-sepharose	GE Healthcare
Hexadimethrine Bromide (Polybrene)	Sigma
Immersion oil	Merck
Indo-1 AM	Invitrogen
IPTG (Isopropyl-β-D-thiogalactopyranosid)	Sigma
MACS columns (LS)	Milteny Biotec
Microscope paper	neoLab
Neubauer improved counting chamber	Brand
Nitrocellulose membrane Hybond ECL	Amersham Biosciences
Prestained Protein Marker, Broad Range (6.5-175 kDa)	NEB
Protease Inhibitor Cocktail (P2714)	Sigma
Pyruvat	Biochrom
Streptavidin-sepharose	GE Healthcare

TransIT®-293 Transfection Reagent	Mirus
Trypsin/EDTA (0.05 %)	Gibco
4-well imaging chambers	Lab Tek
X-gal (5-bromo-4-chloro-3-indolyl-beta-D-galacto-pyranoside)	Roth

3.1.3 Enzymes

All enzymes were used according to the manufacturer's instructions.

Table 3.2: Enzymes used in this study.

Enzymes	Company
Blunting kit	NEB
Calf intestine phosphatase	NEB
Phusion DNA polymerase	NEB
Plasmid-Safe™	Biozym
Restriction endonucleases	NEB
Taq polymerase PCR master mix	Qiagen
T4 DNA ligase	NEB

3.1.4 Reaction systems (kits)

Table 3.3: Reaction systems (kits) used in this study.

Reaction systems	Application	Company
TA Cloning® Kit	Cloning	Invitrogen
Human B Cell Nucleofector® Kit	Nucleofection of DG75 cells	Lonza
Human B cell isolation kit	Isolation of primary human B cells	Milteny Biotec
QIAprep® Spin Miniprep	Plasmid-DNA purification	Qiagen
Wizard® Plus SV Minipreps DNA Purification System	Plasmid-DNA purification	Promega
Pure Yield™ Plasmid Midiprep System	Plasmid-DNA purification	Promega
Wizard® SV Gel and PCR Clean-Up System	PCR clean-up, gel extraction	Promega

3.1.5 Synthetic DNA oligonucleotides

Synthetic DNA oligonucleotides were purchased from Eurofins Genomics and used according to the manufacturer's instructions.

Table 3.4: Primer used in this study.

Primer used for cloning in this study.

Name	Sequence 5'-> 3'	Application
CHLVav1_CTG_fw	TAATGGATCCCTGGAGCTGTGGCGCCAATG	Cloning of Vav1 into pMSCVpuro
CHLVav1_EcoRIfw	TAATGAATTCATGGAGCTGTGGCGCCAATG	Cloning of Vav1 into pMSCVpuro, pCitrine
CHLVav1_XhoI_fw	TAATCTCGAGATGGAGCTGTGGCGCCAATG	Cloning of Vav1 into pMSCVpuro, pCitrine
cVav1_EcoRI_re3	TAATGAATTCTCAGCAGTATTCAGAATAATCTTCCTCC	Cloning of Vav1 into pMSCVpuro
cV1AgeI_re	TAATACCGGTAGGCAGTATTCAGAATAATCTTCCTCCAC	Cloning of Vav1 in pCitrine
XhoI_Vav2_fw	TAATCTCGAGATGGAGCAGTGGCGGCAG	Cloning of Vav2 in pMSCVpuro, pCitrine
AgeI_Vav2_re	TAATACCGGTAGCTGGATGCCCTCCTCTTCTACG	Cloning of Vav2 in pCitrine
Vav3_EcoRI_fw	TAATGAATTCATGGAGCCGTGGAAGCAGTGC	Cloning of Vav3 in pMSCVpuro, pCitrine
Vav3_AgeI_re	TAATACCGGTAGTTCATCCTCTTCCACATATGTGGATGGAAACC	Cloning of Vav3 in pCitrine
mVav1_fw	TAATCTCGAGATGGAGCTCTGGCGACAGTGCAC	Cloning of mVav1 in pMSCVpuro, pCitrine
mVav1_re	TAATACCGGTAGGCAATATTCGGAATAGTCTTCCTCCACATAGTTAGA	Cloning of mVav1 in pCitrine
mVav2_fw	TAATGAATTCATGGAGCAGTGGCGGCAATGCG	Cloning of mVav2 in pMSCVpuro, pCitrine
mVav2_re	TAATACCGGTAGCCTTCTCGCAGTGACAGCTCCCGC	Cloning of mVav2 in pCitrine
mVav3_fw	TAATCTCGAGATGGAGCCGTGGAAGCAGTGCG	Cloning of mVav3 in pMSCVpuro, pCitrine

mVav3_re	TAATACCGGTAGTTCATCTTCTTCCACATATGTGGATGGAAACCAG	Cloning of mVav3 in pCitrine
mVav1_intern_fw	CTCTGCAGCGATTCCTTAAGCCTCA	Sequencing
mVav2_intern_fw	GAGACAGCTGAAAATGATGACGACGTC	Sequencing
mVav2_intern_re	GACGTCGTCATCATTTTCAGCTGTCTC	Sequencing
mVav2_intern_fw2	AGCAAAGGGATCAGGCCATTTCCATCAGAGGAGACAGCTGAAAATGATGA	Sequencing
Vav3_intern_fw	ACAGAAACTTTGGAGTCAATAGAAAAAT	Sequencing
cGFP_EcoRI_re	TAATGAATTCTTTACTTGTACAGCTCGTCCATGC	Cloning of constructs into pMSCVpuro
cGFP_XhoI_re	TAATCTCGAGTTTACTTGTACAGCTCGTCCATGC	Cloning of constructs into pMSCVpuro
deCH_Vav1_fw	TAATGGATCCATGCCCTTCCCCACCGAG	Cloning of ΔCH Vav1
deCH_Vav1_XhoI_fw	TAATCTCGAGATGCGCTCGGAGCCCGTGTC	Cloning of Vav1 CH_{CT}
V1_CH_Nt_fw	CCAACTACGTGGAGGAAGATTATTCTGAATACTGCCTACCGGTCGCCACCCTGGAGCTGTGGCGCCAATGC	Cloning of Vav1 CH_{CT}
V1_CH_Nt_re	GCATTGGCGCCACAGCTCCAGGGTGGCGACCGGTAGGCAGTATTCAGAATAATCTTCCTCCACGTAGTTGG	Cloning of Vav1 CH_{CT}
V1_CH_Ct_re	TAATACCGGTAGGCGCATGAGGTCCTCATAGATCTCGTC	Cloning of Vav1 CH_{CT}
Lyn1-23dCHV1 fw	TAATCTCGAGATGGGATGTATAAAATCAAAAGGGAAAGACAGCTTGAGTGACGATGGAGTAGATTTGAAGACTCAACCACTGCCCTTCCCCACCGAGGAGGAGAG	Cloning of Lyn_{myr}-ΔCH Vav1
CH_Spectrin_fw	TAATCTCGAGATGACGACCACAGTAGCCACAGACTATG	Cloning of $[CH]_2$ β-Spectrin-Vav1

CH_Spec_Vav1_fw	TCTGGTCGGACAGGCCACTGTACATCTTAGAGAAGTAGTGGTAATAAGTCACCA	Cloning of $[CH]_2$ β-Spectrin-Vav1
CH_Spec_Vav1_re	TGGTGACTTATTACCACTACTTCTCTAAGATGTACAGTGGCCTGTCCGACCAGA	Cloning of $[CH]_2$ β-Spectrin-Vav1
CH_IQGAP_fw	TAATCTCGAGATGTCCGCCGCAGACGAGGTTGAC	Cloning of CH IQGAP-Vav1
CH_IQGAP_Vav1_fw	CTCAGTTTGTACCTGTTCAAGCTAGGCCTGTACAGTGGCCTGTCCGACCAGA	Cloning of CH IQGAP-Vav1
CH_IQGAP_Vav1_re	TCTGGTCGGACAGGCCACTGTACAGGCCTAGCTTGAACAGGTACAAACTGAG	Cloning of CH IQGAP-Vav1
V1_deltaAcid_fw	CAGAACAGGGGGATCATGCCCTTCTCCATGCCGCCCAAGATGACAGAG	Cloning of ΔAR Vav1
V1_deltaAcid_re	CTCTGTCATCTTGGGCGGCATGGAGAAGGGCATGATCCCCCTGTTCTG	Cloning of ΔAR Vav1
NSH3_Vav1_fw2	TAATGAATTCGGCCGACATGGGCAAGAT	Cloning of C2 adaptor region into pGEX-4T1
Vav1_cSH3_re1	TAATCTCGAGTCAGCAGTATTCAGAATAATCTTCCTCC	Cloning of C2 adaptor region into pGEX-4T1
Vav1_SH2_fw	TAATGAATTCCCTCCTCAGGACCTGTCTGTT	Cloning of SH2-domain into pGEX-4T1
Vav1_SH2_re	TAATCTCGAGTTAGATGGTTCTCTTTTCAGGCTCCTT	Cloning of SH2-domain into pGEX-4T1
hSLP65SH2_fw	TAATCCTCAGGACTGGTATGCTGGAGCCTGTGATCG	Cloning of Vav1-SLP-65 SH2
hSLP65SH2_re	TAATCCCACTGCTGAAACTTTAACTGCATACTTCAGTCTGGTG	Cloning of Vav1-SLP-65 SH2
SykSH2_fw	TAATCCTCAGGACTCCGGCATGGCTGACAGCG	Cloning of Vav1-Syk $[SH2]_2$
SykSH2_re	TAATCCCACTGCTGGAAGTTGTGGACGGCCTCCAAA	Cloning of Vav1-Syk $[SH2]_2$

OL_SykVav1_fw	TTTGGAGGCCGTCCACAACTTCCAGCAGTGGGAAGCACAAAGTATTTTGGC	Cloning of Vav1-Syk $[SH2]_2$
OL_SykVav1_re	GCCAAAATACTTTGTGCTTCCCACTGCTGGAAGTTGTGGACGGCCTCCAAA	Cloning of Vav1-Syk $[SH2]_2$
Vav1BtkNtSH2_fw2	TGTCCATGGCCCTCCTGAGGACGAAGCAGAAGACTCCATAGAAATGTATGAG	Cloning of Vav1-Btk SH2
Vav1BtkNtSH2_re2	CTCATACATTTCTATGGAGTCTTCTGCTTCGTCCTCAGGAGGGCCATGGACA	Cloning of Vav1-Btk SH2
Vav1BtkCtSH2_fw2	CAAAACAAGAATGCACCTTCCACTGCAGTGGGAAGCACAAAGTATTTTGGC	Cloning of Vav1-Btk SH2
Vav1BtkCtSH2_re2	GCCAAAATACTTTGTGCTTCCCACTGCAGTGGAAGGTGCATTCTTGTTTTG	Cloning of Vav1-Btk SH2
Vav1ItkNtSH2_fw	TGTCCATGGCCCTCCTCAGGACGAAAAATCTCCAAATAATCTGGAAACCTATGAGTGG	Cloning of Vav1-Itk SH2
Vav1ItkNtSH2_re	CCACTCATAGGTTTCCAGATTATTTGGAGATTTTTCGTCCTGAGGAGGGCCATGGACA	Cloning of Vav1-Itk SH2
Vav1ItkCtSH2_fw	TGTTTTGGGAGGCAGAAAGCCCCAGTTGCAGTGGGAAGCACAAAGTATTTTGGC	Cloning of Vav1-Itk SH2
Vav1ItkCtSH2_re	GCCAAAATACTTTGTGCTTCCCACTGCAACTGGGGCTTTCTGCCTCCCAAAACA	Cloning of Vav1-Itk SH2
hSLP65CTGBglIIf	TAATAGATCTCTGGACAAGCTTAATAAAATAACCGTCCCC	Cloning of SLP-65 into pMSCVpuro
hSLP65_BglII_re	TAATAGATCTTTATGAAACTTTAACTGCATACTTCAGTCTGGTG	Cloning of SLP-65 into pMSCVpuro
PIP5KA_BglII_re	TAATAGATCTTTAATGGGTGAACTCTGACTCTGCAACTTC	Cloning of PIP5K1a into pMSCVpuro

PIP5Ka_EcoXho_f	TAATGAATTCCTCGAGATGGCGTCG GCCTCCTCCGC	Cloning of PIP5K1a into pMSCVpuro, pCitrine
PIP5Ka_AgeI_r	TAATACCGGTAGATGGGTGAACTCT GACTCTGCAACTTCAAG	Cloning of PIP5K1a into pCitrine
Vav1Rac1_fw	GGAGGAAGATTATTCTGAATACTGC CTGCAGGCCATCAAGTGTGTG	Cloning of Vav1-Rac1
Vav1Rac1_re	CACACACTTGATGGCCTGCAGGCAG TATTCAGAATAATCTTCCTCC	Cloning of Vav1-Rac1
Rac1_BamHI_re	TAATGGATCCTTACAACAGCAGGCA TTTTCTCTTCCTC	Cloning of Vav1-Rac1
SykSH2_BglII_fw	TAATAGATCTTCCGGCATGGCTGAC AGCG	Cloning of $[SH2]_2$ Syk-PIP5K1a$_{core}$
Syk_PIP5K1a_fw	TTTGGAGGCCGTCCACAACTTCCAG GTGGCGATCCCGCGGTCCCTTCC	Cloning of $[SH2]_2$ Syk-PIP5K1a$_{core}$
Syk_PIP5K1a_re	GGAAGGGACCGCGGGATCGCCACC TGGAAGTTGTGGACGGCCTCCAAA	Cloning of $[SH2]_2$ Syk-PIP5K1a$_{core}$
rPLCg2 fw	TAATCTCGAGCTGACCACCATGGTC AACGTGGACACC	Cloning of rPLCγ2-PIP5K1a$_{core}$
PLCg2_PIP5K1a_fw	GAAGAGAGTGAGTAACAGCAGGTTC TACTCCGGTGGCGATCCCGCGGTC CCTTCC	Cloning of rPLCγ2-PIP5K1a$_{core}$
PLCg2_PIP5K1a_re	GGAAGGGACCGCGGGATCGCCACC GGAGTAGAACCTGCTGTTACTCACT CTCTTC	Cloning of rPLCγ2-PIP5K1a$_{core}$
PIP5K1a_core_re2	TAATGGATCCTTAGGGAATCTTCTTA AATACTGTGTTGCAC	Cloning of PIP5K1a$_{core}$ variants
PIP5K1a_core_re3	TAATCTCGAGTTAGGGAATCTTCTTA AATACTGTGTTGCAC	Cloning of PIP5K1a$_{core}$ variants
PIP5K1a_core_re4	TAATACCGGTTTAGGGAATCTTCTTA AATACTGTGTTGCAC	Cloning of PIP5K1a$_{core}$ variants
PLCg2_intern_fw	ACATGTTCAGTGACCCCAACTTCC	Sequencing

Standard primer used for sequencing in this project.

Name	Sequence 5'-> 3'
EGFPC1 fw	GTCCTGCTGGAGTTCGTG
GEXfw	GGGCTGGCAAGCCACGTTTGGTG
M13fw	TGTAAAACGACGGCCAGT
M13re	CAGGAAACAGCTATGACC
MSCVfw	CCCTTGAACCTCCTCGTTCGACC
MSCVre	CAGACGTGCTACTTCCATTTGTC

Primer used for TALEN in this study.

Name	Sequence 5'-> 3'	Application
pCR8_F1	TTGATGCCTGGCAGTTCCCT	Sequencing
pCR8_R1	CGAACCGAACAGGCTTATGT	Sequencing
TAL_F1	TTGGCGTCGGCAAACAGTGG	Sequencing
TAL_R2	GGCGACGAGGTGGTCGTTGG	Sequencing
SeqTALEN_5-1	CATCGCGCAATGCACTGAC	Sequencing
TALseq3_re	GGGCACCCGTCAGTGCAT	Sequencing
TALseq4_re	TTCAGATTTCTTCTCTTCCAATTCAGA	Sequencing
TALseq5_fw	CGGATCAGGCGTCTTTGCAT	Sequencing
TAL_Seq6_fw	ATACGAGCCGGAAGCATAAAGTGT	Sequencing
TAL_Seq7_re	ACATGCTTAACGTAATTCAACAGAAA	Sequencing
Vav1Ex3Seq_fw	GGCTCATTTGAGAGAACGATGGTAT	Sequencing/activity test
Vav1Ex3Seq_re	CTCAGGCAAGGTTGTGTGCC	Sequencing/activity test
SLP65_Ex5_fw2	TTGAAGTCAACCTCTCCAAGCCTTGT	Sequencing/activity test
SLP65_Ex5_re2	CTGCTTGGAGGTGGCGGGAG	Sequencing/activity test
SLP65_Ex6_fw2	GTCAATAAGCAGTTGAAATTTTGGGCCT	Sequencing/activity test
SLP65_Ex6_re2	GGAGGGGATAATATGAGGGGCACA	Sequencing/activity test
Rac2_Ex3_fw	GCGACAGAGCGTGATTCCATTTCAA	Sequencing/activity test

Rac2_Ex3_re	ACTATCCACCATCTGATTACCGGCC	Sequencing/activity test
CC2_Rac2_Ex3_1	CACCGAGGAGGACTACGACCGTCTC	CC2 construct
CC2_Rac2_Ex3_2	AAACGAGACGGTCGTAGTCCTCCTC	CC2 construct
U6 fwd	GAGGGCCTATTTCCCATGATTCC	Sequencing
pFUS_A5A/B_fw	CGGTGGTCTCGTGCAGCGGCTGTTGCC	Modification
pFUS_A5A/B_re	AGTGAGCGCAACGCAATTAATG	Modification
pFUS_A5A/B_re2	GAGCGCAACGCAATTAATGTGAG	Modification
pFUS_A5A/B_re3	CGGTGGAAAGCGGGCAGT	Modification
pFUSB1-10_fw	TAATCTTAAGCGTCTCAGGACCATGGCCTGACCCCGGAC	Modification
pFUSB1-10_re	TAATGGTACCCAATTCGCCCTATAGTGAGTCGTATTACG	Modification
pFUSB5_fw	TAATGGTACCGGGCCCCCCCTCGAGGTC	Modification
pFUSB5_re	TAATTCTAGAGTCCTGGCACAGCACCGGC	Modification
pFUSB5_re2	TAATTCTAGACGTCTCGGTCCTGGCACAGCACCGGC	Modification
pTAL3+63_fw	TCCCAGCTAGTGAAATCTGAATTGGAAG	Modification
pTAL3+63_re	GGCAACGCGATGGGACG	Modification
+63_mut_fw	ATCGCGTTGCCTCCCAGCTAGTGAAA	Modification
+63_mut_re	TTTCACTAGCTGGGAGGCAACGCGAT	Modification
TAL3 delta152_fw	GTGGATCTACGCACGCTCGG	Modification
TAL3 delta152_re	ATTCTAGACCAACCACTTGCGTCC	Modification
delta152_mu_fw2	GTTGGTCTAGAGTGGATCTACGCAC	Modification
delta152_mu_re2	GTGCGTAGATCCACTCTAGACCAAC	Modification
HA_TAL3_fw	ATGTACCCATACGACGTCCCAGACTACGCTCTGGCTTCCTCCCCTCCAAAGAAA	Modification
HA_TAL3_re	TGTTGAACCTCCTATTGTTACGATATATACAAT	Modification
TAL_HA_Mu_fw	AGGAGGTTCAACAATGTACCCATACG	Modification
TAL_HA_Mu_re	CGTATGGGTACATTGTTGAACCTCCT	Modification
TAL_Kozak_fw	ACAATAGGAGGTCCACCATGGGATACCCATACGACG	Modification

TAL_Kozak_re	CGTCGTATGGGTATCCCATGGTGGACCT CCTATTGT	Modification
Tal4_S418P_fw	AATCGCAAGAAATCCAACTCAGGATAGA ATC	Modification
Tal4_S418P_re	GATTCTATCCTGAGTTGGATTTCTTGCG ATT	Modification
Tal4_K441E_fw	GTTATCGTGGTGAACATTTGGGTGGAT	Modification
Tal4_K441E_re	ATCCACCCAAATGTTCACCACGATAAC	Modification

Primer used for mutagenesis in this study.

Name	**Sequence 5'-> 3'**
Vav1_W10A_fw	TAATCTCGAGATGGAGCTGTGGCGCCAATGCACCCACGCGCT CATCCAGTGCCGGGTGCT
Vav1_D39A_fw	CTGGCCCAGGCCCTCCGGGCTGGTGTCCTTCTGTGTCAGCTG CT
Vav1_D39A_re	AGCAGCTGACACAGAAGGACACCAGCCCGGAGGGCCTGGGC CAG
Vav1_D98A_fw	AGCGAGCTCTTCGAAGCCTTTGCCCTCTTCGATGTGCAGGATT TTG
Vav1_D98A_re	CAAAATCCTGCACATCGAAGAGGGCAAAGGCTTCGAAGAGCT CGCT
L158Q_Vav1_fw2 (L213Q)	GTACACTGACACGCAGGGCTCCATCCAG
L158Q_Vav1_re2 (L213Q)	CTGGATGGAGCCCTGCGTGTCAGTGTAC
Vav1_DH_LK/AAfw (LK334/335AA)	GCTGATGGTGCCTATGCAGCGAGTTGCCGCATATCACCTCCTT CTCCAGGAGCTGG
Vav1_DH_LK/Aare (LK334/335AA)	CCAGCTCCTGGAGAAGGAGGTGATATGCGGCAACTCGCTGCA TAGGCACCATCAGC
Vav1_Q542A_fw	TAATGGTACCTTCTATGCGGGCTACCGCTGCCATCGGTGC
Vav1_Y544A_fw	TAATGGTACCTTCTATCAGGGCGCCCGCTGCCATCGGTGCCG GG
Vav1_R641A_fw (R696A)	CTTGGTGGCGCAGAGGG

Vav1_R641A_re (R696A)	CCCTCTGCGCCACCAAG
hSLP65_Y72F_fw	CTTTGACAGCGACTTTGAAAATCCAGATGA
hSLP65_Y72F_re	TCATCTGGATTTTCAAAGTCGCTGTCAAAG
hSLP65_Y84F_fw	GACTCAGAGATGTTCGTGATGCCCGCCGAG
hSLP65_Y84F_re	CTCGGCGGGCATCACGAACATCTCTGAGTC
hSLP65_Y119F_fw	CGCCAGAGGCGAGTTTATAGACAATCGATCAAGCC
hSLP65_Y119F_re	GGCTTGATCGATTGTCTATAAACTCGCCTCTGGCG
SLP65_R372L_fw	GATGGATCATTTCTTATTCTGAAAAGCTCTGGCCATGATTC
SLP65_R372L_re	GAATCATGGCCAGAGCTTTTCAGAATAAGAAATGATCCATC
pBSKSII_AflII_1	AATTCGATATCTTAAGCTTATCGATACCGTCGACC
pmaxKS_AflII_rev	GGTCGACGGTATCGATAAGCTTAAGATATCGAATT

3.1.6 Vectors and Plasmids

Table 3.5: Plasmids used for cloning and expression in this study.

Vectors for cloning and cDNA sources. cDNA of DG75 cells for the amplification of IQGAP and β-Spectrin CH-domains was kindly provided by Kanika Vanshylla.

Name	**Source**
pBlueScript SK+	Stratagen
pCitrine	M. Engelke
pCR2.1	Invitrogen
pGEX-4T1	GE Healthcare
pmaxKS	N. Engels
pmaxKS IRES-EGFP	N. Engels
pmaxKS IRES-tagRFP	This work
pMiRFP	Lars König
pMSCVpuro	Clontech
pMSCVblast	M. Engelke
pEX-A-5'-CHVav1	Eurofins Genomics
pCR2.1 Btk	N. Engels
pCR2.1 Itk	N. Engels
pOTB7 Vav1	GE Dharmacon
pCR4-TOPO Vav2	GE Dharmacon
pCR-XL-TOPO Vav3	GE Dharmacon
pBluescript mVav1	provided by Klaus-Dieter Fischer

pYX-Asc mVav2	provided by Klaus-Dieter Fischer
pYX-Asc mVav3	provided by Klaus-Dieter Fischer
pCMV-SPORT6 Rac1	GE Dharmacon
pOTB7 PIP5K1a	GE Dharmacon
pMSCVpuro EGFP-rPLCγ2	N. Engels

Retroviral expression vectors.

Name	Insert	Source
pMSCVpuro	EGFP	M. Engelke
pMSCVpuro	Vav1 Cit	This work
pMSCVpuro	Vav2 Cit	This work
pMSCVpuro	Vav3 Cit	This work
pMSCVpuro	mVav1 Cit	This work
pMSCVpuro	mVav2 Cit	This work
pMSCVpuro	mVav3 Cit	This work
pMSCVpuro	Vav1 W10A Cit	This work
pMSCVpuro	Vav1 D39A Cit	This work
pMSCVpuro	Vav1 D98A Cit	This work
pMSCVpuro	Vav1 L213Q Cit	This work
pMSCVpuro	Vav1 LK334/335AA Cit	This work
pMSCVpuro	Vav1 Q542A Cit	This work
pMSCVpuro	Vav1 Y544A Cit	This work
pMSCVpuro	ΔCH Vav1 Cit	This work
pMSCVpuro	Vav1 CH_{CT} Cit	This work
pMSCVpuro	CH IQGAP-Vav1 Cit	This work
pMSCVpuro	[CH]2 β-Spectrin-Vav1 Cit	This work
pMSCVpuro	Lyn_{myr}-ΔCH Vav1 Cit	This work
pMSCVpuro	ΔCH Vav1-Syk $[SH2]_2$ Cit	This work
pMSCVpuro	ΔAR Vav1 Cit	This work
pMSCVpuro	Vav1-Btk SH2 Cit	This work
pMSCVpuro	Vav1-Itk SH2 Cit	This work
pMSCVpuro	Vav1-SLP-65 SH2 Cit	This work
pMSCVpuro	Vav1-SLP-65 SH2 R372L Cit	This work
pMSCVpuro	Vav1-Syk $[SH2]_2$ Cit	This work
pMSCVpuro	Cit Vav1-Rac1	This work

pMSCVpuro	Cit Vav1 L213Q-Rac1	This work
pMSCVpuro	Vav1 L213Q-Syk $[SH2]_2$ Cit	This work
pMSCVpuro	PIP5K1a Cit	This work
pMSCVpuro	Cit $[SH2]_2$ Syk-PIP5K1a$_{core}$	This work
pMSCVpuro	EGFP-rPLCγ2-PIP5K1a$_{core}$	This work
pMSCVpuro	hSLP-65	M. Engelke
pMSCVpuro	hSLP-65 Y72F	This work
pMSCVpuro	hSLP-65 Y84F	This work
pMSCVpuro	hSLP-65 Y119F	This work
pMSCVpuro	hSLP-65 Y72/84F	This work
pMSCVpuro	hSLP-65 Y72/119F	This work
pMSCVblast	Ecotropic Receptor	L. König
pMSCVbleo	CD8/Igα	M. Engelke
pMSCVbleo	CD8/Igα Y204F	M. Engelke

Expression of GST-fusion proteins.

Name	Insert	Source
pGEX-4T1	Vav1 SH2	This work
pGEX-4T1	Vav1 SH2 R696A	This work
pGEX-4T1	Syk $[SH2]_2$	M. Engelke
pGEX-4T1	C2 Vav1	This work
pGEX-4T1	C2 Vav1 R696A	This work
pGEX-4T1	C2 Vav1-SLP-65 SH2	This work
pGEX-4T1	C2 Vav1-Syk $[SH2]_2$	This work
pGEX-4T1	C2 Vav1-Btk SH2	This work
pGEX-4T1	C2 Vav1-Itk SH2	This work

TALEN and CRISPR/Cas cloning vectors.

Name	Source
Golden Gate TALEN and TAL Effector Kit	Addgene
pTal4Titanium	This work
pFusA5A	This work
pFusA5B	This work
pFusA5C	This work

pFusB1B	This work
pFusB2B	This work
pFusB3B	This work
pFusB4B	This work
pSpCas9(BB)-2A-GFP	Addgene

Transient expression of gene targeting constructs.

Name	Insert	Source
pmaxKS IRES EGFP	22	This work
pmaxKS IRES tagRFP	40	This work
pmaxKS IRES EGFP	39	This work
pmaxKS IRES tagRFP	55	This work
pSpCas9(BB)-2A-GFP	CC2	This work

3.1.7 Antibodies

Table 3.6: Antibodies used in this study.

Primary antibodies. Antibodies were mixed in TBS-T with 1 % BSA and 0.01 % NaN_3 and used according to the manufacturer's instructions.

Primary antibody	Isotype	Company
α-Akt	rabbit	CST
α-pAkt (Ser473) (D9E)	rabbit	CST
α-Actin	rabbit	CST
α-pBLNK (pTyr96)	rabbit	CST
α-BLNK	mouse IgG_{2a}	BD
α-CD79a (EP3618)	rabbit	Abcam
α-CD79a (EPR6861)	rabbit	Abcam
α-Erk (16)	mouse IgG_{2a}	BD
α-pErk1/2 (E10)	mouse IgG_1	CST
α-GST	rabbit	Molecular Probes
α-Lyn (44)	rabbit	Santa Cruz
α-PLCγ2 (Q20)	rabbit	Santa Cruz
α-Rac2 (C11)	rabbit	Santa Cruz
α-Syk (4D10)	mouse IgG_{2a}	Santa Cruz
α-pTyr (4G10)	mouse IgG_{2b}	Upstate

α-Vav1 (D45G3)	rabbit	CST
α-Vav2	rabbit	Epitomics
α-Vav3	rabbit	Millipore

Secondary antibodies. Antibodies were mixed in TBS-T 1:10000.

Secondary antibody	Isotype	Company
α-mouse IgG_1-HRPO	goat	Southern Biotech
α-mouse IgG_{2a}-HRPO	goat	Southern Biotech
α-mouse IgG_{2b}-HRPO	goat	Southern Biotech
α-mouse IgG-HRPO	goat	Southern Biotech
α-rabbit IgG-HRPO	goat	Southern Biotech

Antibodies for FACS.

Antibody	Isotype	Company
α-human CD8-FITC (Mem-31)	mouse IgG_{2a}	Immunotools
α-human CD19-PE	mouse IgG_1	MACS Milteny Biotec
α-human IgM-APC	mouse IgG_1	Southern Biotech

Antibodies for stimulation.

Antibody	Type/Isotype	Company
α-human CD8 (Mem-31)	mouse IgG_{2a}	Provided by Vaclav Horejsi
goat-α-human-IgM (Fc5μ fragment specific)	$F(ab')_2$	Jackson ImmunoResearch

3.1.8 Synthetic peptides

The biotinylated peptides of Igα used in this study were purchased from Eurogentec.

Table 3.7: Synthetic peptides used in this study.

Antibody	Type/Isotype	Company
α-peptide I	ENLYEGLNLDDCSMYEDISR	Eurogentec
p-α-peptide I	ENLpYEGLNLDDCSMpYEDISR	Eurogentec
α-peptide II	YEDISRGLQGTYQDVGN	Eurogentec
p-α-peptide II	YEDISRGLQGTpYQDVGN	Eurogentec

3.1.9 Instruments

Table 3.8: Instruments used in this study.

Instruments	Company
Analytical balance MC1	Sartorius
Bacteria incubator Heraeus Kelvitron®t	Heraeus
Bio Photometer	Eppendorf
Cell culture incubator HeraCell 150	Heraeus
Cell culture safety cabinet Herasafe	Heraeus
Centrifuge 5415D	Eppendorf
Centrifuge Multifuge 3 S-R	Heraeus
Centrifuge RC 3B Plus	Sorvall
Centrifuge 5417R	Eppendorf
Chemi Lux Imager	Intas
Confocal Laser scanning microscope TCS SP2	Leica
Cytometer LSRII	BD
Electrophoresis Power Supply	Amersham Biosciences
FACS Calibur	BD
Freezer HERAfreeze	Heraeus
Freezer Platilab 340	Angelantoni
Galaxy Mini centrifuge	VWR
Gel Electrophoresis system	Peqlab
Gel Imager	Intas
Ice machine	Ziegra Eismaschinen
Inverted microscope Axiovert 35	Zeiss
Magnetic stirrer M21/1	Framo®-Gerätetechnik
Mastercycler epgradient	Eppendorf
Mini-PROTEAN Tetra Electrophoresis System	Bio-Rad
MiniRocker MR-1	Peqlab
NanoDrop 2000 Spectrophotometer	Thermo Scientific
Nucleofector®II	Amaxa Biosystems
pH meter	InoLab
Platform shaker Duomax 1040	Heidolph
Platform shaker 3005	GFL

Rotator SB3	Stuart
SE 600 Ruby standard dual cooled vertical unit	Amersham Biosciences
Shaking Incubator Infors	Unitron
TE77 semidry western blot transfer unit	GE Healthcare
Thermomixer comfort	Eppendorf
Ultra-low Temperature Freezer (-150 °C)	Panasonic
Ultrasonic device Sonoplus	Bandelin
UV illuminator	Intas
Vortex-Genie 2	Scientific Industries
Water bath	GFL
Water purification system arium® G11	Sartorius

3.1.10 Software

Table 3.9: Software used in this study.

Software	**Company**
BD FACSDiva Software v 5.0.3.	Flow cytometry data recording
Citatvi 5	Bibliography editing
Core DRAW X7	Graphic editing
Intas Chemostar	Immunoblot imaging
FinchTV	Sequencing viewer
FlowJo (TriStar)	Flow cytometry data analysis
Gel documentation software GDS	Gel imaging
ImageJ	Image editing
Leica Confocal Software	Imaging
MS Office	Text and image editing
pDRAW 32	DNA sequence analysis

3.1.11 Data base

Table 3.10: Data base used in this study.

Program	**Application**
http://crispr.mit.edu/	CRISPR/Cas design
http://elm.eu.org (eukaryotic linear motif resource)	Motif investigations

http://frodo.wi.mit.edu/	Primer3
https://tale-nt.cac.cornell.edu/node/add/talen	TALEN design
http://www.ebi.ac.uk/Tools/msa/	Multiple alignment (clustalw2)
http://www.ensembl.org	Genomic blasts
http://www.ncbi.nlm.nih.gov	Genomic blasts

3.2 Methods

3.2.1 Molecular biology

3.2.1.1 Bacteria strains

Three different *Escherichia coli* (*E. coli*) strains were used during the PhD project. The bacteria strain *E. coli* Top10F' (Invitrogen) was used in standard cloning experiments. For maintenance of basic TALEN plasmids (pHD1-10, pNG1-10, pNI1-10, pNN1-10), the bacteria strain *E. coli* GeneHog (Invitrogen) was used. In the case of protein expression experiments, I used the bacteria strain *E. coli* BL21.

Table 3.11: *Escherichia coli* strains used in this study.

***Escherichia coli* strains**	**Genotyp**
Top10F'	F´[laclq, Tn10(TetR)]mcrAΔ(mrrhsdRMS-mcrBC) Φ80lacZΔM15 ΔlacX74 recA1 araD139 Δ(araleu) 7697 galUgalKrpsL (StrR) endA1 nupG
GeneHog	F- mcrA ∆(mrr-hsdRMS-mcrBC) φ80lacZ∆M15 ∆lacX74 recA1 araD139 ∆(ara-leu)7697 galU galK rpsL (StrR) endA1 nupG fhuA: IS2 (confers phage T1 resistance)
BL21	fhuA2 [lon] ompT gal (λ DE3) [dcm] ∆hsdS λ DE3 = λ sBamHIo ∆EcoRI-B int::(lacI::PlacUV5::T7 gene1) i21 ∆nin5

3.2.1.2 Media for bacteria

LB-medium was used as growing medium for the *E. coli* strains Top10F' and Gene Hog, whereas YT-medium was used for the *E. coli* strain BL21.

LB-medium:	10 g/L tryptone	YT-Medium:	16 g/L tryptone
	5 g/L yeast extract		15 g/L yeast extract
	5 g/L NaCl		5 g/L NaCl
	pH 7.0		pH 7.0

→autoclaved (121 °C, 1.25 bar, 30 min)

Selection was performed using LB-medium or YT-medium with the following antibiotic end concentrations:

Ampicillin	100 µg/ml
Kanamycin	50 µg/ml
Spectinomycin	50 µg/ml
Tetracyclin	10 µg/ml

3.2.1.3 Agar plates

Agar plates were cast with LB-medium containing 2 % (w/v) agar-agar, which was added before autoclaving (121 °C, 1.25 bar, 30 min). After cooling down to 60 °C, the required antibiotic was added and the LB-agar was poured in petri dishes. Agar plates were stored at 4 °C.

3.2.1.4 Sterilisation procedure

Solutions, culture media for bacteria and none-sterile consumables were autoclaved at 121 °C and 1.25 bar for 30 min.

3.2.1.5 Isolation and purification of nucleic acids

3.2.1.5.1 Isolation of genomic DNA

For the isolation of genomic DNA, $1x10^6$ DG75 cells were lysed in 200 µl Tag-lysis buffer containing 1 µl proteinase K (20 mg/ml, Promega) for 2-3 h at 56 °C. Afterwards, the proteinase K was heat-deactivated at 95 °C for 15 min. Storage of genomic DNA was done at -20 °C.

Tag-lysis buffer: 10 mM Tris/HCl pH 8
50 mM KCl
0.45 % NP40
0.45 % Tween20
in $_{dd}H_2O$

3.2.1.5.2 Isolation of plasmid DNA (Mini-preparation)

For the extraction of bacterial plasmid DNA, 4 ml LB-medium containing the required antibiotic were inoculated with one *E. coli* colony. After overnight incubation at 37 °C on a shaker, bacterial plasmid DNA was isolated using the Wizard® Plus SV Miniprep DNA Purification System (Promega) or the QIAprep® Spin Miniprep kit (Qiagen) according to the manufacturer's instructions.

3.2.1.5.3 Isolation of plasmid DNA (Midi-preparation)

To gain higher amounts of bacterial plasmid DNA, 4 ml LB-medium containing the required antibiotic were inoculated with one *E. coli* colony. After 8 h incubation at 37 °C on a shaker, bacteria were used for a second inoculation of 250 ml LB-medium containing again the required antibiotic, followed by an incubation period at 37°C shaking overnight. Finally, isolation of bacterial plasmid DNA was performed with the Promega Pure Yield™ Plasmid Midiprep System kit according to the manufacturer's instruction.

3.2.1.5.4 Measurement of nucleic acid concentration

Measurement of nucleic acid concentration was performed using a NanoDrop2000 according to the manufacturer's instructions.

3.2.1.6 Cloning techniques

3.2.1.6.1 Restriction of DNA using endonucleases

Specific endonucleases (NEB) were used to cleave plasmids, vectors and PCR products to produce compatible sticky or blunt ends. Cleaved DNA fragments were used in ligation and transformation experiments. All enzymes in this study were used according to the manufacturer's instructions.

3.2.1.6.2 DNA gel extraction

The extraction of DNA fragments out of agarose gels was performed using the Promega Wizard® SV Gel and PCR Clean-Up System kit according to the manufacturer's instructions.

3.2.1.6.3 Sub-cloning of PCR products

For sub-cloning of PCR products, *Taq*-polymerase was used to amplify the desired DNA regions. The polymerase contains a transferase activity and thus adds further A-nucleotides at the 3'-end of PCR products, called 'A-tail'. After gel extraction, the PCR products can be directly used in ligation reactions with the pCR2.1 vector, which contains 5'-T-overhangs.

3.2.1.6.4 Ligation of DNA fragments

Ligation reactions were performed with the T4 DNA ligase according to the manufacturer's protocol. In the case of a preceded single endonuclease restriction reaction, the vector was treated with calf intestine phosphatase for 1 h at 37 °C. This removes phosphates from the 5'- and 3'-ends of linearized vectors and thus prevents vector religation. When two or more endonucleases were used for vector linearization, no calf intestine phosphatase treatment was performed. All endonuclease and phosphatase treated vectors were purified via agarose gel extraction using the Promega Wizard® SV Gel and PCR Clean-Up System kit.

3.2.1.6.5 Transformation of competent bacteria

Transformation of *E.coli* Top10F' and GeneHog (50 µl) was done using 5-10 µl of the ligation reaction. After a 30 min incubation on ice, a heat shock was performed for 45 s at 42 °C, followed by a 2 min incubation on ice. Subsequently, the transformation mix was incubated with 500 µl LB-medium without antibiotics for 30 min shaking at 37 °C. In the end, the complete transformation mix was plated on LB-plates containing the required antibiotic. Transformations of *E.coli* Top10F' with the pCR2.1 and TALEN plasmid were performed with blue-white screening. Therefore, 50 µl X-gal (5-bromo-4-chloro-3-indolyl-beta-D-galacto-pyranoside) (50 mg/ml in DMF) and 50 µl IPTG (Isopropyl-β-D-thiogalacto-pyranoside) (0.1 M) had been distributed on agar plates before the transformation mix was added.

3.2.1.7 Gel electrophoresis

Gel electrophoresis was done using 1 % agarose gels containing 0.5 µg/ml ethidium bromide in TAE buffer. Before loading, samples were mixed with 6x DNA-loading buffer (NEB). DNA fragments were separated at 220 mA and 100 V for 30-50 min depending on the DNA fragment size. A 1 kb DNA-ladder (Fermentas) was used as scale to determine the size of DNA fragments.

TAE buffer:	40 mM	Tris/acetic acid pH 7.8
	10 mM	NaOAc
	1 mM	EDTA
		$_{dd}H_2O$
		pH 8

3.2.1.8 Polymerase chain reaction (PCR)

The PCR reaction is used to amplify specific DNA fragments *in-vitro* (Erlich et al., 1988). It can be divided into three steps. First, double stranded template DNA is denaturized to allow annealing of oligonucleotides (primers) within the second step. Third, elongation of annealed primers is started using optimal conditions for the specific polymerase according to the manufacturer's instructions. Repetition of the described three step process leads to vast amplification of DNA fragments.

3.2.1.8.1 Standard PCR

The standard PCR reaction was used to amplify specific DNA regions of genomic or plasmid DNA templates. In my PhD project, I exclusively used the phusion polymerase for DNA fragment amplification. The annealing temperature was chosen according to the primer3 software recommendation and elongation was performed following the manufacturer's instructions. The basic PCR cycle is described in table 3.11.

Table 3.12: Standard PCR cycle conditions. *with regard to the annealing temperature calculated with the primer3 software.

Step	Time	Cycles	Temperature
Initial denaturation	2 min	1	98 °C
Denaturation	20 s	⎫	98 °C
Annealing	20-40 s	⎬ 30	*
Elongation	0.5-4 min	⎭	72 °C
Final elongation	1-5 min	1	72 °C

3.2.1.8.2 Overlap PCR

The overlap PCR reaction was used to connect two different DNA fragments. To do that, phusion polymerase was used according to the PCR cycle program described in table 3.11. However, the first 10 PCR cycles were carried out without primer to increase the amount of desired template using the internal overlapping DNA regions of the two DNA fragments as elongation start points.

3.2.1.8.3 Sequencing PCR

Sequencing was carried out by the Seqlab company. Samples were prepared according to the company guidelines. In brief, 1.2 µg DNA and 3 µl of primer (10 pmol/µl) were mixed with $_{dd}H_2O$ in a total volume of 15 µl.

3.2.2 Biochemistry

3.2.2.1 Preparation of cleared cellular lysate

Cleared cellular lysates (CCL) were prepared from resting or stimulated human cell lines or primary B cells to analyse proteins by western blotting. Therefore, $1x10^6$ cells per 20 µl NP40-lysis buffer were lysed in 1.5 microcentrifuge tube for 30 min on ice. Afterwards, the cell lysates were centrifuged for 10 min, at 4 °C and 16000 x g. The resulting CCL was transferred into a new 1.5 microcentrifuge tube and the cell debris was discarded. In the end, the CCL was mixed with 3x Laemmli buffer, heated for 5 min at 95 °C and stored at -20 °C.

NP40-lysis buffer:	0.1375 M	NaCl
	0.05 M	Tris/HCl (pH 7.8)
	1 mM	sodium-ortho-vanadate
	0.5 mM	EDTA
	10 %	Glycerol
	1 %	NP40
		+ Protease inhibitor (Sigma P2714)
		in $_{dd}H_2O$

3x Laemmli buffer:	62.5 mM	Tris/HCl pH 6.8
	2 % (w/v)	SDS
	0.025 % (w/v)	Bromphenol blue
	20 % (v/v)	Glycerol
	5 %	β-mercaptoethanol
		in $_{dd}H_2O$

3.2.2.2 Stimulation of B cells

DG75 cells were harvested and washed once with 1x PBS (300 g, 4 °C, 4 min). Cells were resuspended in 1 ml FCS-free RPMI 1640 medium (R0) with a final cell number of $3x10^7$ DG75 cells/ml. After the transfer of cells to 1.5 ml microcentrifuge tubes, they were incubated for 30 min at 30 °C to reduce pre-stimulatory effects of the FCS containing RPMI culture medium. Stimulation was done using 20 µg/ml anti-human IgM $F(ab')_2$ fragments or 10 µg/ml anti-human CD8 antibodies for desired time points. Subsequently, DG75 cells were spun down in a microcentrifuge, the medium was discarded and cells were lysed in 200 µl NP40-lysis buffer per $1x10^7$ DG75 cells on ice for 15-25 min. Then, cell debris was removed by centrifugation (16000 x g, 4 °C, 10 min) and the cleared cellular lysate (CCL) was transferred into a new 1.5 ml microcentrifuge tube. Afterwards, 30 µl of the CCL was mixed with 3x Leammli buffer and incubated for 5 min at 95 °C for denaturation of proteins. The remaining CCL was used for affinity purification experiments.

PBS:	137 mM	NaCl
	2.4 mM	KCl
	4.3 mM	Na_2HPO_4 x 12 HPO_4
	1.4 mM	KH_2PO_4
		$_{dd}$H2O
		pH 7.4

3.2.2.3 Expression of recombinant GST-fusion proteins

For the generation of GST-fusion proteins, the respective cDNA was cloned into the pGEX-4T1 vector (GE Healthcare). The resulting plasmid was transformed into the *E.coli* strain BL21 and plated on a LB-agar plate (37 °C, overnight). Next, an overnight culture was inoculated using one *E.coli* colony and 4 ml LB-medium containing ampicillin (37° C, shaking). The following day, the overnight culture was used to inoculate 200-300 ml YT-medium containing ampicillin (37 °C, shaking). The expression of the GST-fusion protein

was induced at OD 0.6 with 100 µM IPTG at 37 °C shaking for 4 h. In the case of low yield of GST-fusion protein, the temperature was reduced to 25 °C or 30 °C during protein expression. Afterwards, the bacteria were harvested in 50 ml tubes by centrifugation (3000 x g, 15 min, 4 °C) and the obtained bacteria pellet was stored at -80 °C.

3.2.2.4 Preparation of recombinant GST-fusion proteins

One bacteria pellet was resuspended in 20 ml cold 1x PBS and lysed by ultrasonification on ice (3x30 s, 1 cycle, 50 %). To support the lysis of bacteria, 200 µl 10 % Triton-X-100 were added, followed by an incubation for 10-15 min on ice. Next, the bacteria cell debris was removed by centrifugation (3000 x g, 20 min, 4 °C). The supernatant was used for GST-fusion protein purification. For that purpose, 200 µl of gluthatione-sepharose beads were added to the supernatant, followed by a 2-3 h incubation at 4 °C on a rotator. Afterwards, beads were pelleted by centrifugation (400 x g, 5 min, 4 °C), the supernatant discarded and the beads transferred into a 1.5 ml microcentrifuge tube, followed by three washing steps with 1 ml cold 1x PBS (300 x g, 3 min, 4 °C). In the end, the beads were resuspended in 250 µl cold 1x PBS and stored at 4 °C.

3.2.2.5 Elution of GST-fusion proteins

200 µl of sepharose beads binding the desired GST-fusion protein were mixed with 100 µl reduced L-Glutahione (10 mM in 1x PBS) in a 1.5 ml microcentrifuge tube. The mixture was incubated for 10 min on a rotator at RT followed by a centrifugation step (500 x g, 5 min, RT). The GST-fusion protein containing supernatant was transferred to a new 1.5 microcentrifuge tube and stored at 4 °C, whereas the sepharose beads were mixed again with 100 µl reduced L-Glutahtione. In total, three elution cycles were performed. The preparation (3.2.2.4) as well as the elution of GST-fusion proteins were controlled by SDS-PAGE followed by Coomassie staining. For Coomassie staining, SDS-gels were incubated for 15 min at RT on a shaker. Afterwards, the Coomassie solution was replaced with tap water to de-stain the SDS-gel overnight.

Coomassie staining solution: 0.1 % Coomassie Brilliant Blue R-250
40 % MeOH
10 % acetic acid

3.2.2.6 Affinity purification (AP)

Affinity purifications were perfomed in three different ways using either GST-fusion proteins, synthetic peptides or antibodies. For affinity purification with GST-fusion proteins, 15 µg of the desired GST-fusion protein was added to the CCL and incubated for 4 h rotating at 4 °C. In the case of synthetic peptides, 2 µM of biotinylated peptides were added and incubated for 1 h rotating at 4 °C. Afterwards, 25 µl Streptavidin-sepharose beads were added, followed by 1 h incubation at 4 °C on a rotator. For the affinity purification with antibodies, 2 µg/ml anti-PLCγ2 antibodies were added to the CCL and rotated for at least one hour at 4° C. Following, 25 µl protein A/G-agarose beads (Santa Cruz Biotechnology, 50 % slurry) were added and incubated for one hour at 4° C on a rotator. In the end, beads were washed three times (300 x g, 5 min, 4 °C) with NP40-lysis buffer, mixed with 40 µl 3x Laemmli buffer, incubated for 5 min at 95 °C and subjected to western blot analysis or stored at -20 °C.

3.2.2.7 SDS-Polyacrylamide Gel Electrophoresis (SDS-PAGE)

The separation of proteins from CCLs and affinity purification experiments was performed by SDS-PAGE. Therefore, proteins were denatured and reduced using Laemmli buffer (see chapter 3.2.2.1), so that the separation of proteins could be done according to their molecular weight (Weber and Osborn, 1969). Protein samples were concentrated in a 5 % SDS stacking gel (20 mA, 250 V per gel) and separated in a 10 % SDS resolving gel (20 mA, 300 V per gel). The determination of the protein size was done with the help of a prestained protein marker (broad range, 6.5-175 kDa, NEB).

Resolving gel:	8 ml	Lower buffer (1.5 M Tris/HCl pH 8.8, 14 mM SDS, in $_{dd}H_2O$)
	6 ml	30 % AA/BAA
	13.4 ml	$_{dd}H_2O$
	30 µl	TEMED
	200 µl	10 % APS

Stacking gel:	3.75 ml	Upper buffer (0.5 M Tris/HCl pH 6.8, 14 mM SDS, in $_{dd}H_2O$)
	2.4 ml	30 % AA/BAA
	8.9 ml	$_{dd}H_2O$
	15 µl	TEMED
	150 µl	10 % APS

SDS running buffer:	25 mM	Tris/HCl
	192 mM	Glycine
	0.1 % (w/v)	SDS
		in $_{dd}H_2O$

3.2.2.8 Western blot analysis

The detection of SDS-PAGE separated proteins was done by western blot analysis. Therefore, proteins were transferred onto a nitrocellulose membrane by semi-dry blotting (Towbin et al., 1979). To this end, two Whattman paper, a nitrocellulose membrane and the SDS-polyacrylamide gel were soaked in blotting buffer and stacked according to the following arrangement: Whattman paper, membrane, gel, Whattman paper. Importantly, air bubbles were removed by rolling with a glass pipette for efficient blotting. Blotting was performed at 1 mA/cm^2 for 60 min.

Blotting buffer:	48 mM	Tris/HCl
	39 mM	Glycine
	0.0375 % (v/v)	SDS
	20 %	MeOH
		in $_{dd}H_2O$

3.2.2.9 Immunostaining

Immunostaining was performed to visualize proteins that were previously transferred onto a nitrocellulose membrane. Here, specific antibodies (primary antibodies), which bind to the proteins of interest, and secondary HRPO-coupled antibodies, which recognize the Fc-region of primary antibodies, were used in combination with the ECL detection system for protein visualization. To do this, the membrane was blocked with 5 % BSA in TBS-T for 1 h at RT on a shaker, followed by two washing steps with TBS-T in excess for 5 min each. Incubation with the primary antibodies was done overnight shaking at 4 °C. Next

day, the membrane was washed three times with TBS-T in excess and incubated with secondary antibodies for 1 h at RT on a shaker. In the end, the membrane was washed again three times with TBS-T in excess and visualization of proteins was done using 4 ml ECL solution in combination with the Chemilux Camera System (Intas).

TBS-T:	25 mM	Tris/HCl pH 8.0
	125 mM	NaCl
	0.1 %	Tween20
		in $_{dd}H_2O$
		adjust to pH 7.4

ECL solution:	4 ml	Solution A:	250 mg/ml Luminol in 0.1 M Tris/HCl pH 8.6
	400 µl	Solution B:	1.1 g/L para-hydroxycoumaric acid in DMSO
	1.2 µl	30 % H_2O_2	

3.2.3 Cell biology

3.2.3.1 Media for cell culture

Media for cell culture were bought from the company Biochrom. For culturing of DG75, HEK 293 and Plat E cells further ingredients were added:

Medium for DG75, HEK 293 and Plat E cells (R10):	RPMI 1640 (+GlutaMax)
	10 % FCS
	1 % Penicillin/Streptomycin
	1 mM L-glutamine
	50 µM ß-mercaptoethanol

3.2.3.2 Cell lines

DG75 (DSMZ-No: ACC 83)

The DG75 cell line constitutes the human B cell model cell line in my PhD project. It was derived from a pleural diffusion of a 10-year-old boy with a burkitt lymphoma (refractory, terminal) in 1975. It is a male, diploid B cell line with the translocation: t(8;14)(q24;q32) (Ben-Bassat et al., 1977).

Table 3.13: DG75 characteristics. – indicates not detected, + indicates detected characteristics in immunology and viruses.

Topic	Characteristic
Immunology	CD3 -, CD10 +, CD13 -, CD19 +, CD34 -, CD37 +, CD38 +, CD80 +, CD138 -, HLA-DR +, cyIgG -, cyIgM +, cykappa +, cylambda -
Fingerprint	multiplex PCR of minisatellite markers revealed a unique DNA profile
Cytogenetic	human near diploid karyotype with 6% polyploidy - 46<2n>XY, t(8;14)(q24;q32)
Viruses	ELISA: reverse transcriptase negative; PCR: EBV -, HBV -, HCV -, HHV-8 -, HIV -, HTLV-I/II -, MLV -, SMRV -

In my PhD project, different DG75 sub-lines were used in genetic and biochemical approaches. To this end, DG75 cells were equipped with an ecotropic receptor (referred to as EB) to enable retroviral infection with Moloney Murine Leukemia Virus.

Table 3.14: DG75 knock out sub-lines.

DG75 genetic background	Reference
***RAC2*$^{-/-}$**	This work
***SLP-65*$^{-/-}$**	This work
***VAV1*$^{-/-}$**	This work

HEK 293

The HEK (human embryonic kidney) 293 cell line is an adherent cell line that is often used in cell biology due to its easy handling. In this project, HEK 293 cells were exclusively used as negative control for Vav1 expression.

Platinum E (Plat E)

The Plat E cell line (platinum retroviral packaging cell line) originates from HEK 293 cells. It contains Moloney Murine Leukemia Virus (MMLV) genes, which are stably integrated into the genome, coding for gag, pol and env proteins. For the generation of a virus that

can infect non-murine cells, Plat E cells are transiently transfected with a plasmid encoding for the glycoprotein of the vesicular stromatitis virus (VSV-G) enabling efficient infection (Morita et al., 2000). In the case of DG75 EB cells, additional transient transfection of Plat E cells with VSV-G constructs is not necessary any more due to the ecotropic expressed receptor.

3.2.3.3 Cell culture of none-adherent cells

The none-adherent human DG75 cell line (3.2.3.2) was used as model system in my PhD project. Cells were grown in culture dishes using R10 an incubated in a HeraCell 150 incubator with 5 % CO_2 at 37 °C. Every second day, cells were passed 1:10.

3.2.3.4 Cell culture of adherent cells

The adherent Plat E and HEK 293 cell lines were cultured under the same conditions as DG75 cells. For passaging, medium was removed, cells were washed once with 1x PBS and treated with 0.05 % trypsin-EDTA (Invitrogen) to detach them from the bottom of the culture dish. Subsequently, fresh R10 medium was added to dilute the trypsin-EDTA, which stops the detachment process. Every second day, cells were passed 1:10.

3.2.3.5 Long-term storage of cells

Cells were harvested (300 x g, 5 min, RT) and resuspended in freezing medium (10 % DMSO in FCS) with a cell number of $1x10^7$ cells/ml. After the transfer into a cryo-tube, cells were stored subsequently at -80 °C in a polystyrene box. The next day, the cryo-tubes were placed at -150 °C for long-term storage.

3.2.3.6 Revitalization of cells

Cells stored at -150 °C were thawed in a water bath (37 °C). Subsequently after thawing, cells were transferred into 9 ml fresh medium (RT). Cells were centrifuged (300 x g, 4 °C, 5 min), the supernatant was discarded and cells were taken up in 10 ml fresh medium (RT).

3.2.3.7 Isolation of primary human B cells

Blood samples were taken from volunteers using syringes coated with heparin to prevent clotting of blood. Blood was transferred into 50 ml tubes and mixed 1:1 with 1x PBS

containing 1 mM EDTA. The equal amount of Ficoll (Amersham Bioscience) was provided in a fresh 50 ml tube and the blood-PBS mix was transferred by very gently pipetting. Centrifugation of the Ficoll gradient was done using 800 x g, 20 min and RT (lowest setting for break). Afterwards, the PBMC ring (interface) was carefully transferred into a new 50 ml tube. Washing of PBMCs was done with 30 ml 1x PBS containing 1 mM EDTA and 0.5 % BSA (300 x g, 15 min, RT). The PBMC pellet was resuspended in 20 ml of the previous buffer and cells were counted. Two 100 µl aliquots were taken and kept on ice for later FACS analysis.

B cell purification was performed using the B cell purification kit II (MACS Milteny). PBMCs were centrifuged (300 x g, 10 min, RT), the supernatant completely aspirated and the cell pellet resuspended in 40 µl MACS buffer per $10x10^6$ cells. Afterwards, 10 µl Biotin-antibody-cocktail per $10x10^6$ cells were added, mixed and incubated for 5 min at 4° C. Subsequently, 20 µl Biotin-antibody-cocktail per $10x10^6$ cells were added, mixed and incubated for 10 min at 4 °C. The minimal volume for magnetic separation is 500 µl, so that the volume was adjusted with MACS buffer. LS-column was placed to the separator and rinsed with 3 ml MACS buffer. The cell suspension was added and the flow through was collected in a 15 ml tube. In addition, 3 ml MACS buffer were added to the column and collected. Eluted B cells were counted and aliquots were taken for purity control using FACS analysis with anti-human CD19-Pe and anti-human IgM-APC antibodies.

MACS buffer: 1x PBS
0.5 % BSA
2 mM EDTA
pH 7.2

3.2.3.8 Transfection methods

3.2.3.8.1 Transfection via nucleofection

Nucleofection of DG75 cells was done using the Lonza Human B cell Nucleofector® Kit according to the manufacturer's instructions. In brief, $2x10^6$ cells were harvested (90 g, 10 min, RT), the supernatant was completely removed and cells were resuspended in the nucleofection mix containing 82 µl human B cell Nucleofector® solution and 18 µl supplement 1. After addition of 2 µg plasmid DNA, the cell suspension mix was transferred into a nucleofection cuvette and nucleofection was done using the Amaxa Nucleofector™ II (program T-015). In the case of a nucleofection with two plasmids, 2 µg of plasmid DNA were used of each plasmid. Finally, cells were cultured on a 6 well plate containing 2 ml pre-warmed R10 medium per well.

3.2.3.8.2 Retroviral transfection/infection

For retroviral transfection, the packaging cell line Plat E was used, which expresses gag/pol and env genes derived from the Moloney Murine Leukemia Virus (MMLV). 24 h before retroviral transfection, roughly 1.5x10^6 cells were seeded on a 6 cm dish to reach 60-70 % confluence the next day. For transfection, 250 µl R0 medium were mixed with 8 µl Trans-IT solution (Mirus) and 3-4 µg plasmid DNA, followed by 30 min incubation at RT. In the meanwhile, the old R10 medium from Plat E cells was replaced with 2 ml fresh, pre-warmed R10 medium. The transfection mix was carefully distributed over the Plat E cells. After 24 h, further 3 ml R10 medium were added carefully on the 6 cm dish, so that Plat E cells were not detached from the plate bottom. Further 24 h later, the virus containing Plat E supernatant was taken and centrifuged for 5 min at 300 x g and RT to remove detached Plat E cells from the virus supernatant. Simultaneously, 1-2x10^6 DG75 cells were centrifuged using the same conditions. After removing the supernatant from DG75 cells, 4 ml virus supernatant was used to resuspend the DG75 cells and to plate them on a 6 cm culture dish. In addition, 1 ml R10 medium supplemented with the cationic polymer polybrene (Sigma) with a final concentration of 3-4 µg/ml was added to the cells. After 48 h, infection was stopped by replacement of the virus containing medium with 5 ml R10 medium (300 x g, 5 min, RT). The next day, cells were selected by the addition of the required antibiotic.

Antibiotic	**Concentration**
Puromycin	1 µg/ml
Blasticidin	10 µg/ml
Bleomycin	50 µg/ml

3.2.3.9 Flow cytometry

3.2.3.9.1 Expression analysis of surface receptors

To measure the amount of cell surface receptors, 0.5-1.0x10^6 DG75 cells were harvested and washed once with 4 ml 1x PBS (300 x g, 5 min, RT). The supernatant was discarded and the remaining cell pellet resupended in 100 µl 1x PBS containing 1 µl of anti-human IgM-APC (0.1 mg/ml), anti-human CD19-PE or anti-human CD8-FITC. After a 20 min incubation on ice in the dark, cells were washed once with 1x PBS (300 x g, 5 min, RT) and subjected to flow cytometry.

3.2.3.9.2 Expression analysis of ectopic expressed fluorophore-tagged proteins

For expression analysis of fluorophore-tagged proteins, approximately $0.5x10^6$ cells were washed once with 3-4 ml 1x PBS (300 x g, 5 min, RT), resuspended in 400 µl 1x PBS and subjected to flow cytometry.

3.2.3.9.3 Cell sorting

Cell sorting was done in cooperation with the cell sorting facility of the university medical center. In brief, $1\text{-}5x10^6$ cells were washed once with 10 ml 1x PBS (300 x g, 5 min, RT) and resuspended in 500 µl 1x PBS for cell sorting. Cells were stored on ice until the beginning of cell sorting. Afterwards, cells were washed and resuspended in R10 medium (300 x g, 5 min, RT).

3.2.3.9.4 Analysis of Ca^{2+}-mobilization

Ca^{2+}-mobilization measurements were done to investigate Ca^{2+} changes within the cytoplasm of DG75 cells after BCR stimulation. The measurement is based on a Ca^{2+} sensitive dye, named Indo-1 AM, which changes its fluorescence emission from ~475 nm to ~400 nm after binding of Ca^{2+}. For Ca^{2+}-mobilization measurement, $2\text{-}3x10^6$ DG75 cells per sample were centrifuged at 300 x g, 5 min, RT. The supernatant was discarded, cells were resuspended in 500 µl R10 and transferred into light protected tubes. After the addition of 200 µl master mix containing 1 µM Indo-1 and 0,015 % pluronic acid, cells were incubated for 20 min shaking at 30 °C, followed by an incubation for 10 min shaking at 37 °C (Grynkiewicz et al., 1985). Next, cells were washed twice with 1x Krebs-Ringer solution containing 1 mM $CaCl_2$ (300 x g, 3 min, RT). Finally, cells were resuspended in 900 µl 1x Krebs-Ringer solution (1 mM $CaCl_2$) and kept on 30 °C for 30 min before measurement. Measurements were recorded with the LSRII (Becton Dickinson, San Jose, CA, USA). A 25 s base line was recorded before cells were stimulated with 20 µg/ml anti-human IgM $F(ab')_2$ fragments. The total measurement time was set to 5 min.

Krebs-Ringer buffer:	10 mM	HEPES, pH 7.0
	140 mM	NaCl
	4 mM	KCl
	1 mM	$MgCl_2$
	1 mM	$CaCl_2$
	10 mM	glucose
		in $_{dd}H_2O$

3.2.3.10 Confocal microscopy

A confocal laser scanning microscope was used (Leica, objective HCX OL APO 63.0x1.32 OIL UV) to detect the intracellular localization of fluorescent labeled proteins. To do this, 0.5-1.0x10^6 DG75 cells were washed twice with 1 ml 1x Krebs-Ringer buffer containing 1 mM $CaCl_2$ (300 x g, 3 min, RT), resuspended in 400 µl 1x Krebs-Ringer buffer (1 mM $CaCl_2$) and transferred into a 4-well chamber. After 20-30 min of cell settlement, images were recorded before and 3 min after stimulation with 20 µg/ml α-human IgM F(ab')$_2$ fragments. For each measurement, a 4x digital zoom was used.

3.2.4 Gene targeting methods

3.2.4.1 Transcription Activator-like Effector Nucleases - TALEN

TALEN is a gene targeting method that can be used to generate knock out cell lines. It is based on transiently expressed fusion proteins that contain a DNA binding segment for specific DNA targeting and an endonuclease that introduces DNA double-strand breaks. The plasmid kit used for the generation of TALENs was a gift from Daniel Voytas and Adam Bogdanove (Addgene kit # 1000000024). The generation of TALEN constructs was done according to the manufacturer's protocol. Noteworthy, changes within the TALEN vectors were done for improved TALEN assembly and efficiency.

Design of TALEN constructs

The design of TALEN constructs was done with the help of the TALEN targeter software. Here, the desired Exon sequence was analysed for possible TALEN sites. TALEN constructs were chosen that have the following attributes:

1. TALEN constructs contain 15-18 DNA binding modules.
2. The spacer region between the two TALEN constructs is 17 bp in size.
3. The predicted TALEN cleavage site overlaps with a endonuclease binding/restriction site for later activity screening.

Assembly of TALEN constructs - Optimization of the Golden Gate Ligation

TALEN constructs were assembled according to the protocol of the Voytas lab. For the assembly, the Golden Gate Ligation method is used to minimize the number of cloning steps. Following the protocol, up to ten cDNAs encoding DNA binding modules can be

cloned in one cloning step. However, the procedure revealed some obstacles regarding efficiency and reliability. Therefore, I reconstructed the Golden Gate Ligation kit. In detail, I changed the DNA backbone of the cloning vectors resulting in different sticky ends, so that I divided a '10 module cloning step' in two '5 module cloning steps'. Hence, I also had to change sticky ends of additional cloning vectors to ensure a consensus of sticky ends and to allow cloning into the backbone vector. Changes are outlined below:

Table 3.15: Optimization of Golden Gate Ligation kit.

Old vector	Number of modules	New vector	Number of modules
pFusA30A	10 modules	pFusA5A	5 modules
pFusA30B	10 modules	pFusA5B	5 modules
pFusB5	5 modules	pFusA5C	5 modules
pFusB1	1 module	pFusB1B	1 module
pFusB2	2 modules	pFusB2B	2 modules
pFusB3	3 modules	pFusB3B	3 modules
pFusB4	4 modules	pFusB4B	4 modules

Example of the TALEN construct 22 used for the generation of a Vav1-deficient DG75 sub-line:

Table 3.16: Vectors and modules used for the generation of TALEN construct 22.

Vector	Number of modules	Modules
pFusA5A	5 modules	pNI, pHD, pNI, pHD, pHD
pFusA5B	5 modules	pHD, pNG, pNN, pNG, pHD
pFusB4	4 modules	pNG, pNN, pHD, pNG
pLR-HD	half module	half HD module
pTAL4Tit	final backbone	Containing FokI endonuclease, NLS, HA-tag

In addition, I changed the vector backbone of the pTAL4 vector that contains the FokI endonuclease cDNA and renamed the new designed backbone vector into pTAL4Titanium (pTAL4Tit). Changes were done according to Miller et al.. Here deletions were introduced into the DNA backbone, reducing the linker regions N-terminal and C-terminal of the DNA binding modules. In addition, I introduced 'SHARKEY' mutations in the FokI endonuclease leading to a higher activity without increasing off-target effects (Guo et al., 2010). To enable TALEN protein expression determination by western blot analysis, I introduced an HA-tag N-terminal of the TALEN construct. Finally, to increase translation efficiency, I equipped the pTAL4Tit vector with a Kozak consensus sequence

5’ of the TALEN start codon. The described changes are shown in figure 4.1 in the results chapter.

Nucleofection and expression of TALEN constructs

For expression of TALEN proteins the pmax vector from the company LONZA was used. This was modified by Niklas Engels with a multiple cloning site derived from the pBlueScript KS vector and an IRES-EGFP site (pmaxKS IRES-EGFP). In addition, I introduced an AflII restriction site into the multiple cloning site and erased a present AflII site from the vector backbone. Furthermore, I used the newly designed vector backbone to generate the pmaxKS IRES-tagRFP vector. The pmaxKS IRES-EGFP and pmaxKS IRES-tagRFP were used for transient expression of TALEN constructs. Nucleofection of TALEN constructs was done using the Lonza Human B cell Nucleofector® Kit.

Cell sorting, activity test and sub-cloning of DG75 cells

36-48 h after nucleofection, cells were sorted for EGFP/tagRFP double-positive cells in the cell sorting facility of the university medical center. After recovery of the cells, they were used in a TALEN activity test. Therefore, a proportion of cells were harvested (300 x g, 5 min, RT) and genomic DNA was isolated. Afterwards, the targeted exon region was amplified by PCR, purified and used in the TALEN activity assay with an endonuclease, whose binding/restriction site overlaps with the TALEN target site. In the case of a high TALEN activity, exon restriction should be dramatically diminished. If TALEN constructs were active, cells were sub-cloned onto 96-well plates and grown until a sufficient number of cells was reached for western blot analysis.

3.2.4.2 CRISPR/Cas

The CRISPR/Cas gene targeting method was used according to Ran et al. 2013. In my project, I used the pSpCas9(BB)-2A-GFP vector for CRISPR/Cas gene targeting. The pSpCas9(BB)-2A-GFP (PX458) vector was a gift from Feng Zhang (Addgene plasmid # 48138). This offers the advantage of a one vector system, which encodes for all necessary elements. The design of CRISPR/Cas constructs was done with the help of the CRISPR/Cas Design software. Constructs were chosen that showed a high score indicating a low number of off-target sites and that had an overlapping targeting site with an endonuclease binding/restriction site. Assembly of the CRISPR/Cas construct is faster

compared to the TALEN system, since only a phosphorylated 25 bp oligonucleotide dimer has to be cloned into the backbone vector. Phosphorylated oligonucleotides were ordered from Eurofins Genomics. Cloning of oligonucleotides was done according to the protocol of the Feng Zhang group (Ran et al., 2013). Further steps are identical to the TALEN gene targeting method (see chapter 3.2.4.1).

4 Results

4.1 The guanine nucleotide exchange factor Vav1 is a key regulator of BCR-proximal signaling in human B cells

4.1.1 Establishment of the TALEN method to generate a Vav1-deficient sub-line of DG75

In order to investigate the function of the guanine nucleotide exchange factor (GEF) Vav1 in BCR-proximal signaling events in a human B cell line, I had to establish the recently developed Transcription Activator-like Effector Nuclease (TALEN) gene targeting method in our laboratory. The TALEN method is based on chimeric proteins that can introduce DNA double strand breaks (DSBs) in specific genomic DNA loci. The DSB repair mechanisms of cells are error prone, so that insertions or deletions frequently occur at the repair site that can cause frame shift mutations, which lead to a disturbed gene expression (Cermak et al., 2011; Sanjana et al., 2012).

An individual TALEN protein consists of an N-terminal nuclear localization signal (NLS), a central DNA binding region and a C-terminal FokI nuclease, which needs to dimerize to be enzymatically active (figure 4.1 A). The central DNA binding region is composed of 15-30 DNA binding modules that contain 34 amino acids each. In total, four different module types exist, which have a nearly identical amino acid sequence. Only the amino acids at positions 12 and 13 differ between the DNA binding modules. This amino acid pair is responsible for the DNA contact with the respective nucleotide and thus determines the module's binding specificity (figure 4.1 A). For genomic targeting, two TALEN constructs have to bind 17-18 base pairs (bps) apart from each other on opposite DNA strands to allow efficient FokI dimerization and activity (figure 4.1 B).

For generation of TALEN constructs, the Golden Gate TALEN assembly kit was retrieved from Addgene and used following the instructions of the Voytas lab (Cermak et al., 2011). However, some changes were made to increase TALEN efficiency according to the modifications described by the group of Rebar (Miller et al., 2011). Deletions within the regions N-terminal and C-terminal of the DNA binding region were made to increase TALEN efficiency (figure 4.1 C). In addition, deletions reduced the final vector size, thus improving transfection rates. Furthermore, two amino acid substitutions S418P and K441E ('SHARKEY' variant) inside the FokI nuclease were introduced to increase FokI activity (Guo et al., 2010). Moreover, a Kozak consensus sequence was introduced into the expression plasmids to increase translation efficiency and thereby the amount of active

TALEN proteins in the transfected cells. For detection of the TALEN proteins via western blot, they were equipped with an N-terminal HA-tag (figure 4.1 C).

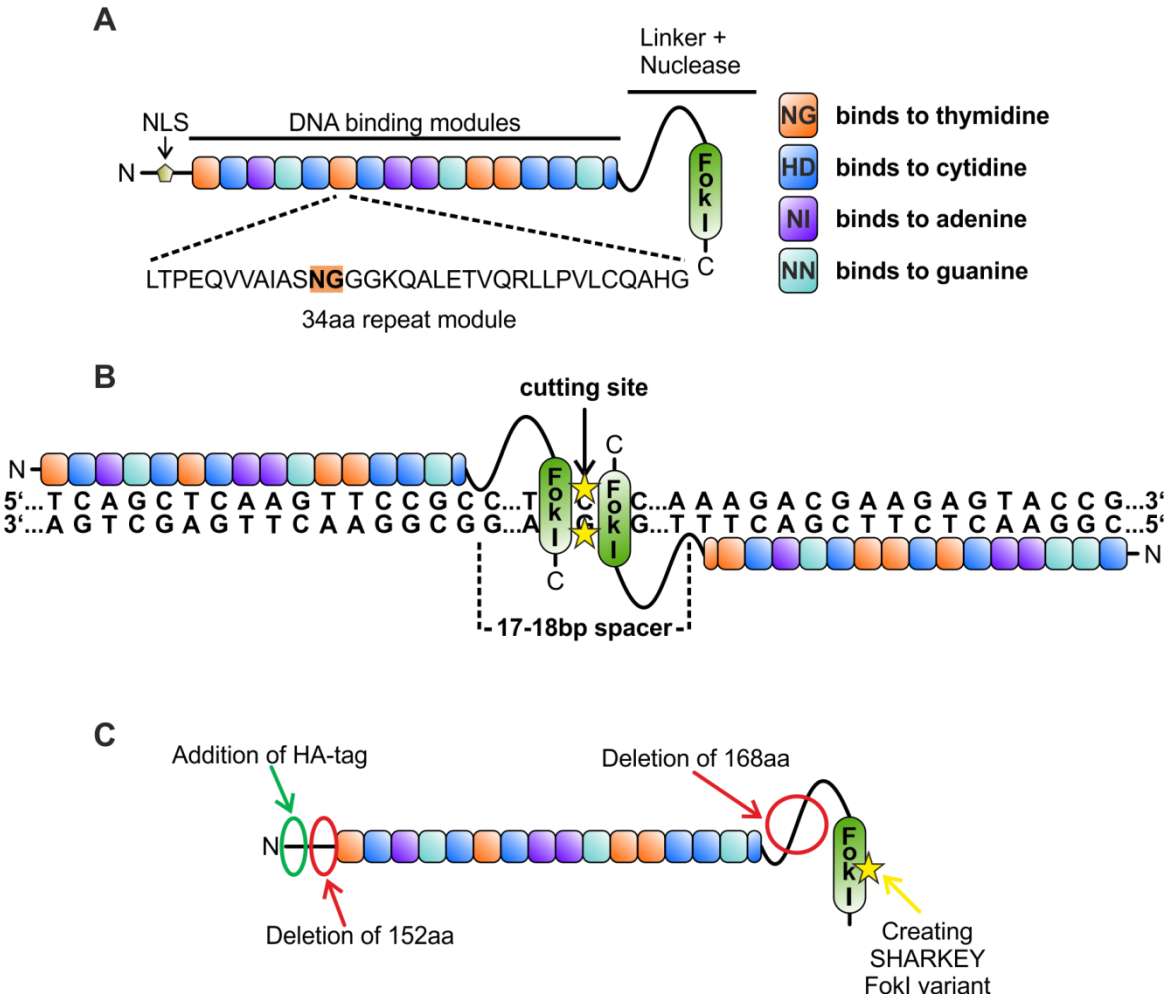

Figure 4.1: Schematic overview of the TALEN method. A) Schematic drawing of the domain architecture of an individual TALEN construct, which is composed of a N-terminally located nuclear localization signal (NLS), an array of centrally located DNA binding modules, which are followed by a linker region and the FokI nuclease domain at the C-terminal end. The central DNA binding modules are composed of 34 amino acids each. The amino acids at positions 12 and 13 are responsible for DNA interaction and determine the specificity of the module. Four different DNA binding modules exist, which specifically bind to their respective nucleotide. **B)** Schematic drawing of a TALEN construct pair binding its genomic target. The TALEN constructs have to bind 17-18 base pairs apart from each other at opposite DNA strands to achieve efficient FokI dimerization and cleavage of DNA. **C)** Schematic drawing of TALEN construct modifications to improve TALEN efficiency. TALEN constructs were equipped with an HA-tag to allow detection via western blot. In addition, two amino acids substitutions (SHARKEY variant) within the FokI nuclease were introduced to increase FokI enzymatic activity. Furthermore, N-terminal and C-terminal deletions in linker regions were generated to decrease the size of TALEN constructs and thus improving transfection efficiency of TALEN expression vectors. Finally, a Kozak sequence was introduced 5' of start codons of the TALEN constructs to increase their translation rate (not shown). (Adapted from Sanjana et al., 2012)

For the expression of TALEN constructs, the pmax vector from the company Lonza was used because of its minimal size of 2.8 kbps. It was equipped with either an IRES-EGFP (pmax-IE) or an IRES-tagRFP (pmax-IR) cassette, respectively, to allow for indirect expression control of the TALEN constructs as well as sorting of doubly transfected cells to increase the overall efficiency.

After optimization of TALEN constructs and expression vectors, the gene targeting system was used to generate a Vav1-deficient variant of the human B cell line DG75. As target site, the *VAV1* exon 3 was chosen, since it is contained in all described protein coding *VAV1* mRNA isoforms (based on Ensembl data base, figure 4.2 A). Furthermore, TALEN constructs were designed in a way that the restriction enzyme AvaII could be used for TALEN activity screening.

Cloning of TALEN constructs was done as described in chapter 3.2.4.1. The TALEN constructs 22 and 40 cloned into pmax-IE and pmax-IR, respectively, were nucleofected into DG75 cells to achieve a transient construct expression. Next, EGFP/tagRFP double-positive cells were sorted to get rid of all non-transfected or single-transfected cells. Roughly 6 % double positive cells were collected for further cultivation and subsequent analysis (figure 4.2 B).

To test the activity of the TALEN construct pair 22/40, genomic DNA was isolated from EGFP/tagRFP-sorted cells as well as parental DG75 cells and the exon 3 containing genomic region (referred to as ‘exon 3’) of *VAV1* was amplified via PCR. The ‘exon 3’ amplicon was cut using the restriction enzyme AvaII, whose binding site overlays with the TALEN target site (see figure 4.2 A). Figure 4.2 C shows that the ‘exon 3’ of parental DG75 cells was completely cut by the AvaII restriction enzyme, whereas the amplicon of TALEN-treated DG75 cells was not cut at all indicating that the AvaII site was damaged by TALEN mediated indel (insertion/deletion) mutations. In conclusion, the TALEN construct pair 22/40 is active in DG75 cells. To further verify TALEN activity, sequencing of the ‘exon 3’ amplicon from the sorted DG75 cells was performed (figure 4.2 D). The sequencing chromatogram shows that the ‘exon 3’ was derived from a polyclonal population.

To isolate Vav1-deficient clones from the polyclonal population, sorted DG75 cells were sub-cloned by limited dilution and the resulting cell clones were analyzed by western blot for Vav1 protein expression. Figure 4.2 E shows that twelve analyzed clones (#1 - #12) lack Vav1 expression, which indicates that the generation of Vav1-deficient DG75 cell clones was successful. Altogether, 36 clones were tested for Vav1 expression, 33 of which were negative for Vav1. The total efficiency of my strategy was >90 %.

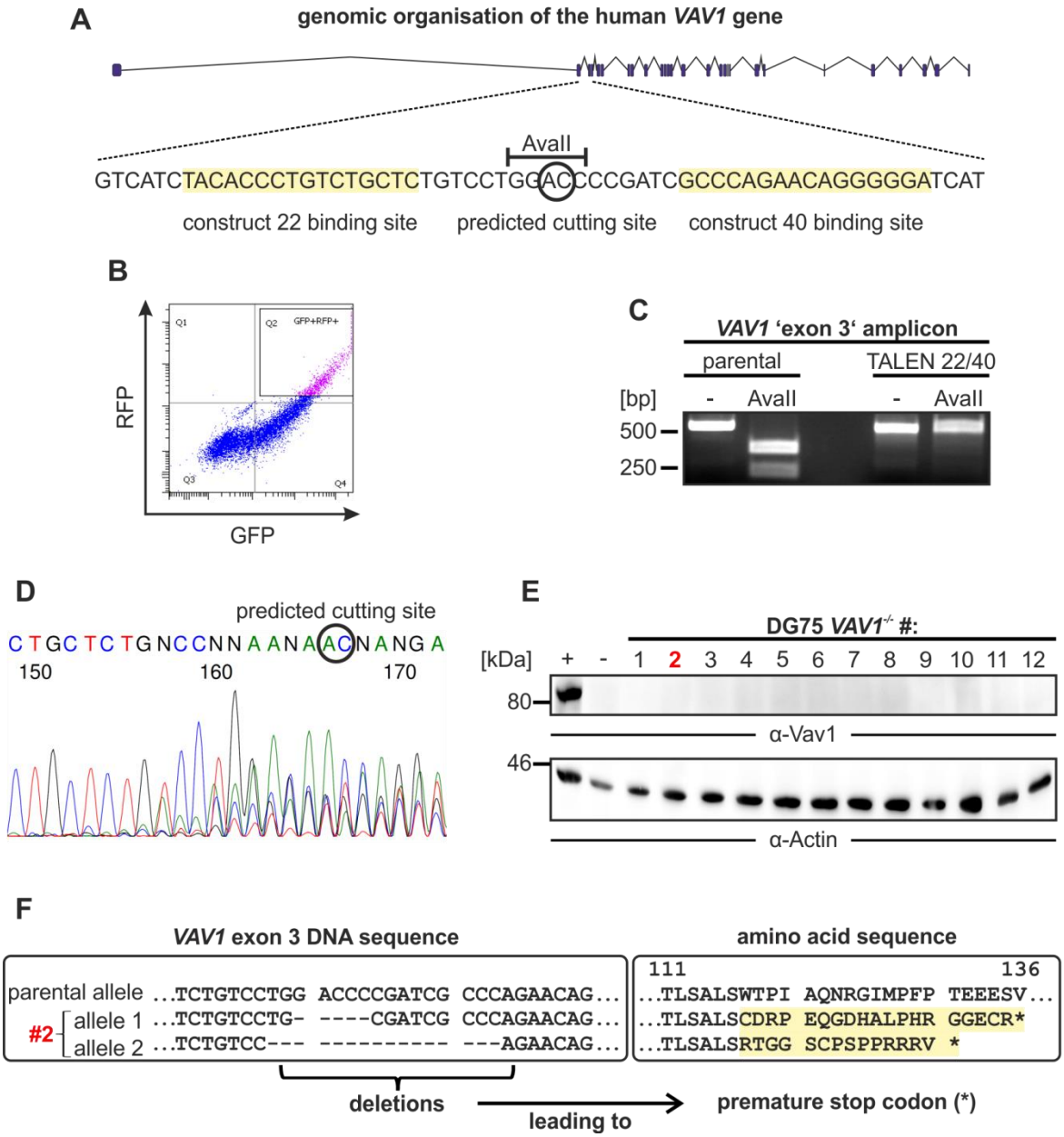

Figure 4.2: Generation of a Vav1-deficient DG75 sub-line. A) Schematic drawing of the *VAV1* genomic organization indicating the TALEN target region in exon 3. **B)** DG75 cells were nucleofected with pmax expression vectors containing the TALEN constructs 22 and 40 along with either an IRES-EGFP or IRES-tagRFP cassette. Subsequently, double-positive cells (GFP+, RFP+ gate) were sorted for further cultivation. **C)** To test the activity of the TALEN construct pair 22/40, the genomic region containing the targeted *VAV1* exon 3 was amplified by PCR and cleaved with the restriction enzyme AvaII. The AvaII binding site overlaps with the TALEN target site and therefore can be used for TALEN activity testing. **D)** Sequencing result of the *VAV1* 'exon 3' amplicon from sorted cells. The predicted targeting site of TALEN constructs 22 and 40 is indicated. **E)** Screening of DG75 cell clones for Vav1 deficiency was done using western blot analysis. Cleared cellular lysates of $1x10^6$ DG75 cells were loaded per lane and separated by SDS-PAGE. Immunoblots were probed with anti-Vav1 and anti-Actin antibodies as indicated below individual blots. The molecular weight of marker proteins (in kDa) is indicated on the left. **F)** Characterization of Vav1-deficient DG75 clone #2 was done by cloning the *VAV1* 'exon 3' amplicon into the pCR2.1 vector and subsequent sequencing of individual alleles. The result is representative of seven sequencing reactions.

To analyze the underlying genetic alterations that cause the loss of Vav1 protein expression, the Vav1-deficient DG75 clone #2 was used for further characterization. To sequence both *VAV1* alleles separately, the *VAV1* 'exon 3' amplicon was cloned into the pCR2.1 cloning vector. The sequencing results show that both alleles carry nucleotide deletions (figure 4.2 F). In detail, allele 1 has a deletion of 5 nucleotides, whereas allele 2 has a deletion of 16 nucleotides resulting in premature stop codons in both cases. DG75 *VAV1*$^{-/-}$ clone #2 was used in all following experiments and is hereafter referred to as Vav1-deficient DG75 cells.

4.1.2 Vav1 is essential for BCR-induced Ca^{2+}-mobilization

Since Vav1 is described to be an essential regulator of various signaling pathways including BCR signaling (see introduction), the generation of a Vav1-deficient DG75 cell line using the TALEN method opened new opportunities for Vav1 investigations.

One key event in BCR signaling is the influx of Ca^{2+} from the endoplasmic reticulum (ER) and external sources into the cytoplasm of B cells. For that reason, I investigated the influence of Vav1 on Ca^{2+}-mobilization upon BCR stimulation in DG75 cells. Figure 4.3 A shows that the three Vav1-deficient DG75 cell clones #2, #3 and #6 have a dramatically reduced Ca^{2+}-mobilization compared to parental DG75 cells, which indicates an obligatory role of Vav1 for BCR-induced Ca^{2+}-mobilization. To exclude that the observed phenotype is caused by off-target TALEN effects, Vav1-deficient cells were reconstituted with a Citrine-tagged variant of wild-type Vav1. Figure 4.3 C shows that this reconstitution restored BCR-induced Ca^{2+}-mobilization and even led to elevated Ca^{2+}-mobilization upon BCR stimulation compared to parental DG75 cells. In accordance, additional ectopic expression of wild-type Vav1 in DG75 cells also led to an elevation of Ca^{2+}-mobilization compared to parental cells (figure 4.3 E,F,G). In conclusion, BCR-induced Ca^{2+}-mobilization requires the presence of Vav1 and its intensity is regulated by the amount of Vav1 protein expression.

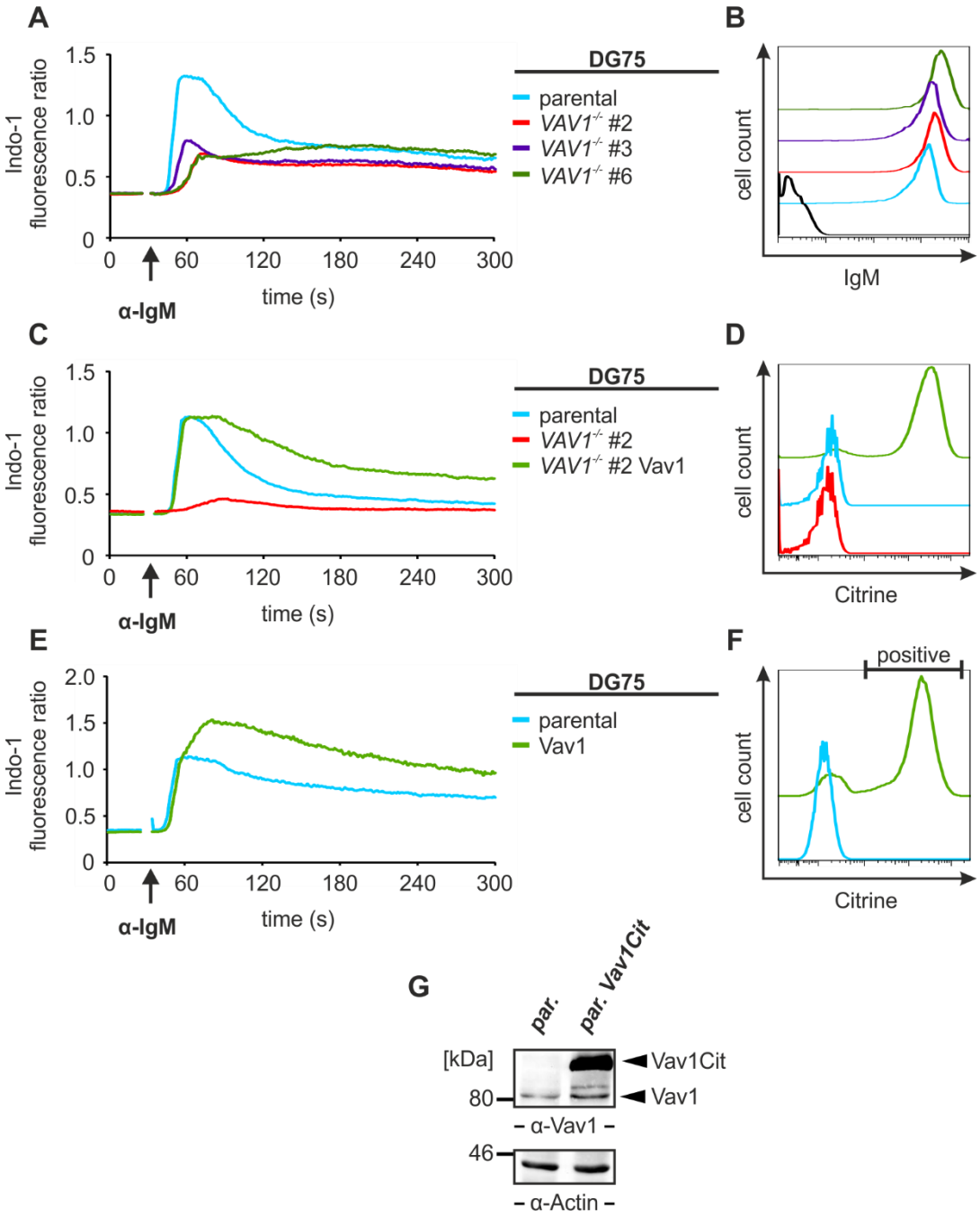

Figure 4.3: Vav1 controls Ca^{2+}-mobilization upon BCR stimulation in DG75 cells. A) Parental DG75 as well as Vav1-deficient cell clones #2, #3 and #6 were analyzed for Ca^{2+}-mobilization upon BCR stimulation. Cells were loaded with the Ca^{2+}-sensitive fluorophore Indo-1 AM in order to measure intracellular Ca^{2+}-changes by flow cytometry. After base line recording for 25 s, cells were stimulated with 20 µg/ml anti-human IgM $F(ab')_2$ fragments (α-IgM) as indicated by an arrow. The graph is representative of three independent experiments. **B)** Surface BCR expression measured by flow cytometry. Surface staining was performed using anti-human IgM-APC antibodies. The unstained negative control is depicted in black. Samples have the same color code as in A). **C)** Vav1-deficient DG75 cells expressing Citrine-tagged wild-type Vav1 were analyzed for Ca^{2+}-mobilization as in A). Parental DG75 cells were used as positive and Vav1-deficient DG75 cells as negative control, respectively. **D, F)** Expression levels of Citrine-tagged proteins were determined by flow cytometry. **E)** DG75 cells expressing Citrine-tagged wild-type Vav1 were analyzed for BCR-induced Ca^{2+}-mobilization as in A). Untransfected cells were excluded by gating on Citrine-positive cells shown in F). **G)**

Cleared cellular lysates of $1x10^6$ DG75 cells were loaded per lane and separated by SDS-PAGE. Immunoblots were probed with anti-Vav1 and anti-Actin antibodies as indicated below individual blots. The molecular weight of marker proteins (in kDa) is indicated on the left.

4.1.3 Vav1 and Vav3 control Ca^{2+}-mobilization upon BCR stimulation in DG75 B cells

Vav1 is expressed exclusively in the hematopoietic cell lineage indicating that it has specialized functions in these cells. However, the Vav protein family contains two additional family members, namely Vav2 and Vav3, which may also have important functions in BCR signaling. Therefore, I investigated the expression of Vav proteins in primary and DG75 B cells by western blot analysis with antibodies against the three Vav family members. Differences were observed with regard to the abundance of individual Vav members. Vav1 levels are elevated in DG75 cells, whereas Vav2 and Vav3 have a higher abundance in primary B cells (figure 4.4 A).

Having shown the expression of all Vav family members in human DG75 B cells, the question arose whether Vav2 and Vav3 have a function in BCR signaling. To analyze their influence on BCR-induced Ca^{2+}-mobilization, Vav1-deficient DG75 cells were retrovirally transfected with constructs encoding Citrine-tagged Vav2 or Vav3 followed by Ca^{2+}-mobilization analysis. Figure 4.4 B shows that Vav2 was not capable to replace Vav1 in Ca^{2+}-mobilization upon BCR stimulation, even though it was expressed in higher amounts (figure 4.4 C). In contrast, additional ectopic expression of Vav3 did not only restore the Ca^{2+}-mobilization defect of Vav1-deficient DG75 cells, but led to an elevated and more sustained Ca^{2+}-influx compared to cells reconstituted with Vav1. This result may indicate that the remaining Ca^{2+}-mobilization upon BCR stimulation in Vav1-deficient DG75 cells is brought about by the relatively weak expression of Vav3. Even though Vav3 was only poorly expressed in DG75 cells in comparison to primary B cells, Vav3 appears to be the most potent protein member within the Vav protein family in the context of BCR-induced Ca^{2+}-mobilization. In summary, Vav1 and Vav3 have the potential to control Ca^{2+}-mobilization upon BCR stimulation in human DG75 B cells, whereas Vav2 seems to have no function in that context.

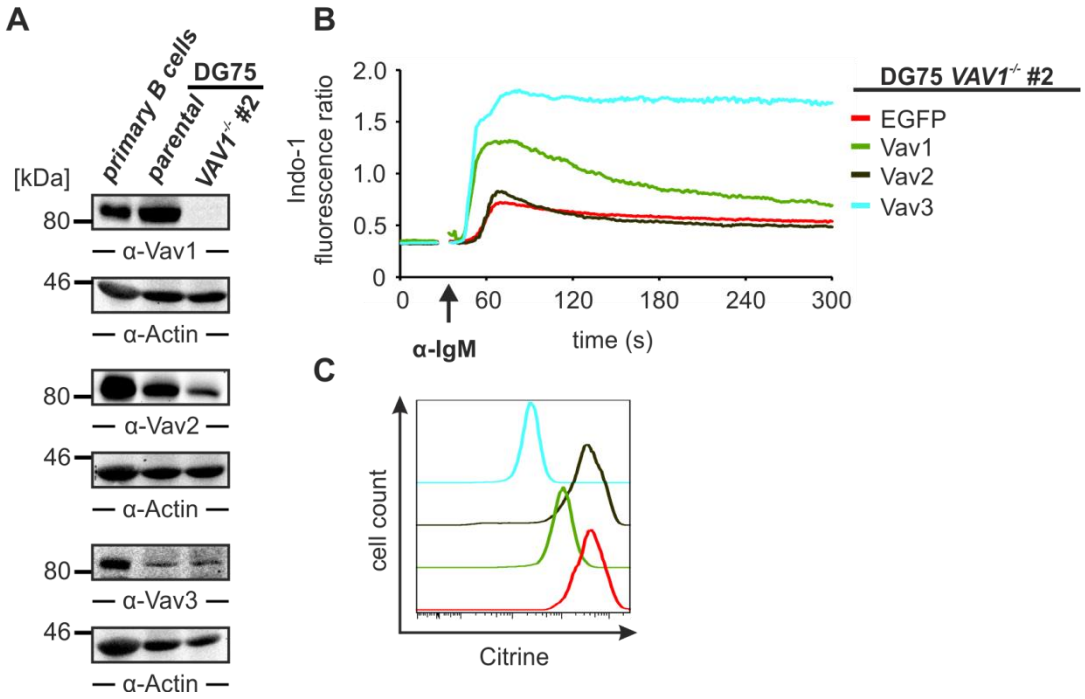

Figure 4.4: Vav3, but not Vav2, can restore Ca^{2+}-mobilization in Vav1-deficient DG75 B cells. A) Expression analysis of Vav family members in human B cells. Cleared cellular lysates of $1x10^6$ cells were loaded per lane and separated by SDS-PAGE. Immunoblots were probed with antibodies against the three Vav proteins and Actin as indicated below individual blots. The molecular weight of marker proteins (in kDa) is indicated on the left. **B)** Vav1-deficient DG75 cells expressing Citrine-tagged wild-type Vav1, Vav2, Vav3 or EGFP as negative control were analyzed for Ca^{2+}-mobilization upon BCR stimulation as before. The graph is representative of three independent experiments. **C)** Expression levels of the analyzed proteins were determined by flow cytometry.

In contrast to the functions of Vav family members in the human DG75 B cell model system (figure 4.4), Vav proteins behave differently in primary mouse B cells. The group of Klaus-Dieter Fischer showed that an individual loss of either Vav1 or Vav2 in mice has no effect on BCR-induced Ca^{2+}-mobilization (Tedford et al., 2001). Only in Vav1/Vav2 double-deficient mice a severe impact on Ca^{2+}-mobilization could be detected, whereas in the human DG75 B cell line the loss of Vav1 is sufficient to dramatically reduce Ca^{2+}-mobilization.

To test potential differences between mouse and human Vav family members, I retrovirally transfected Vav1-deficient DG75 cells with constructs coding for Citrine-tagged murine Vav proteins and investigated their ability to restore the Ca^{2+}-mobilization defect. The results show that mouse Vav1 and mouse Vav3 were both capable to restore Ca^{2+}-mobilization and thus seem to have the same function as their human counterparts (figure 4.5 A, E). Murine Vav2, like human Vav2, was not capable to restore the Ca^{2+}-mobilization defect. However, expression of mouse Vav2 was very weak in the transfected cells (figure

4.5 C, D). In summary, mouse Vav proteins closely resembled their human counterparts with regard to their ability to support Ca^{2+}-mobilization upon BCR stimulation in human B cells. Therefore, the described phenotypical differences between Vav-deficient murine B cells and the human model system might depend on cell-intrinsic differences rather than on Vav proteins themselves.

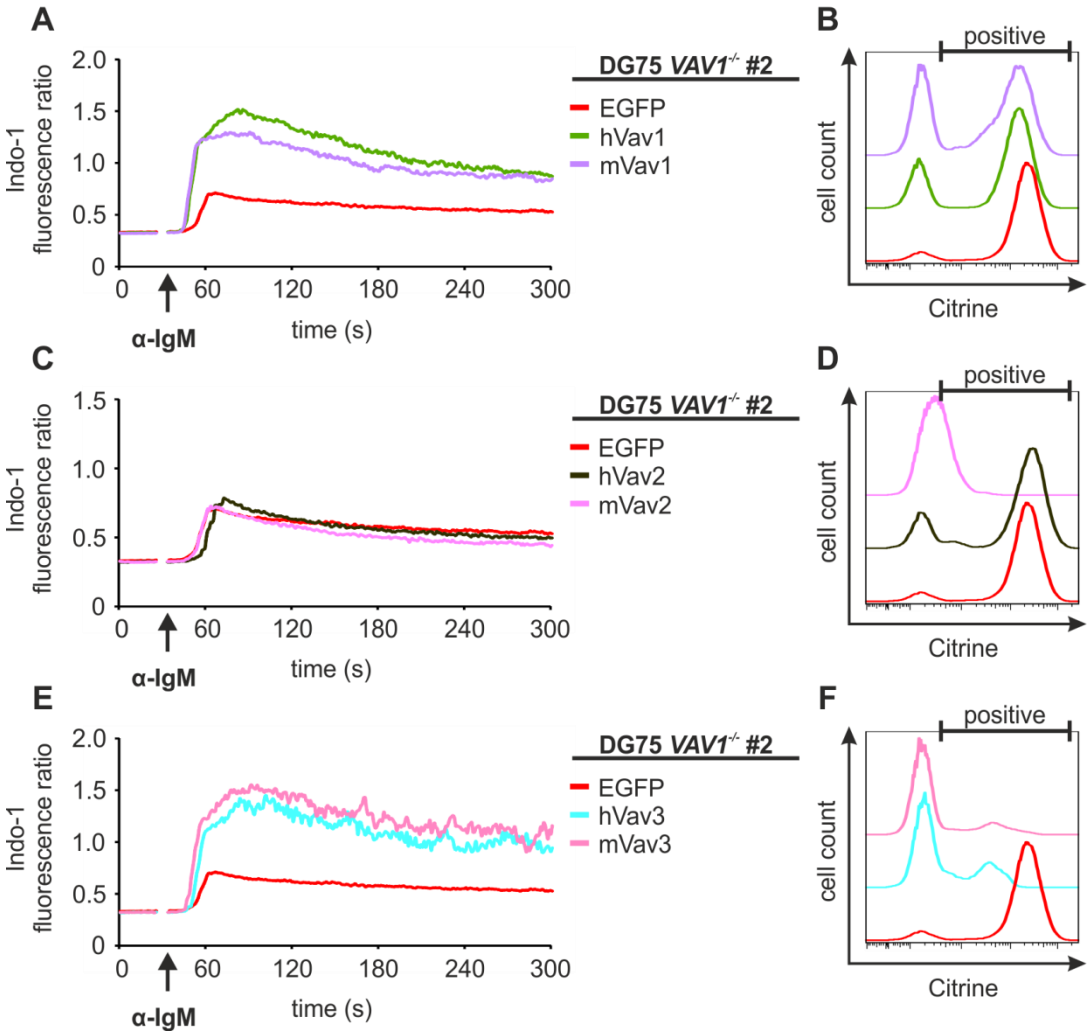

Figure 4.5: The mouse Vav protein family behaves similar to their human counterparts in the context of BCR-induced Ca^{2+}-mobilization. A, C, E) Vav1-deficient DG75 cells expressing Citrine-tagged human (h) Vav1 or mouse (m) Vav1 (A), hVav2 or mVav2 (C), hVav3 or mVav3 (E) or EGFP as negative control were analyzed for Ca^{2+}-mobilization upon BCR stimulation as before. The graphs show Ca^{2+}-mobilization of gated cells (positive gates (B, D, F)) and are representative of three independent experiments. **B, D, F)** Expression levels of analyzed proteins were determined by flow cytometry.

4.1.4 Loss of Vav1 does not influence the assembly of the Ca^{2+}-initiation complex

The analysis of BCR-induced Ca^{2+}-mobilization in Vav1-deficient DG75 B cells showed that Vav family members are essential signaling components in that process. Ca^{2+}-mobilization critically depends on the correct formation of the Ca^{2+}-initiation complex consisting of the adaptor protein SLP-65, the tyrosine kinase Btk and the phospholipase PLCγ2 (Engelke et al., 2007). Since Vav1-deficient DG75 cells showed a reduced Ca^{2+}-mobilization, it appeared possible that the lack of Vav1 disturbs the formation of the Ca^{2+}-initiation complex. The outcome of the Ca^{2+}-initiation complex formation is the phosphorylation and thereby activation of PLCγ2. This is followed by the production of the key second messenger IP_3 that induces the release of Ca^{2+} from the ER.

To test the influences of Vav1 on activation of PLCγ2, I analyzed BCR-induced PLCγ2 phosphorylation in DG75 cells lacking or expressing Vav1. To this end, PLCγ2 was affinity purified from cellular lysates followed by western blot analysis with α-pTyr antibodies. Figure 4.6 A shows the phosphorylation kinetics of PLCγ2 and PLCγ2-associated proteins upon BCR stimulation in each of the cell lines. The PLCγ2 tyrosine phosphorylation intensity is similar in the tested cell lines. In addition, further phospho-tyrosine signals of co-purified proteins at roughly 60 kDa and between 30-46 kDa were indicative of phosphorylated SLP-65 (Engels et al., 2009) and Igα/Igβ proteins, respectively. Moreover, phosphorylation of SLP-65 and Igα/Igβ proteins was slightly increased in Vav1-deficient DG75 cells. Since PLCγ2 tyrosine phosphorylation as well as the binding to SLP-65 was not affected in the absence of Vav1, I assume that the formation of the Ca^{2+}-initiation complex is not disturbed.

To verify that finding, I investigated SLP-65 phosphorylation and plasma membrane recruitment, which both are necessary for Ca^{2+}-initiation complex formation (Abudula et al., 2007). To determine the influence of Vav1 on the phosphorylation status of SLP-65, I analyzed SLP-65 phosphorylation in Vav1-deficient cells compared to Vav1-expressing cells (figure 4.6 B). As seen in figure 4.6, SLP-65 phosphorylation was slightly increased in Vav1-deficient cells compared to DG75 parental cells.

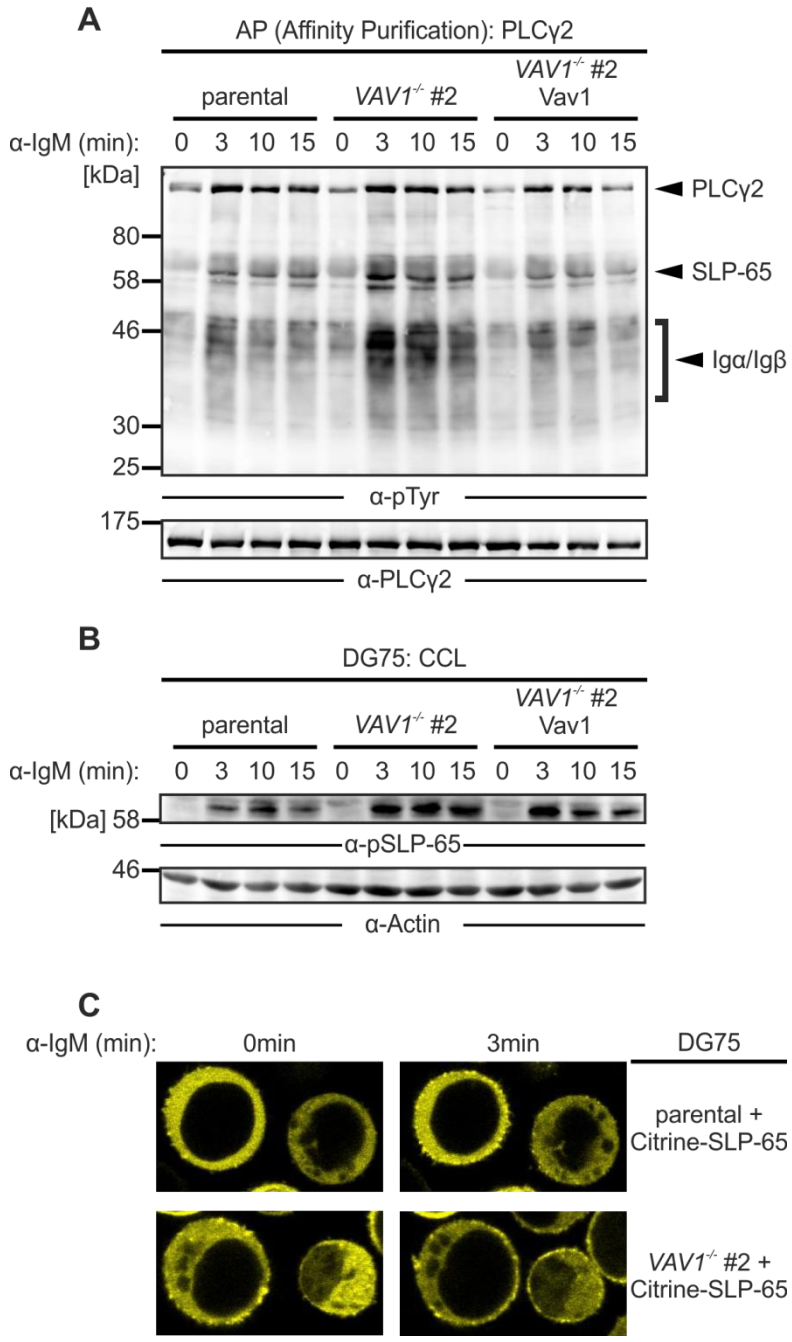

Figure 4.6: The formation of the Ca^{2+}-initiation complex is not altered in Vav1-deficient DG75 cells. A) Affinity purification of PLCγ2 to check its phosphorylation status upon BCR stimulation. DG75 cells, Vav1-deficient cells and Vav1-deficient cells reconstituted with Citrine-tagged wild-type Vav1 were stimulated with 20 µg/ml α-IgM $F(ab')_2$ fragments for different periods of time (0 min, 3 min, 10 min ,15 min). PLCγ2 was affinity purified from cleared cellular lysates with anti-PLCγ2 antibodies followed by western blot analysis with anti-pTyr and anti-PLCγ2 antibodies as loading control. The molecular weight of marker proteins (in kDa) is indicated on the left. Data are representative of three independent experiments. **B)** Cleared cellular lysates (A) were used for western blot analysis with anti-pSLP-65 antibodies and anti-Actin antibodies as loading control. Data are representative of three independent experiments. **C)** Confocal microscopy of DG75 and Vav1-deficient DG75 cells expressing constructs encoding N-terminally Citrine-tagged wild-type SLP-65. Images were taken before and 3 min after BCR stimulation with 20 µg/ml α-IgM $F(ab')_2$ fragments. Data are representative of three independent experiments.

To investigate whether membrane recruitment of SLP-65 relies on Vav1, I expressed an N-terminally Citrine-tagged SLP-65 variant in parental and Vav1-deficient DG75 cells and analyzed SLP-65 localization using confocal microscopy. There was no difference in SLP-65 plasma membrane recruitment between parental DG75 and Vav1-deficient DG75 cells (figure 4.6 C). In both cell lines, SLP-65 was located in the cytoplasm of non-stimulated cells, whereas a pool of SLP-65 was recruited to the plasma membrane upon BCR stimulation. Based on these findings, the reduced Ca^{2+}-mobilization in Vav1-deficient DG75 cells cannot be attributed to an alteration in Ca^{2+}-initiation complex formation.

4.1.5 Vav1 influences Akt activation upon BCR stimulation

Having described an essential role of Vav1 in BCR-proximal Ca^{2+}-signaling, further characterization of distal BCR signaling effectors was performed. Since DG75 cells are a Burkitt lymphoma cell line in which proliferation-promoting pathways are more active than in primary cells, investigation of certain effectors was not possible due to pre-activation (data not shown). Therefore, I investigated the phosphorylation of Akt and the MAPK Erk as representatives for distal effectors in Vav1-deficient and Vav1-expressing DG75 cells.

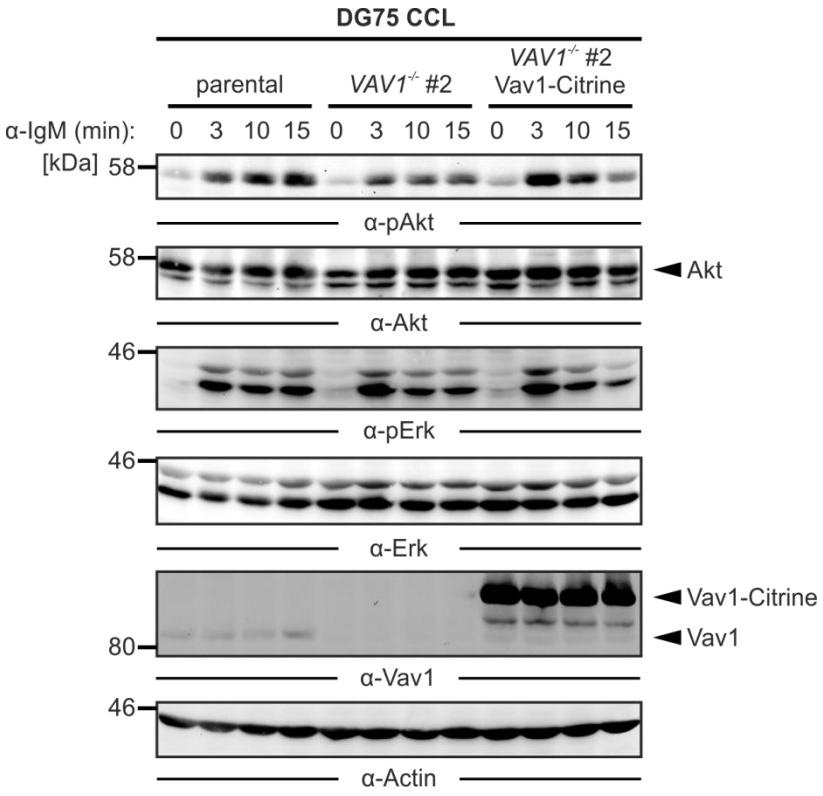

Figure 4.7: Vav1 positively influences the Akt signaling pathway. DG75 cells, Vav1-deficient DG75 cells and Vav1-deficient DG75 cells reconstituted with Citrine-tagged wild-type Vav1 were stimulated for 3 min, 10 min and 15 min with 20 µg/ml anti-human IgM $F(ab')_2$ fragments. Unstimulated cells served as control. Cleared cellular lysates of $1x10^6$ cells were loaded per lane and separated by SDS-PAGE. Immunoblots were

probed with antibodies indicated below individual blots. Anti-Actin and anti-Vav1 antibodies served as loading controls. The molecular weight of marker proteins (in kDa) is indicated on the left. Data are representative of three independent experiments.

The results show that phosphorylation of Akt was reduced in Vav1-deficient DG75 compared to Vav1-expressing cells (figure 4.7). However, the Akt phosphorylation kinetic over time was not identical between parental DG75 and Vav1-deficient DG75 cells reconstituted with Vav1, which might be due to differences in Vav1 expression levels in these cell lines (figure 4.7). Collectively, it seems that Vav1 has the ability to influence the phosphorylation of Akt besides its involvement in Ca^{2+}-mobilization. In contrast, BCR-induced Erk phosphorylation occurs independently of Vav1 in DG75 B cells.

4.2 Recruitment of Vav1 to phosphorylated BCR ITAMs enables Ca^{2+}-mobilization

4.2.1 The Vav1 SH2-domain can directly bind to the BCR ITAMs and is essential for Ca^{2+}-mobilization upon BCR stimulation

Since I described in the previous chapter that Vav1 is involved in BCR-induced Ca^{2+}-mobilization without affecting formation and activation of the Ca^{2+}-initiation complex, the question arose how exactly Vav1 is controlling BCR-induced Ca^{2+}-mobilization. To investigate this issue, I first checked the interaction of Vav1 with possible Ca^{2+}-regulating effector proteins. The C-terminus of Vav1 contains three protein binding-domains and therefore represents the adaptor region of Vav1. The center of that adaptor region consists of an SH2-domain, which was described to bind to the adaptor protein SLP-65 and to the BCR-proximal tyrosine kinase Syk (Deckert et al., 1996; Wienands et al., 1998).

To analyze the role of the Vav1 SH2-domain in BCR-induced Ca^{2+}-mobilization, the capacity of an SH2-domain-inactivated variant of Vav1 (Vav1 R696A) (Zugaza et al., 2002) to restore Ca^{2+}-mobilization upon BCR stimulation was analyzed. Figure 4.8 A shows that the Vav1 R696A variant induced a Ca^{2+}-mobilization profile that resembled that of Vav1-deficient DG75 cells. In conclusion, the SH2-domain is essential for Vav1 to promote Ca^{2+}-mobilization in antigen activated B cells.

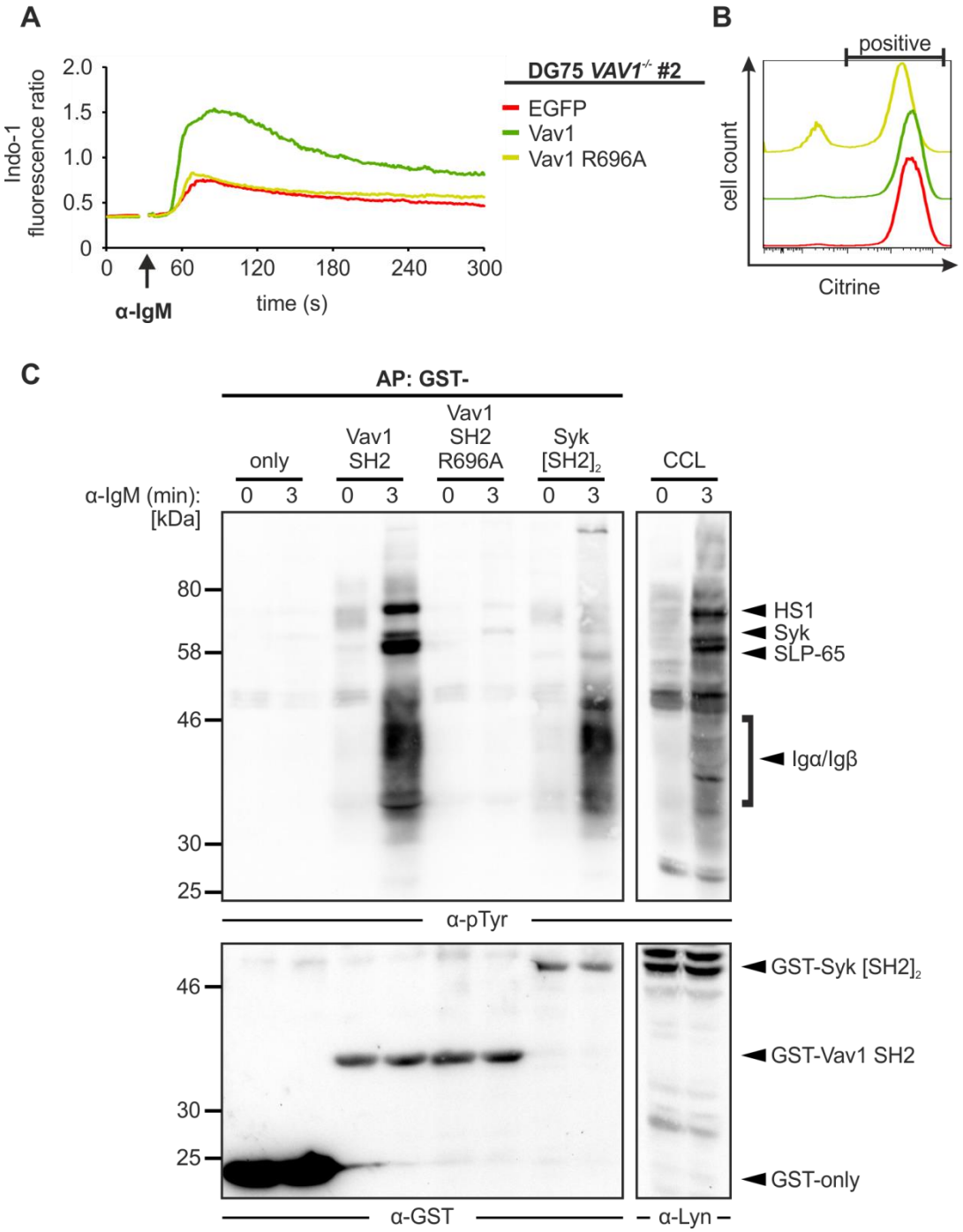

Figure 4.8: The SH2-domain of Vav1 is essential to promote BCR-induced Ca^{2+}-mobilization. A) Vav1-deficient DG75 cells expressing Citrine-tagged Vav1 or Vav1 R696A or EGFP as negative control were analyzed for Ca^{2+}-mobilization upon BCR stimulation as before. The graph shows BCR-induced Ca^{2+}-mobilization of gated cells (positive gate (B)). Data are representative of three independent experiments. **B)** Expression levels of analyzed proteins were determined by flow cytometry. **C)** Affinity purification of Vav1 SH2-domain binding partners. DG75 cells were stimulated with 20 µg/ml α-IgM $F(ab')_2$ fragments for 3 min or left untreated. Affinity purification of proteins was done with GST-Vav1 SH2, GST-Vav1 SH2 R696A, GST-Syk $[SH2]_2$ or GST-only. Samples were subjected to western blot analysis with anti-pTyr antibodies to detect phosphorylated interaction partners of the Vav1 SH2-domain. The molecular weight of marker proteins (in kDa) is indicated on the left. Data show one representative example of at least three independent experiments.

To identify B cell specific interaction partners of the Vav1 SH2-domain in BCR signaling, I tested its binding capacity in affinity purification experiments. To this end, DG75 cells were stimulated with anti-IgM F(ab')$_2$ fragments for 3 min or left untreated. The cleared cellular lysates were used in affinity purification experiments with GST-fusion proteins containing the wild-type Vav1 SH2-domain or the R696A variant. In addition, the tandemly arranged SH2-domains of Syk (GST-Syk [SH2]$_2$) and GST-only were used. Samples were subjected to immunoblot analysis with antibodies to anti-pTyr to detect tyrosine-phosphorylated binding partners.

Figure 4.8 C shows binding of the GST-Vav1 SH2-domain to proteins that resemble the molecular weight of the already described binding partners SLP-65 and Syk. Furthermore, so far undescribed interaction partners between 30 kDa and 46 kDa were detected. The molecular weight of these proteins was similar to that of the BCR components Igα and Igβ, which are specifically bound by the GST-Syk [SH2]$_2$-domains (Fütterer et al., 1998). Figure 4.8 C shows a similar Igα/Igβ phospho-protein signal for both GST-SH2-domain fusion proteins, indicating that Vav1 can interact with Igα and/or Igβ. Moreover, neither the inactive Vav1 SH2 R696A variant nor GST-only were able to interact with any tyrosine-phosphorylated protein.

To verify the newly identified interaction between Vav1 and the BCR, phosphorylated and non-phosphorylated peptides containing either the ITAM or the non-ITAM sequence of Igα were used for affinity purification of binding partners from lysates of DG75 B cells (figure 4.9 A). The results show that Vav1 could be purified with the phosphorylated peptide containing the Igα-ITAM sequence (figure 4.9 A, B). This binding resembles the interaction between the phosphorylated Igα-ITAM peptide and its known interaction partner Syk (Fütterer et al., 1998). In addition, a weak interaction between Vav1 and the phosphorylated non-ITAM tyrosine of Igα was detected. However, this interaction is negligible compared to the interaction of this phosphorylation motif with its known binding partner SLP-65 (Engels et al., 2001) (figure 4.9 B).

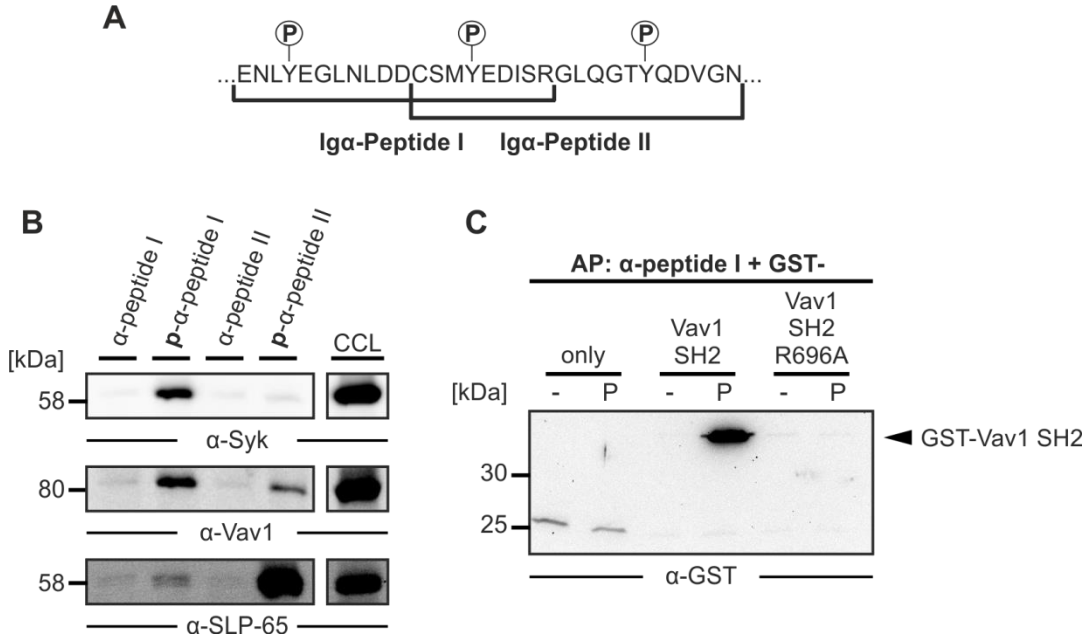

Figure 4.9: Vav1 can directly bind to the ITAMs of the Igα/Igβ heterodimer of the BCR. A) Schematic drawing of Igα-peptides used for affinity purifications. **B)** Affinity purification of proteins from cleared cellular lysate of DG75 cells using phosphorylated and non-phosphorylated Igα-peptides I and II. Samples were subjected to western blot analysis with anti-Vav1, anti-Syk and anti-SLP-65 antibodies as indicated. **C)** Affinity purifications were performed using the non-phosphorylated or phosphorylated form of the Igα-peptide I in combination with the purified GST-Vav1 SH2-domain, the GST-Vav1 SH2 R696A-domain (negative control) or GST-only (negative control). Samples were subjected to western blot analysis with anti-GST antibodies. The molecular weight of marker proteins (in kDa) is indicated on the left. Data of B) and C) show one representative example of two independent experiments.

Furthermore, to exclude that the interaction between Vav1 and the Igα/Igβ heterodimer is indirectly mediated by other proteins like SLP-65 and Syk, an affinity purification was performed using the non-phosphorylated or phosphorylated α-peptide I in combination with the purified GST-Vav1 SH2-domain. In addition, GST-only and the GST-Vav1 SH2 R696A-domain were used as negative controls. Samples were analyzed by western blot with anti-GST antibodies to check for protein-peptide binding. The results show a strong interaction between the phosphorylated peptide containing the Igα-ITAM sequence and the GST-Vav1 SH2-domain, whereas no interaction could be detected with the non-phosphorylated Igα-ITAM peptide and the negative controls (figure 4.9 C).

Summarized, the ITAMs of the Igα/Igβ heterodimer of the BCR could be identified as a new binding partner of Vav1. This interaction is mediated by the Vav1 SH2-domain, which was shown to be essential for Vav1 function in Ca^{2+}-mobilization upon BCR stimulation.

4.2.2 The Vav1 SH2-domain can be functionally replaced by SH2-domains of other Igα/Igβ interacting proteins

Having established that Vav1 can directly interact with the BCR, it remained unknown if this interaction is functionally relevant for BCR signaling. Inactivation of the Vav1-interacting ITAM-tyrosines would corrupt the entire BCR signaling cascade. To circumvent this problem, I generated Vav1 constructs that contain either the SH2-domain of SLP-65 or the tandem SH2-domains of Syk instead of the Vav1 SH2-domain (figure 4.10 A). Both, the SLP-65 and Syk SH2-domains are well known to interact primarily with the Igα/Igβ heterodimer of the BCR (Fütterer et al., 1998; Engels et al., 2001), so that the resulting chimeric Vav1 proteins should bind the BCR. Constructs encoding Vav1, Vav1-Syk $[SH2]_2$, Vav1-SLP-65 SH2 or EGFP were expressed in Vav1-deficient DG75 cells and Ca^{2+}-mobilization was measured. The results show that Vav1-deficient DG75 cells expressing wild-type Vav1 or either of the chimeric proteins had an increased Ca^{2+}-mobilization compared to control cells (figure 4.10 B), even though cells expressing the Vav1-SLP-65 SH2 chimera showed a somewhat reduced Ca^{2+}-mobilization compared to cells reconstituted with wild-type Vav1. In contrast, Vav1-deficient DG75 cells expressing the Vav1-Syk $[SH2]_2$ chimera showed a dramatically enhanced Ca^{2+}-mobilization. Collectively, both chimeric proteins could restore Ca^{2+}-mobilization in Vav1-deficient DG75 cells albeit with different efficiencies.

To prove that the chimeric proteins can indeed bind the Igα/Igβ heterodimer, I tested their binding capability in affinity purification experiments. Therefore, I generated GST-fusion proteins consisting of the C-terminal adaptor region of Vav1 (hereafter referred to as C2) containing either the wild-type Vav1 SH2 or the SH2 domains of SLP-65 or Syk (figure 4.10 D). In addition, GST-only was used as negative control. Purified proteins were subjected to western blot analysis with antibodies to Igα, Igβ or GST, showing that all chimeric proteins could bind Igα as well as Igβ, except the negative controls (figure 4.10 E).

Taken together, I could show that Vav1 chimeric proteins containing other BCR-binding SH2-domains can functionally replace the Vav1 SH2-domain in the context of BCR-induced Ca^{2+}-mobilization. This indicates that Vav1 needs to be localized close to the BCR for efficient Ca^{2+}-mobilization.

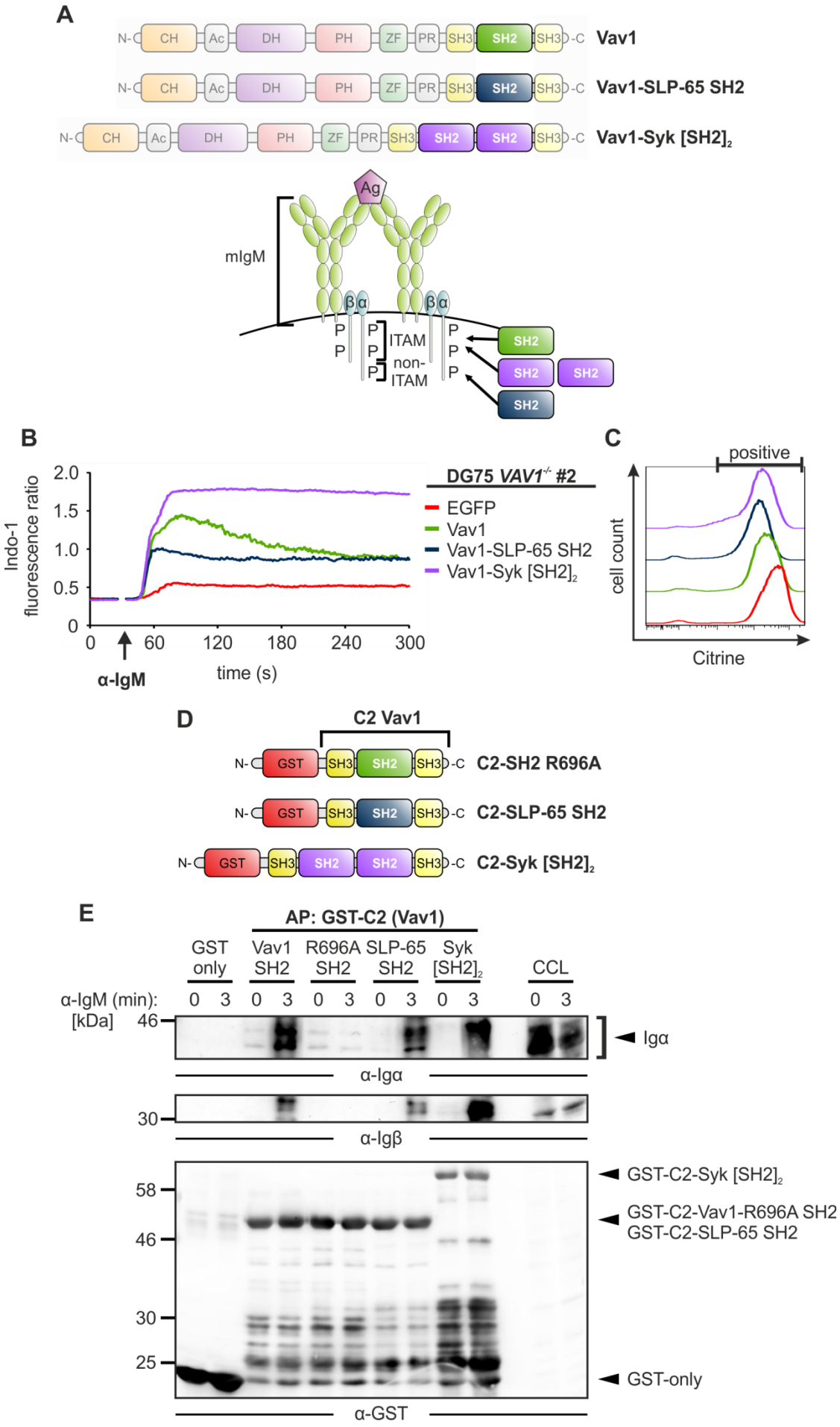
A
N-
CH
Ac
DH
PH
ZF
PR
SH3
SH2
SH3
-C
Vav1
Vav1-SLP-65 SH2
Vav1-Syk [SH2]2
Ag
mIgM
β α
P
ITAM
non-ITAM
B
Indo-1 fluorescence ratio
2.0
1.5
1.0
0.5
0
0
60
120
180
240
300
α-IgM
time (s)
DG75 VAV1-/- #2
EGFP
Vav1
Vav1-SLP-65 SH2
Vav1-Syk [SH2]2
C
positive
cell count
Citrine
D
C2 Vav1
GST
C2-SH2 R696A
C2-SLP-65 SH2
C2-Syk [SH2]2
E
AP: GST-C2 (Vav1)
GST only
Vav1 SH2
R696A SH2
SLP-65 SH2
Syk [SH2]2
CCL
α-IgM (min):
0 3 0 3 0 3 0 3 0 3 0 3
[kDa]
46
Igα
α-Igα
30
α-Igβ
58
46
30
25
GST-C2-Syk [SH2]2
GST-C2-Vav1-R696A SH2
GST-C2-SLP-65 SH2
GST-only
α-GST

Figure 4.10: BCR-binding SH2-domains can replace the Vav1 SH2-domain in the context of BCR-induced Ca^{2+}-mobilization. A) Schematic drawing of the domain architecture of Vav1 and the chimeric Vav1-SLP-65 SH2 and Vav1-Syk $[SH2]_2$ proteins. In addition, the binding capabilities of the individual SH2-domains are depicted, which can bind different phosphorylated tyrosines (P) in the cytoplasmic tails of Igα/Igβ. **B)** Vav1-deficient DG75 cells expressing Citrine-tagged wild-type Vav1, Vav1-SLP-65 SH2, Vav1-Syk $[SH2]_2$ or EGFP were analyzed for Ca^{2+}-mobilization upon BCR stimulation as before. The graph shows Ca^{2+}-mobilization of gated cells (positive gate (C)). Data show one representative example of three independent experiments. **C)** Expression levels of analyzed proteins were measured by flow cytometry. **D)** Domain architecture of the used GST-fusion proteins in affinity purifications. **E)** Affinity purifications with C2 regions of chimeric Vav1 proteins. DG75 cells were stimulated with 20 µg/ml α-IgM $F(ab')_2$ fragments for 3 min or left untreated. Cleared cellular lysates were used for affinity purification with GST-C2 Vav1, GST-C2 Vav1 SH2 R696A, GST-C2 Vav1-Syk $[SH2]_2$, GST-C2 Vav1-SLP-65 SH2 or GST-only. Samples were subjected to western blot analysis with anti-Igα, anti-Igβ and anti-GST antibodies as indicated. The molecular weight of marker proteins (in kDa) is indicated on the left. Data show one representative example of three independent experiments.

To further characterize the functional relevance of the Vav1-BCR interaction for Ca^{2+}-mobilization upon BCR stimulation, I generated an experimental system that combines the Vav1-SLP-65 SH2-chimera and a chimeric receptor consisting of the extracellular part of CD8 and the intracellular part of Igα (figure 4.11 A). The intracellular part of Igα contains the non-ITAM tyrosine (Y204), which is described as exclusive binding site for SLP-65 (Engels et al., 2001). Vice versa, The SLP-65 SH2-domain is described to bind primarily to the phosphorylated non-ITAM Y204 of Igα, so that binding of the Vav1-SLP-65 SH2 chimera to the CD8/Igα chimera can be selectively investigated and is supposed to resemble the interaction between the Vav1 SH2-domain and the BCR.

I first expressed CD8/Igα or CD8/Igα Y204F chimeric proteins in Vav1-deficient DG75 cells. Next, the resulting two cell lines were retrovirally transfected with constructs coding for wild-type Vav1, Vav1-SLP-65 SH2, Vav1-SLP-65 SH2 R372L or EGFP and Ca^{2+}-mobilization was measured upon stimulation of the CD8 chimeras with anti-CD8 antibodies. Figure 4.11 B shows that expression of Vav1 and Vav1-SLP-65 SH2 in Vav1-deficient DG75 cells led to Ca^{2+}-mobilization, which resembles the Ca^{2+}-mobilization signal of DG75 cells stimulated via the endogenous BCR (figure 4.10). This indicates that the chimeric receptor can mimic the endogenous BCR. The function of the chimeric Vav1-SLP-65 SH2-domain fusion protein relies on its SH2-domain since inactivation of the SH2-domain (Vav1-SLP-65 SH2 R372L) led to a Ca^{2+}-mobilization defect similar to Vav1-deficient DG75 cells (figure 4.11 B).

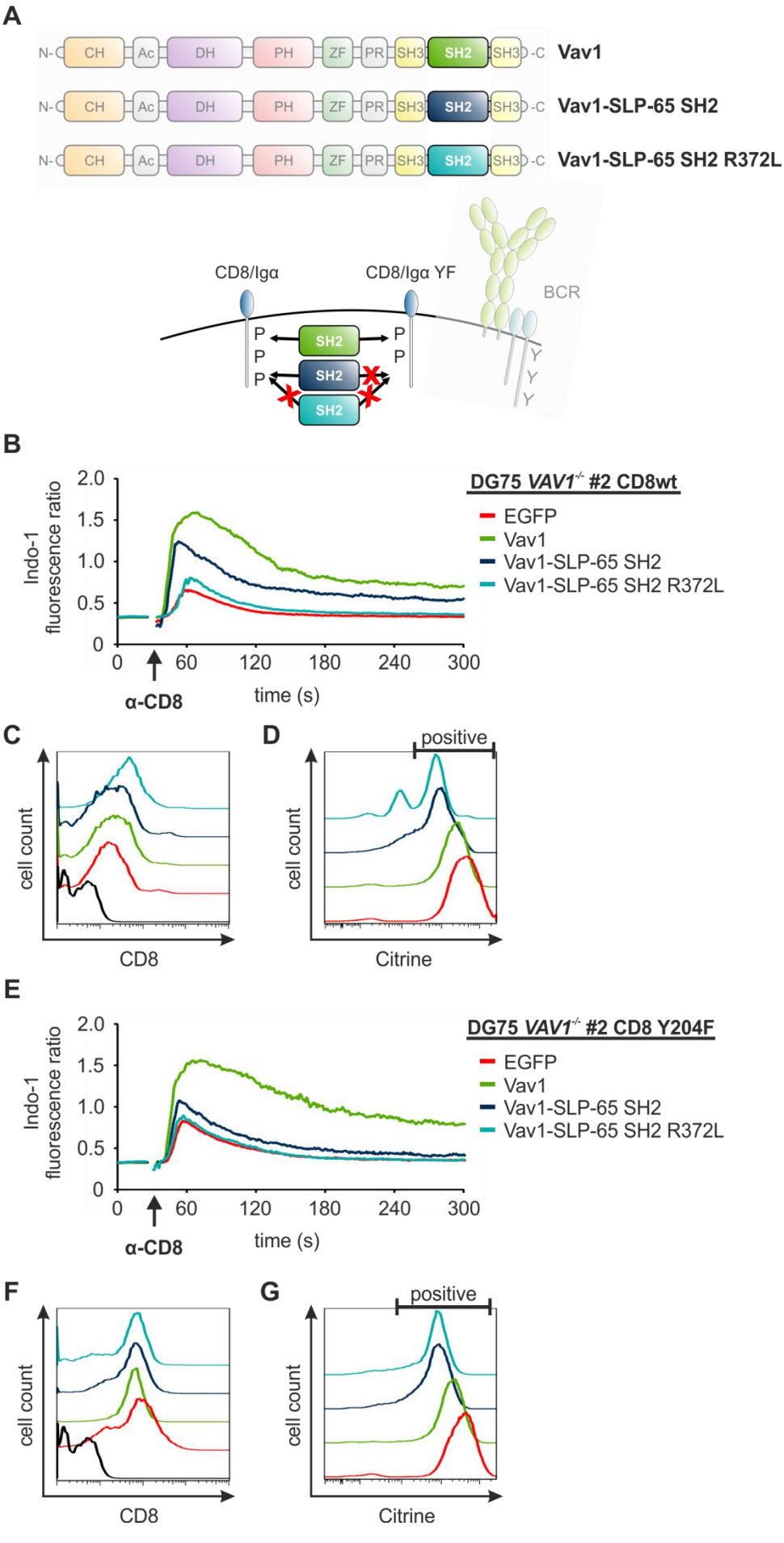
A
N-
CH
Ac
DH
PH
ZF
PR
SH3
SH2
SH3
-C
Vav1
Vav1-SLP-65 SH2
Vav1-SLP-65 SH2 R372L
CD8/Igα
CD8/Igα YF
BCR
P
Y
B
Indo-1 fluorescence ratio
2.0
1.5
1.0
0.5
0
0
60
120
180
240
300
time (s)
α-CD8
DG75 VAV1-/- #2 CD8wt
EGFP
Vav1
Vav1-SLP-65 SH2
Vav1-SLP-65 SH2 R372L
C
cell count
CD8
D
positive
cell count
Citrine
E
Indo-1 fluorescence ratio
time (s)
α-CD8
DG75 VAV1-/- #2 CD8 Y204F
EGFP
Vav1
Vav1-SLP-65 SH2
Vav1-SLP-65 SH2 R372L
F
cell count
CD8
G
positive
cell count
Citrine

Figure 4.11: Interaction of Vav1 with the BCR is sufficient for Vav1 function in Ca^{2+}-mobilization. A) Schematic drawing of the domain architecture of Vav1 and the chimeric Vav1-SLP-65 SH2 and Vav1-SLP-65 SH2 R372L proteins. In addition, the binding capability of the individual SH2-domains is depicted, which can bind different phosphorylated tyrosines (P) in the cytoplasmic tail of CD8/Igα or CD8/Igα Y204F. **B, E)** Vav1-deficient DG75 cells expressing CD8/Igα or CD8/Igα Y204 were retrovirally transfected with constructs coding for Citrine-tagged wild-type Vav1, Vav1-SLP-65 SH2, Vav1-SLP-65 SH2 R372L or EGFP and analyzed for Ca^{2+}-mobilization as before. Cells were stimulated with 10 µg/ml anti-human CD8 antibodies. The graph shows Ca^{2+}-mobilization of gated cells (positive gate (D, G)). One representative example of three independent experiments is shown. **C, D, F, G)** CD8 staining was performed with anti-human CD8-FITC antibodies and expression levels of analyzed proteins were determined by flow cytometry. Colour code is equivalent in B), C), D). The same is true for E), F), G).

Moreover, when cells expressed the CD8/Igα Y204F variant, only Vav1, which binds to phospho-ITAMs, could mobilize Ca^{2+} upon CD8 stimulation (figure 4.11 E). By contrast, the Vav1-SLP-65 SH2 chimera could not restore Ca^{2+}-mobilization, when its docking site, Y204, was inactivated. Collectively, I could show by mutational analysis that recruitment of Vav1 to phosphorylated BCR tyrosine residues enables BCR-induced Ca^{2+}-mobilization.

4.3 The interaction between Vav1 and SLP-65 permits BCR-induced Ca^{2+}-mobilization

4.3.1 Generation of a SLP-65-deficient DG75 sub-line

The previously described results of my PhD thesis show an important function of Vav1 in BCR-induced Ca^{2+}-mobilization. Furthermore, I could show an interaction between Vav1 and the BCR, which is sufficient for Vav1 to function in the context of Ca^{2+}-mobilization upon BCR stimulation in DG75 B cells. Besides this novel signaling mechanism, SLP-65 was reported to be involved in Vav1 localization and function (Johmura et al., 2003). The interaction between Vav1 and SLP-65 is mediated by the SH2-domain of Vav1 (figure 4.8, chapter 4.2.1), which is supposed to bind tyrosine 72 of human SLP-65 based on the results by the group of Andrew Chan (Chiu et al., 2002). However, the Vav1 SH2-domain is able to bind a diverse set of tyrosine-phosphorylated proteins upon BCR stimulation (figure 4.8, chapter 4.2.1), so that Vav1 with a non-functional SH2-domain loses interaction to many proteins and thus is not conclusive. To be able to investigate specifically the Vav1-SLP-65 interaction, I generated a SLP-65-deficient DG75 sub-line to have a genetic model system for the analysis of SLP-65 variants.

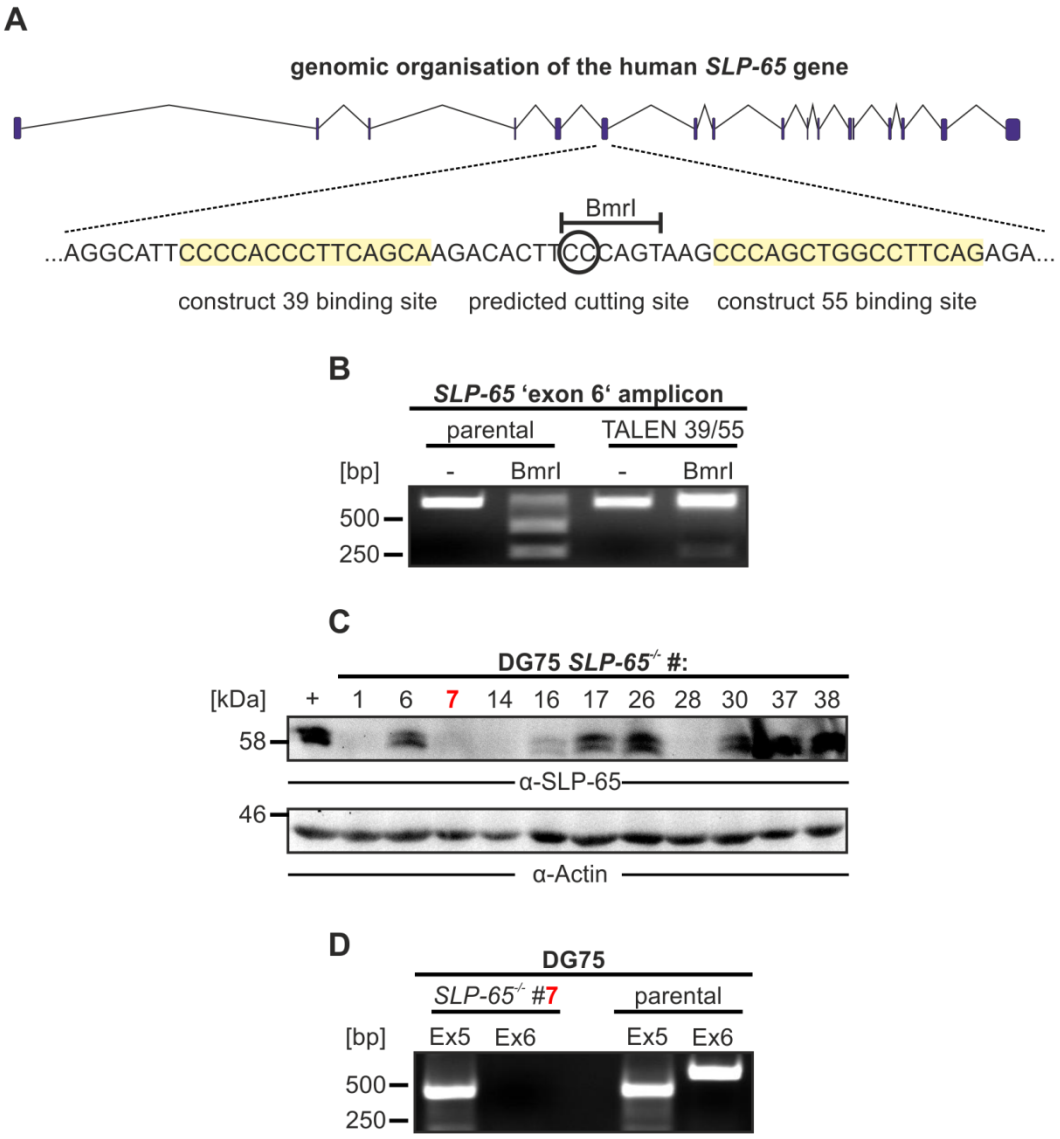

Figure 4.12: Generation of a SLP-65-deficient DG75 sub-line. A) Schematic drawing of the genomic organization of the *SLP-65* gene indicating the TALEN target region. **B)** To test the activity of the TALEN constructs, the genomic region containing the targeted *SLP-65* exon 6 was amplified by PCR from DG75 cells that had been transiently transfected with TALEN constructs 39 and 55 and sorted. The PCR product was cut with the restriction enzyme BmrI, whose binding site overlaps with the TALEN target site and therefore can be used for TALEN activity testing. **C)** Screening of DG75 cell clones for SLP-65 deficiency was done using western blot analysis. Cleared cellular lysates of $1x10^6$ DG75 cells were loaded per lane and separated by SDS-PAGE. Immunoblots were probed with anti-SLP-65 and anti-Actin antibodies as indicated below the individual blots. Cleared cellular lysates of DG75 cells served as positive control (+). The molecular weight of marker proteins (in kDa) is indicated on the left. **D)** Characterization of the SLP-65-deficient DG75 clone #7. The genomic region containing exon 6 of the SLP-65-deficient DG75 cell clone #7 could not be amplified by PCR for further genomic characterization. To test PCR conditions, I amplified the *SLP-65* exon 5 genomic region by PCR to prove the quality of the genomic DNA template and I amplified the *SLP-65* exon 6 genomic region by PCR from parental, genomic DNA.

To this end, a TALEN pair was constructed to target exon 6 of the human *SLP-65* gene located on chromosome 10 (figure 4.12 A). Exon 6 was chosen as target region, because it is present in all described protein coding SLP-65 mRNAs (based on Ensembl data base) and it showed a good availability of restriction enzyme sites for later activity screening. Transient transfection of TALEN constructs, cell sorting, activity test and subsequent sub-cloning was performed as before (see chapter 4.1.1). Resulting cell clones were screened for SLP-65 protein expression by western blot with anti-SLP-65 antibodies. Figure 4.12 C shows no detectable SLP-65 signal in cell clones #1, #7, #14 and #28 indicating that the TALEN pair 39/55 was active in these cell clones. In addition, a decreased SLP-65 signal compared to parental DG75 cells was detected in cell clones #6, #16 and #17.

To characterize the SLP-65-deficient DG75 clone #7 genetically, I amplified the exon 6 containing genomic region (referred to as 'exon 6') of *SLP-65* via PCR for subsequent cloning and sequencing. However, despite of using different primer pairs, amplification of the 'exon 6' was not successful. To test the PCR conditions, I amplified the genomic region of *SLP-65* exon 5 to prove the quality of the genomic DNA template. In addition, I amplified the 'exon 6' of *SLP-65* from genomic DNA of parental cells. Both controls showed optimal PCR results (figure 4.12 D). In conclusion, the TALEN targeting of *SLP-65* exon 6 in clone #7 led to a genomic deletion that includes surrounding intron regions and thus interfered with primer annealing and PCR amplification of 'exon 6'. At any rate, based on western blot analysis and PCR-assays, DG75 cell clone #7 was considered a SLP-65-deficient sub-line and was used in the following experiments. It is hereafter referred to as SLP-65-deficient DG75 cells.

4.3.2 SLP-65 is essential for BCR-induced Ca^{2+}-mobilization in DG75 cells

Previous experiments of several laboratories including our group have established an essential function of SLP-65 in Ca^{2+}-mobilization in murine B cells and the chicken DT40 cell line (Fu et al., 1998; Jumaa et al., 1999; Chiu et al., 2002). In accordance with these results, SLP-65-deficient DG75 cell clones showed a decreased Ca^{2+}-mobilization signal compared to parental DG75 cells (figure 4.13 A). Reconstitution of SLP-65-deficient DG75 cells with wild-type SLP-65 fully restored BCR-induced Ca^{2+}-mobilization and thus proved that the Ca^{2+}-mobilization defect in the knock out cells was due to the lack of SLP-65 expression (figure 4.13 C).

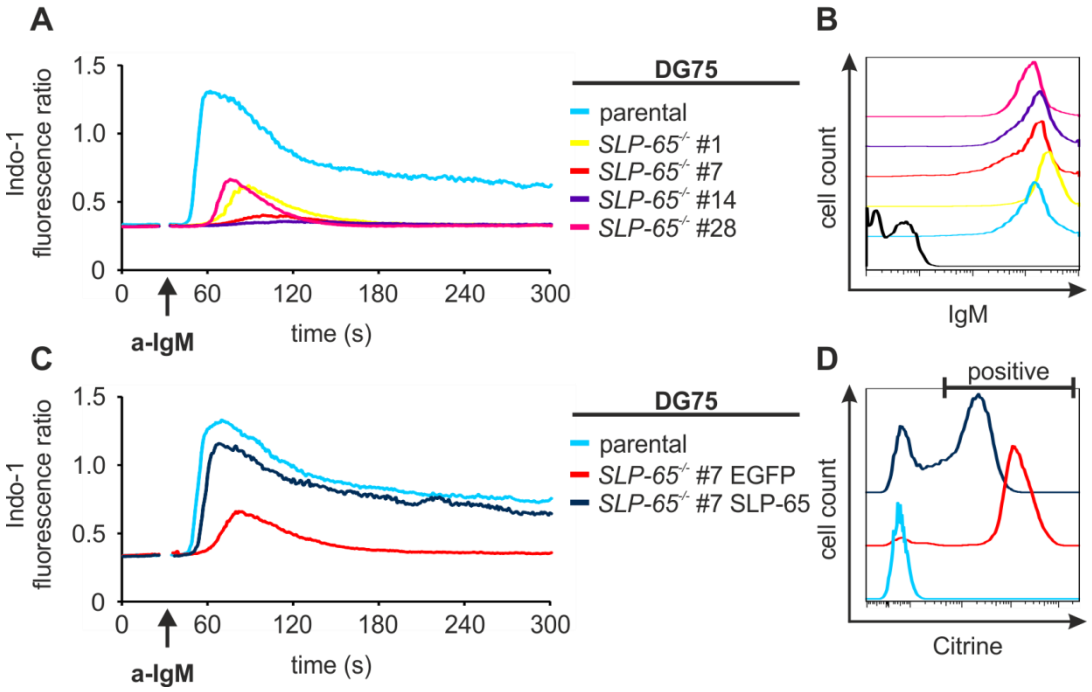

Figure 4.13: Human SLP-65 has a pivotal role in Ca^{2+}-mobilization upon BCR stimulation. A) Parental DG75 as well as SLP-65-deficient cell clones #1, #7, #14 and #28 were analyzed for Ca^{2+}-mobilization upon BCR stimulation as before. The graph is representative of three independent experiments. **B)** Expression levels of BCRs were measured by flow cytometry. Surface staining was done using anti-human IgM-APC antibodies. Unstained cells are depicted in black. Samples have the same color code as in A). **C)** SLP-65-deficient DG75 cells expressing Citrine-tagged wild-type SLP-65 were analyzed for Ca^{2+}-mobilization as before. Parental DG75 cells and SLP-65-deficient EGFP-expressing cells were used as positive and negative control, respectively. The graph shows Ca^{2+}-mobilization of gated cells (positive gate (B)) and it is representative of three independent experiments. **D)** Expression levels of analyzed proteins were determined by flow cytometry.

4.3.3 SLP-65 tyrosines 72, 84 and 119 are important for its function in BCR-induced Ca^{2+}-mobilization

The 3D structure of SLP-65 is not completely defined. The N-terminus is predicted to bind phospho-lipids of membranes (Herrmann, 2009), whereas the C-terminus contains a phospho-tyrosine binding SH2-domain. The center of SLP-65 is described as principally unstructured (Pirkuliyeva, 2015) and contains a number of tyrosines that on phosphorylation can serve as docking sites for proteins like Btk (Y96) and PLCγ2 (Y84, Y119, Y178 and Y189) (Chiu et al., 2002; Engelke et al., 2013). Importantly, SLP-65 tyrosine 72 (Y72) was described to be the interaction site for Vav1 (Chiu et al., 2002).

To analyze whether Vav1-SLP-65 binding is indeed mediated by Y72, I checked the binding capability of Vav1 to several tyrosine-to-phenylalanine (YF) mutant variants of SLP-65 (SLP-65 Y72F, Y84F, Y119F, Y72/84F and Y72/119F) in affinity purification

experiments with the Vav1 SH2-domain. Purified proteins were subjected to western blot analysis with anti-SLP-65 antibodies. Each SLP-65 YF variant could be bound by the GST-Vav1 SH2-domain (figure 4.14 A, B), although binding was reduced compared to wild-type SLP-65. SLP-65 Y72F and SLP-65 Y84F showed the weakest interaction with the Vav1 SH2-domain. Furthermore, the Vav1 SH2-domain was still able to interact with double YF variants of SLP-65, with SLP-65 Y72/84F showing the weakest interaction. Collectively, the tyrosines 72, 84 and 119 of SLP-65 showed impaired binding of Vav1. However, a complete loss of SLP-65 binding by Vav1 could not be detected, so that I assume that Vav1 has the ability to bind more than one phosphorylated tyrosine of SLP-65.

Next, I tested the functional importance of the interaction between Vav1 and SLP-65 for BCR-induced Ca^{2+}-mobilization. Each SLP-65 YF variant was able to mobilize Ca^{2+} after BCR stimulation, yet to different extents, which in any case did not reach the level of cells expressing wild-type SLP-65 (figure 4.14 C, E). The strongest decrease in Ca^{2+}-mobilization was seen in cells expressing the SLP-65 Y119F variant. In comparison, Ca^{2+}-mobilization in SLP-65-deficient DG75 cells expressing either the SLP-65 Y72F or the SLP-65 Y84F variant was only marginally reduced.

Furthermore, SLP-65 Y72/84F and SLP-65 Y72/119F double mutant variants were investigated. Here, in addition to the substitution of tyrosine 72, also tyrosine 84 or tyrosine 119 were substituted with phenylalanine. Both SLP-65 double YF-mutant variants showed a reduced Ca^{2+}-mobilization compared to the SLP-65 Y72F single mutant variant (figure 4.14 C, E). In conclusion, I could show that the SLP-65 tyrosines 72, 84 and 119 are involved in BCR-induced Ca^{2+}-mobilization. In addition, each tyrosine might interact with a specific protein indicated by the additive effect in Ca^{2+}-mobilization upon BCR stimulation.

Taken together, Vav1 binding to SLP-65 YF-mutant variants correlates to the signaling competence of these variants in BCR-induced Ca^{2+}-mobilization. However, whether the reduced Ca^{2+}-mobilization of cells expressing individual YF-mutant SLP-65 variants depends exclusively on the reduced interaction between Vav1 and SLP-65, needs to be unraveled.

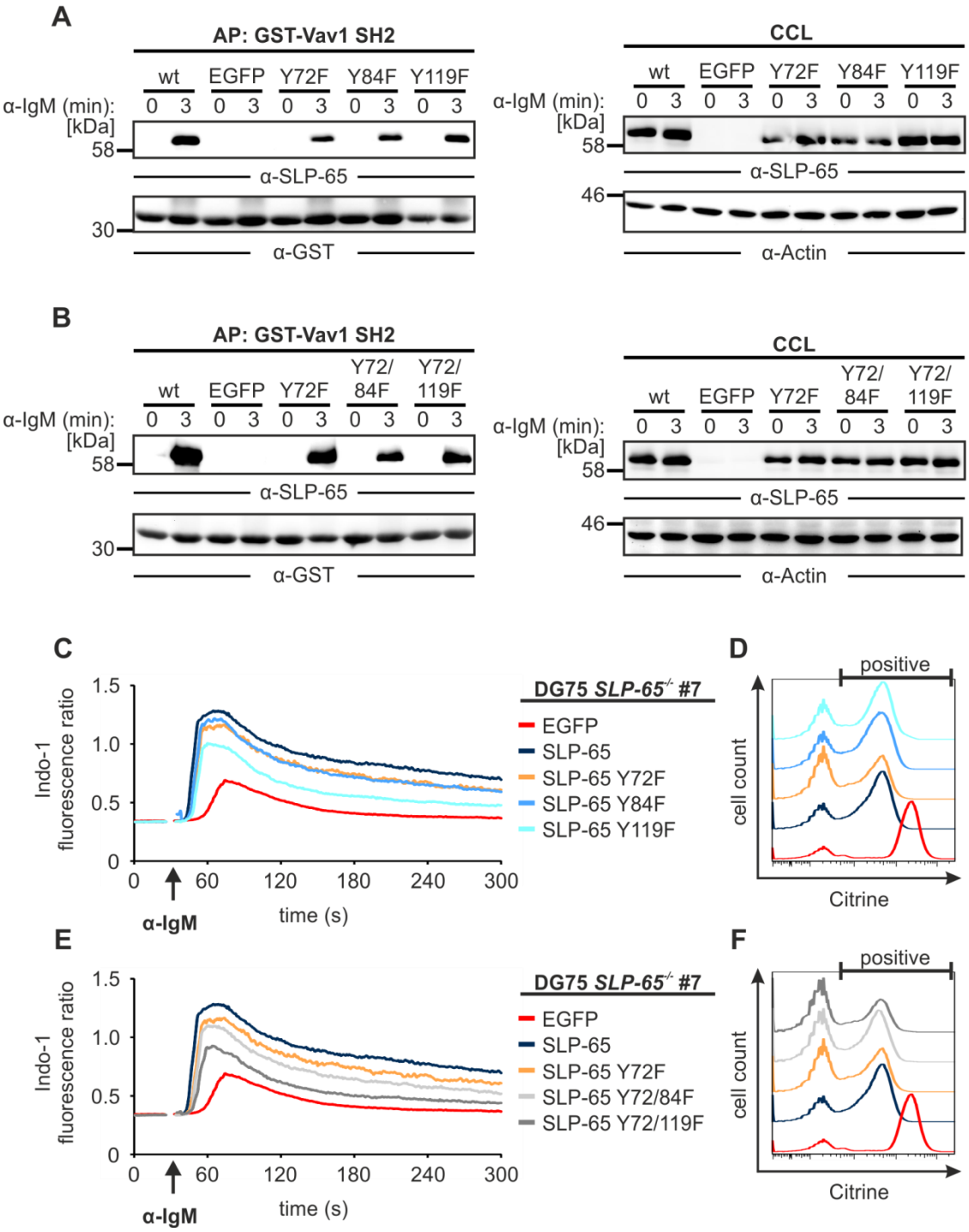

Figure 4.14: Phosphorylation of several SLP-65 tyrosines is important for BCR-induced Vav1 binding and Ca^{2+}-mobilization. A, B) Cells were stimulated with 20 µg/ml α-IgM $F(ab')_2$ fragments for 3 min or left untreated. SLP-65 YF-mutant variants were affinity purified from cleared cellular lysates using the GST-Vav1 SH2-domain. Samples were subjected to western blot analysis with anti-SLP-65, anti-Actin and anti-GST antibodies as indicated. The molecular weight of marker proteins (in kDa) is indicated on the left. Data show one representative example of three independent experiments. **C, E)** SLP-65-deficient DG75 cells expressing Citrine-tagged wild-type SLP-65, SLP-65 Y72F, SLP-65 Y84F, SLP-65 Y119F, SLP-65 Y72/84F, SLP-65 Y72/119F or EGFP were analyzed for Ca^{2+}-mobilization upon BCR stimulation as before. The graph shows Ca^{2+}-mobilization of gated cells (positive gate (D, F)). Data show one representative result of three independent experiments. **D, F)** Expression levels of analyzed proteins were determined by flow cytometry.

4.3.4 Recruitment of Vav1 to SLP-65 enables BCR-induced Ca^{2+}-mobilization.

Due to the fact, that I could not generate a variant of SLP-65 that selectively lost its interaction with Vav1, it remained unclear whether the Vav1-SLP-65 interaction is important for BCR-induced Ca^{2+}-mobilization. To check the functional relevance of this protein-protein interaction, chimeric Vav1 proteins were designed containing the SH2-domain of either Btk or Itk instead of the Vav1 SH2-domain and expressed in Vav1-deficient DG75 cells (figure 4.15 A). These SH2-domains are described to bind SLP-65 at tyrosine 96 (Y96) (Su et al., 1999).

Figure 4.15 B shows a slightly increased Ca^{2+}-mobilization in cells expressing the Vav1-Btk SH2-chimera compared to EGFP-expressing control cells (figure 4.15 B). In contrast, the Vav1-Itk SH2-chimera led to a significantly higher Ca^{2+}-mobilization even though it did not reach the level of cells expressing wild-type Vav1 (figure 4.15 B). These results show that the recruitment of Vav1 to SLP-65 enabled BCR-induced Ca^{2+}-mobilization. In addition, the different extent of Ca^{2+}-mobilization indicates that the binding affinities of the Btk and Itk SH2-domains to phospho-tyrosine 96 in SLP-65 might differ.

To test whether the chimeric Vav1 proteins can indeed bind phospho-SLP-65, affinity purifications were performed using GST-fusion proteins consisting of the C-terminal adaptor region (referred to as C2) containing the different SH2-domains of Btk or Itk (figure 4.15 D). The results show that each of the GST-fusion proteins could bind to the adaptor protein SLP-65 although with different affinity. In detail, the GST-fusion protein containing the wild-type C2 region of Vav1 showed the strongest interaction with phospho-SLP-65, followed by the C2 region containing the SH2-domain of Itk. On the contrary, affinity purification performed with the C2-Btk SH2 region showed only a weak SLP-65 interaction. This suggests that the affinity of the interaction between Vav1 and SLP-65 regulates the intensity of BCR-induced Ca^{2+}-mobilization. Note that only the wild-type C2 region of Vav1 could bind to the Igα protein of the BCR, which might explain why this protein gives rise to the strongest Ca^{2+}-signal (figure 4.15 E).

In summary, the association of Vav1 and the adaptor protein SLP-65 enables BCR-induced Ca^{2+}-mobilization even if no direct interaction of Vav1 with the BCR is possible.

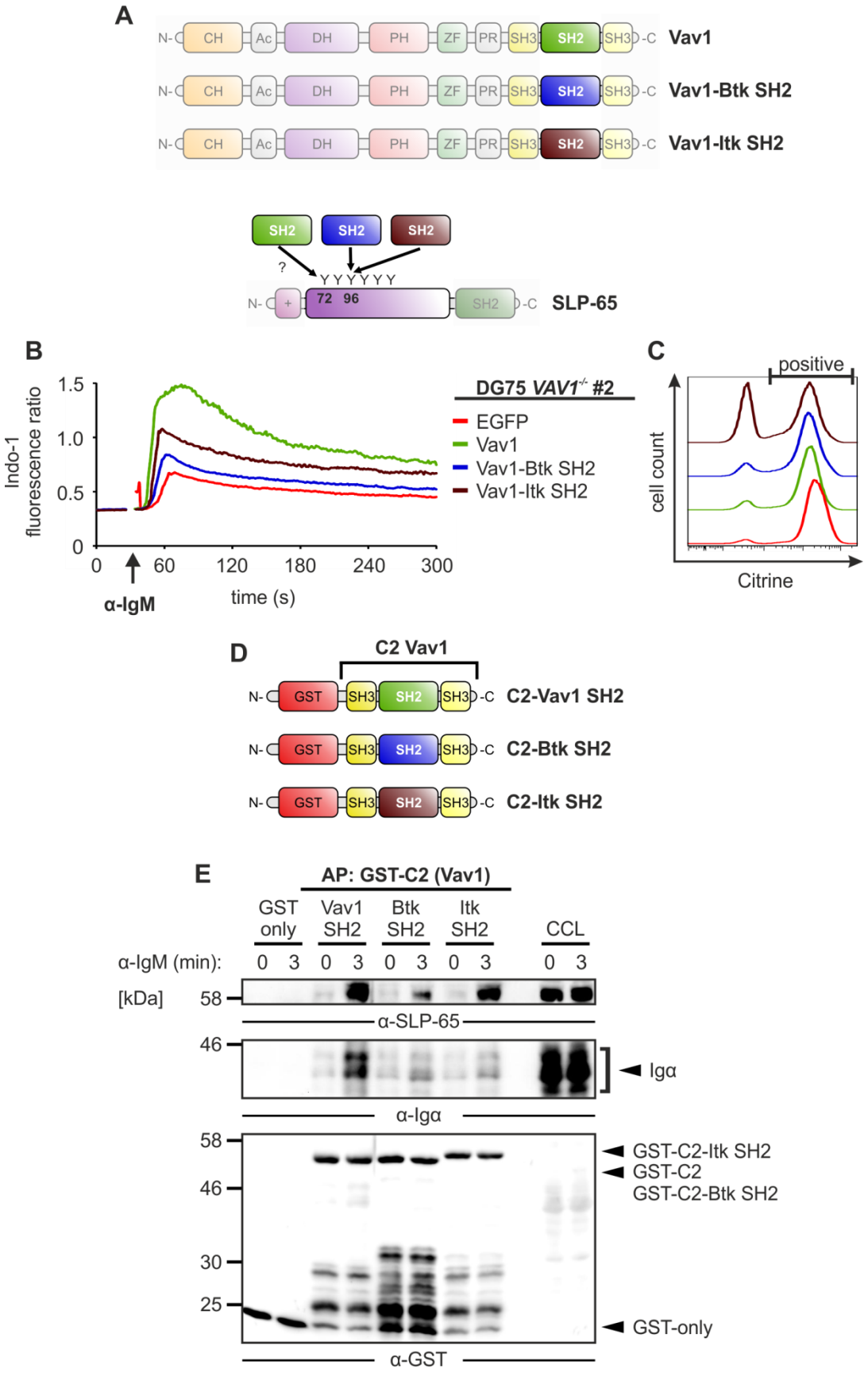

Figure 4.15: The interaction between Vav1 and SLP-65 enables Ca^{2+}-mobilization upon BCR stimulation. A) Schematic drawing of Vav1 SH2-chimeras and their binding sites in SLP-65. **B)** Vav1-deficient DG75 cells expressing Citrine-tagged wild-type Vav1, Vav1-Btk SH2, Vav1-Itk SH2 or EGFP were

analyzed for Ca^{2+}-mobilization upon BCR stimulation as before. The graph shows Ca^{2+}-mobilization of gated cells (positive gate (C)). Data show one representative example of three independent experiments. **C)** Expression levels of analyzed proteins were determined by flow cytometry **D)** Schematic structure of the GST-fusion proteins used in affinity purifications. **E)** Affinity purifications with C2 regions from chimeric Vav1 proteins. DG75 cells were stimulated with 20 µg/ml α-IgM $F(ab')_2$ fragments for 3 min or left untreated. SLP-65 was affinity purified with GST-C2 Vav1, GST-C2 Vav1-Btk SH2, GST-C2 Vav1-Itk SH2 or GST-only. Samples were subjected to western blot analysis with anti-Igα, anti-SLP-65 and anti-GST antibodies as indicated. The molecular weight of marker proteins (in kDa) is indicated on the left. Data show one representative example of three independent experiments.

4.3.5 CD19-mediated Vav1 recruitment is not involved in BCR-induced Ca^{2+}-mobilization

Besides the interactions between Vav1 and the BCR as well as Vav1 and SLP-65, a SH2-domain-mediated interaction of Vav1 with the co-stimulatory B cell receptor CD19 is well established (O'Rourke et al., 1998). However, it remains unclear if the Vav1-CD19 interaction is important in the context of BCR-induced Ca^{2+}-mobilization.

To address this question, a CD19-negative population of DG75 cells that was isolated by repeated cell sorting (N. Engels, unpublished) was analyzed for Ca^{2+}-mobilization upon BCR stimulation. Figure 4.16 A shows that CD19-negative DG75 cells had a BCR-induced Ca^{2+}-mobilization, which resembled that of parental DG75 cells. In conclusion, CD19 is not involved in BCR-induced Ca^{2+}-mobilization, which indicates that the Vav1-CD19 interaction is not important in that context.

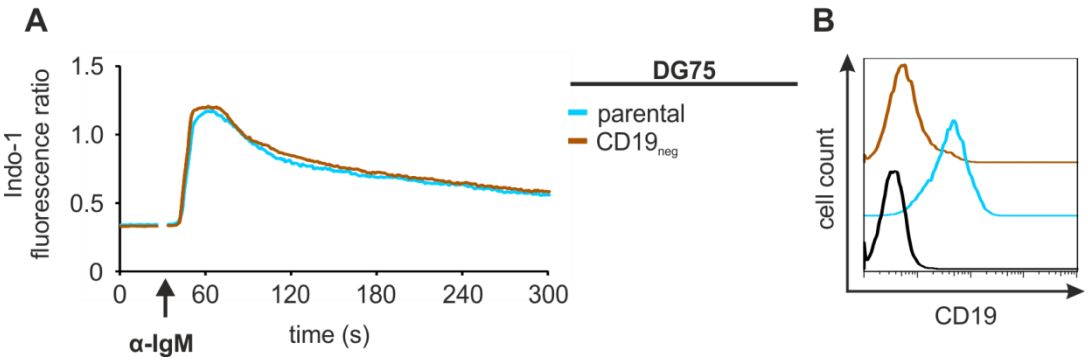

Figure 4.16: CD19 is not involved in Ca^{2+}-mobilization upon BCR stimulation. A) Parental DG75 cells as well as CD19-negative cells were analyzed for Ca^{2+}-mobilization upon BCR stimulation as before. Data show one representative example of three independent experiments. **B)** Surface expression levels of CD19 on the cells analyzed in A) were measured by flow cytometry. Surface staining was done using anti-human CD19-PE antibodies. Unstained cells are depicted in black. Samples have the same color code as indicated in figure A).

4.4 The structural integrity of the DH-PH-ZF-domain unit of Vav1 is essential for BCR-induced Ca^{2+}-mobilization

4.4.1 The Vav1 DH-domain is critical for Vav1 function in the context of BCR-induced Ca^{2+}-mobilization

In the previous chapters, I focused on the identification of functionally important interaction partners of Vav1 and its connection to the BCR signalosome. However, it remains to be elucidated, which functions Vav1 fulfills in Ca^{2+}-mobilization upon BCR stimulation. The best studied function of Vav1 is its GEF activity for the Rho family of small G-proteins (Movilla et al., 2001; Zugaza et al., 2002; Palmby et al., 2004). Activation of small G-proteins results most commonly in cell growth and proliferation (Tybulewicz and Henderson, 2009). In B cells, it is not known if the Vav1 GEF function is involved in BCR-induced Ca^{2+}-mobilization.

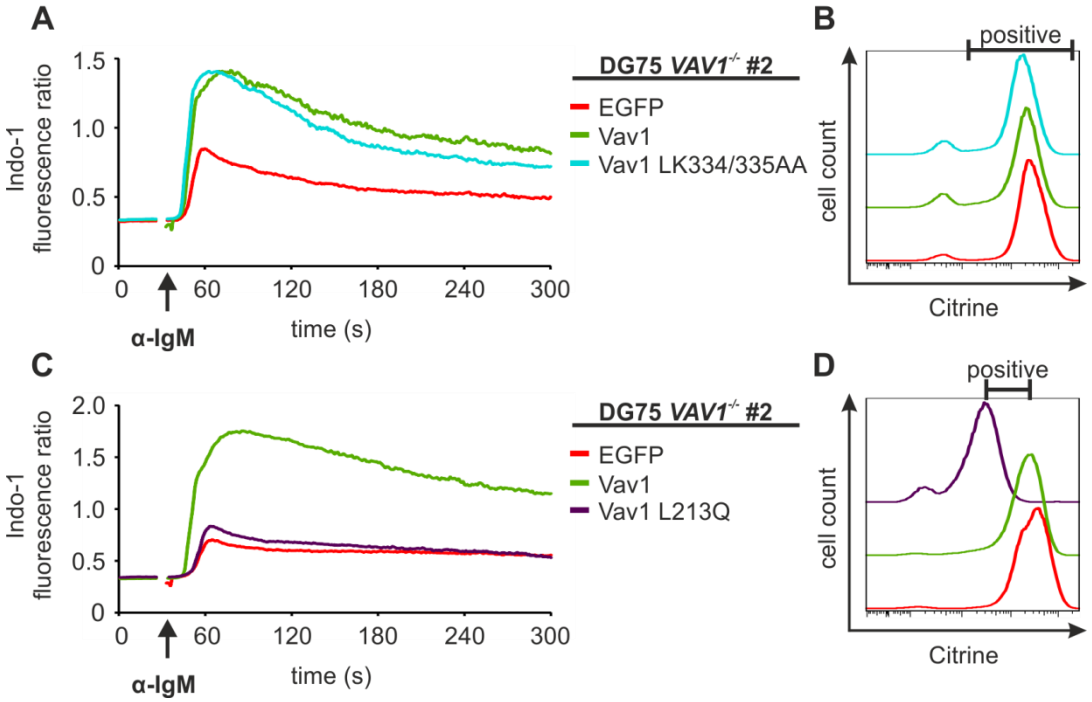

Figure 4.17: The structural integrity of the Vav1 DH-domain is crucial for BCR-induced Ca^{2+}-mobilization. A, C) Vav1-deficient DG75 cells expressing Citrine-tagged wild-type Vav1, Vav1 LK334/335AA, Vav1 L213Q or EGFP were analyzed for Ca^{2+}-mobilization upon BCR stimulation as before. The graph shows Ca^{2+}-mobilization of gated cells (positive gate in (B D)). Data show one representative example of three independent experiments. **B, D)** Expression levels of analyzed proteins were determined by flow cytometry.

To address this question, I generated two Vav1 variants with non-functional DH-domains based on previous publications. One Vav1 variant carries two amino acid substitutions, leucine-to-alanine at position 334 and lysine-to-alanine at position 335 (LK334/335AA),

that are located directly in the active center of the DH-domain without affecting its structural integrity (Saveliev et al., 2009). The other Vav1 variant contains a leucine-to-glutamine substitution at amino acid position 213 (L213Q) that is located away from the active center and is affecting the overall structure of the DH-domain (Zugaza et al., 2002). The Vav1 mutant variants were expressed in Vav1-deficient DG75 cells and BCR-induced Ca^{2+}-mobilization was measured. Figure 4.17 A shows that Ca^{2+}-mobilization was fully restored in cells expressing the Vav1 LK334/335AA variant. Hence, Vav1 DH-domain GEF activity is most likely not involved in BCR-induced Ca^{2+}-mobilization. In contrast, the Vav1 L213Q variant failed to restore Ca^{2+}-mobilization (figure 4.17 C). Derived from these results, the structural integrity of the Vav1 DH-domain appears to be essential for BCR-induced Ca^{2+}-mobilization in the human DG75 B cell line, whereas the catalytic GEF activity of the DH-domain seems to be dispensable in that process.

4.4.2 The DH-domain is not involved in plasma membrane recruitment of Vav1

Even though I could show that the structural integrity of the Vav1 DH-domain is important for BCR-induced Ca^{2+}-mobilization, it remained unknown what function the Vav1 DH-domain fulfills in BCR signaling. Since GEF activity might be excluded as possible function (see chapter 4.4.1), I investigated whether plasma membrane recruitment via specific binding partners could be a possible function. The small G-protein Rac1 is a well described interaction partner for the Vav1 DH-domain (Zugaza et al., 2002; Broun et al., 2007). Rac1 contains a so-called CAAX box at its C-terminus, which is responsible for Rac1 plasma membrane targeting via fatty acid modification (Roberts et al., 2008). Hence, Vav1 plasma membrane recruitment could be mediated through binding of the Vav1 DH-domain to plasma membrane attached Rac1.

To test this hypothesis, I generated a chimeric construct containing Vav1 fused to the N-terminus of Rac1. This construct was expressed in Vav1-deficient DG75 cells to analyze its localization and plasma membrane recruitment upon BCR stimulation using confocal microscopy. Figure 4.18 A shows that the Vav1-Rac1 chimeric protein was preferentially localized in the cytoplasm of DG75 cells. Only a small proportion of the chimeric protein was localized at the plasma membrane. Upon BCR stimulation, the Vav1-Rac1 chimera translocated from the cytoplasm to the plasma membrane. In contrast, plasma membrane translocation was not observed for wild-type Vav1 (data not shown). Hence, fusion of Rac1 to the C-terminus of Vav1 enhances its plasma membrane translocation.

Next, I investigated the Vav1-Rac1 chimera in the context of a functional or a non-functional DH-domain in Ca^{2+}-mobilization upon BCR stimulation. To this end, I inactivated the DH-domain in the Vav1-Rac1 chimera by introducing the L213Q mutation (Vav1 L213Q-Rac1). Figure 4.18 B shows that the Vav1-Rac1 chimeric protein was able to restore Ca^{2+}-mobilization in Vav1-deficient DG75 cells, whereas the L213Q-mutant chimera was non-functional.

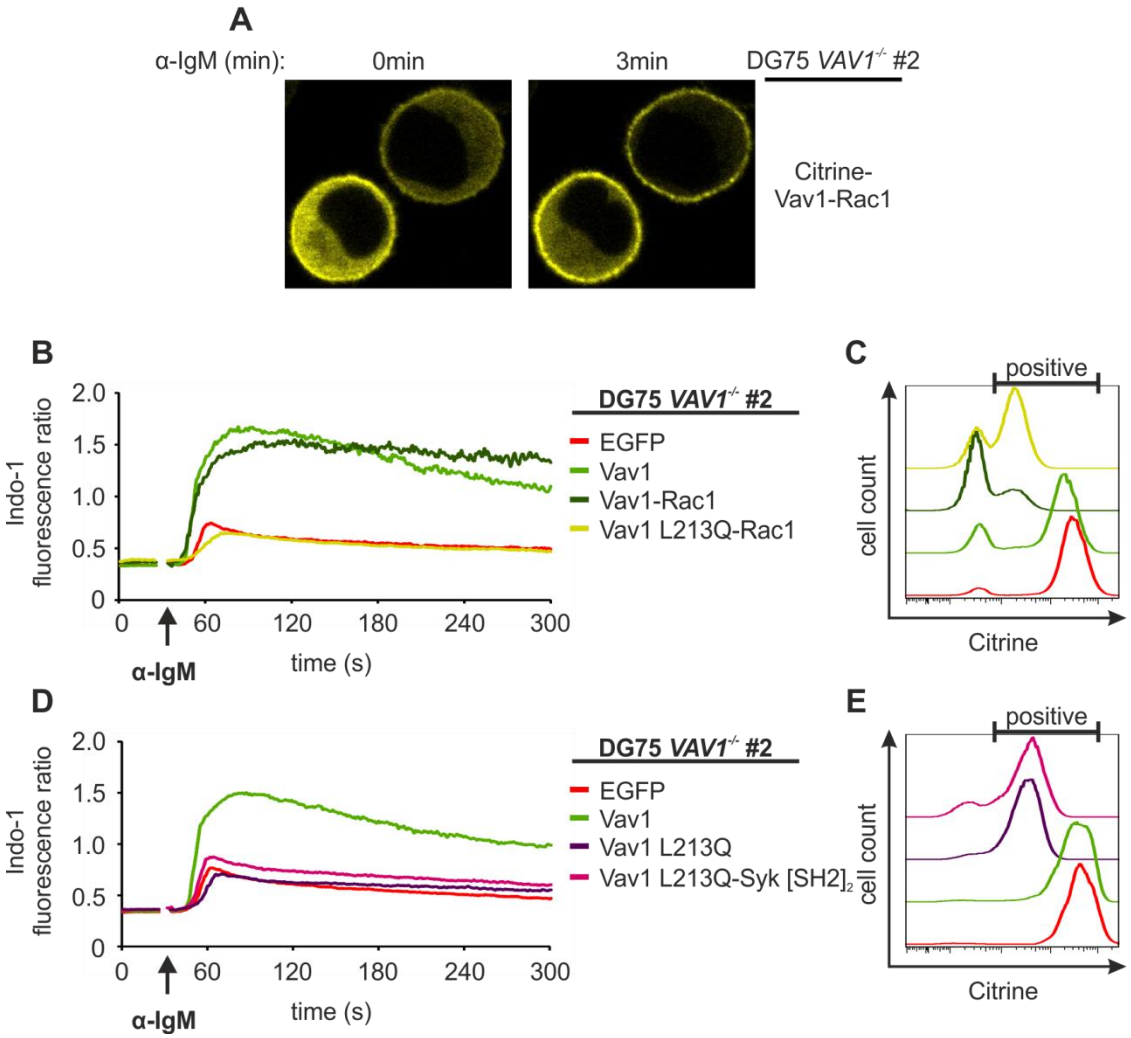

Figure 4.18: The DH-domain does not mediate the translocation of Vav1 to the plasma membrane. A) Confocal microscopy of Vav1-deficient DG75 cells expressing a N-terminally Citrine-tagged Vav1-Rac1 chimera. Images were taken before and 3 min after stimulation with 20 µg/ml α-IgM $F(ab')_2$ fragments. The data show one representative example of two independent experiments. **B, D)** Vav1-deficient DG75 cells expressing either Citrine-tagged wild-type Vav1, Vav1-Rac1, Vav1 L213Q, Vav1 L213Q-Syk $[SH2]_2$, Vav1 L213Q-Rac1 or EGFP were analyzed for Ca^{2+}-mobilization upon BCR stimulation as before. The graph shows Ca^{2+}-mobilization of gated cells (positive gate (C, E)). Data show one representative example of three independent experiments. **C, E**) Expression levels of analyzed proteins were determined by flow cytometry.

To further elucidate the role of the Vav1 DH-domain in translocation processes, I generated another Vav1 chimera containing the L213Q substitution as well as the tandem

SH2-domains of Syk instead of the Vav1 SH2-domain. The Syk SH2-domains mediate strong binding to the BCR and lead in the context of the Vav1 protein to increased BCR-induced Ca^{2+}-mobilization (see chapter 4.2.2). The constructs were expressed in Vav1-deficient DG75 cells and Ca^{2+}-mobilization was measured. Figure 4.18 D shows that the Vav1 L213Q-Syk-$[SH2]_2$ variant was not able to mobilize more Ca^{2+} than Vav1-deficient cells upon BCR stimulation. This indicates, that the positive effect of the tandem SH2-domains of Syk within the Vav1 protein cannot rescue the function of the DH-domain. In conclusion, plasma membrane recruitment can be excluded as possible function of the Vav1 DH-domain in the context of Ca^{2+}-mobilization.

4.4.3 DH-domain surrounding regions of Vav1 influence its Ca^{2+}-promoting function

In addition to the DH-domain itself, other regions of Vav1 were described to influence the function and stability of the DH-domain. Structural analyses of Chrencik et al. revealed that the N-terminally located CH domain as well as the acidic region between the CH and DH-domains of Vav1 adopt a specific protein folding that is described as inhibitory loop. This regulates Vav1 GEF activity on the one hand by blocking the active center of the DH-domain and on the other hand by structural stabilization of the DH-domain (Chrencik et al., 2008). The ZF-domain of Vav1 has a contact interface with the Vav1 DH-domain (Chrencik et al., 2008). Mutations inside the ZF-domain impair GEF activity of Vav1 (Zugaza et al., 2002). This indicates a ZF-domain-mediated structural stabilization of the DH-domain, since the mutations inside the Zn-finger are far away from the Vav1 catalytic center.

To test the importance of the ZF-domain in BCR-induced Ca^{2+}-mobilization, I generated Vav1 variants containing different mutations inside the Zn-finger, glutamine-to-alanine and tyrosine-to-alanine at positions 542 and 544, respectively. These were described to lead to a loss of Vav1-mediated Rac1 activation (Zugaza et al., 2002). The constructs were expressed in Vav1-deficient DG75 cells and Ca^{2+}-mobilization was measured. Figure 4.19 A shows that both Vav1 Q542A and Vav1 Y544A severely affected Ca^{2+}-mobilization. These results are in line with previous results of the Vav1 L213Q variant (see chapter 4.4.1) that showed the importance of a structurally intact Vav1 DH-domain in BCR signaling.

The acidic amino acid region between the CH and the DH-domain of Vav1 contains three specific tyrosines (Y142 ,Y160 ,Y172) that are reported to inhibit DH-domain by blocking its active center (Zugaza et al., 2002; Chrencik et al., 2008). Upon phosphorylation of

these tyrosines, the so-called inhibitory loop loosens up and Vav1 GEF activity increases. To test, if the deletion of the acidic region has an influence on Vav1's function in BCR-induced Ca^{2+}-mobilization, I generated a Vav1 variant that lacks the acidic stretch including the three inhibitory tyrosines (ΔAR Vav1, figure 4.19 C). Figure 4.19 D shows that this ΔAR Vav1 variant led to an increased Ca^{2+}-mobilization compared to control cells. Given that the Vav1 GEF activity was not involved in BCR-induced Ca^{2+}-mobilization (see chapter 4.4.1), the increased Ca^{2+}-mobilization in cells expressing the ΔAR Vav1 variant might be a result of a better accessibility of the DH-domain for effector proteins. However, since interactions with small G-proteins appear to be transient and could not be detected in affinity purification experiments (data not shown), it remains unclear whether binding of small G-proteins is the task of the Vav1 DH-domain that allows Ca^{2+}-mobilization in human B cells.

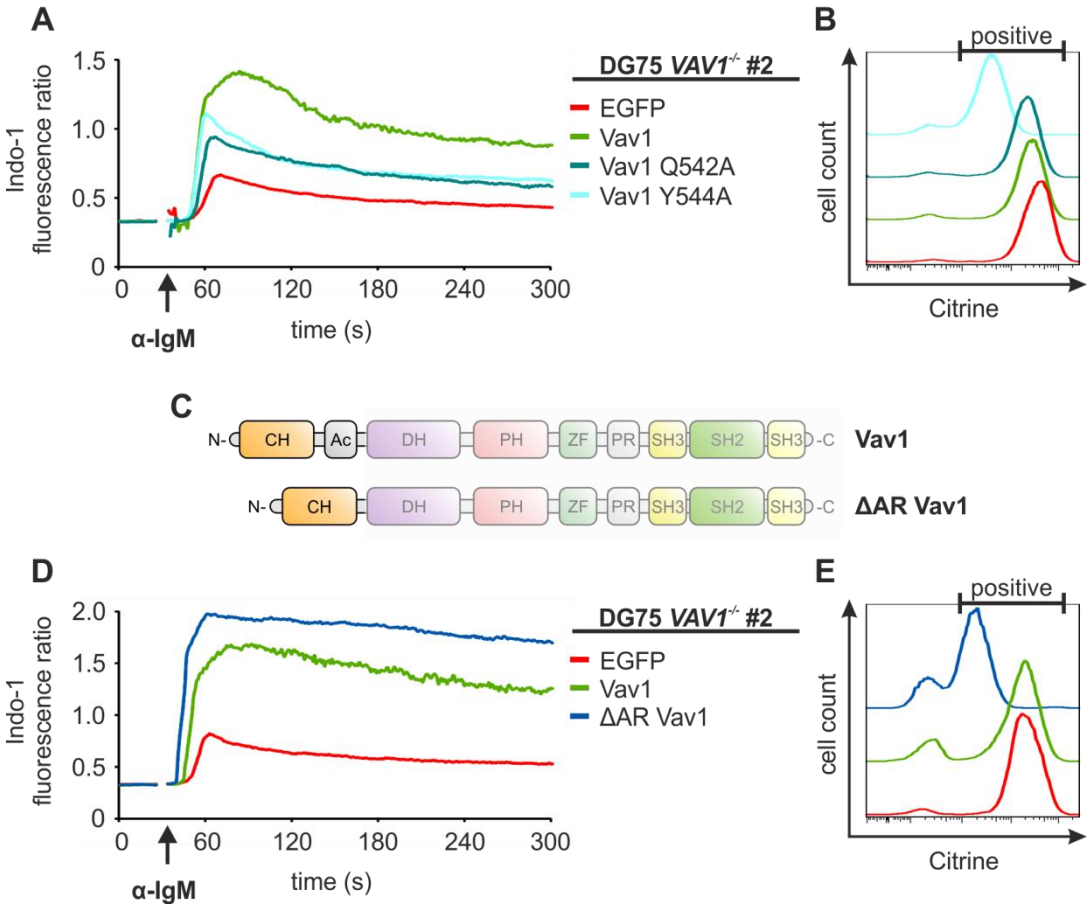

Figure 4.19: The ZF-domain and the acidic region regulate Vav1 activity in BCR-induced Ca^{2+}-mobilization. A, D) Vav1-deficient DG75 cells expressing Citrine-tagged wild-type Vav1, Vav1 Q542A, Vav1 Y544A, ΔAR Vav1 or EGFP were analyzed for Ca^{2+}-mobilization upon BCR stimulation as before. The graph shows Ca^{2+}-mobilization of gated cells (positive gate (B, E)). Data show one representative example of three independent experiments. **B, E)** Expression levels of analyzed proteins were determined by flow cytometry. **C)** Schematic drawing of wild-type Vav1 and the ΔAR Vav1 variant.

4.4.4 Do Rac family proteins influence BCR-induced Ca^{2+}-mobilization? - Generation of a Rac2-deficient DG75 sub-line

Since I demonstrated in chapter 4.4.1 and 4.4.3 that a structurally intact Vav1 DH-domain is indispensable for Ca^{2+}-signaling in human B cells and given that small G-proteins of the Rho family are the only reported binding partners of the Vav1 DH-domain, an interaction between these proteins might be essential to allow BCR-induced Ca^{2+}-mobilization. However, a direct interaction between Vav1 and Rac1 in BCR-induced Ca^{2+}-mobilization could not be observed in affinity purification experiments so far (data not shown).

Nevertheless, there are some indications in the literature that small G-proteins might be involved in BCR-induced Ca^{2+}-signaling. Experiments performed with Rac1/Rac2 double-deficient mice demonstrated a pivotal role of both proteins for B cell development and signaling (Walmsley et al., 2003) and resemble partially the phenotype of Vav1/Vav2 double-deficient mice. In addition, Walliser et al. reported that Rac2 has the ability to bind to PLCγ2 and thus might influence PLCγ2 enzymatic activation in a chicken B cell line.

Since Rac2 was reported to be more important than Rac1 in B cells (Walmsley et al., 2003; Walliser et al., 2015), I generated a Rac2-deficient DG75 sub-line to check the influence of Rac2 on BCR-induced Ca^{2+}-mobilization in DG75 cells. Therefore, I used the CRISPR/Cas method to target exon 3 of the *RAC2* gene located on chromosome 22 (figure 4.20 A). Transfection, cell-sorting, sub-cloning and screening for Rac2-deficient DG75 cells (figure 4.20 B-D) was performed as described for the TALEN method (see chapter 4.1.1). Subsequently, the Rac2-deficient DG75 clone #4 was further analyzed with regard to its genomic mutations in the *RAC2* exon 3. A genomic region containing exon 3 of the *RAC2* gene (referred to as ‘exon 3’) was amplified by PCR and ligated into a cloning vector for sequencing of single alleles. In total, 10 sequencing reactions were performed, which documented a 2 nucleotide deletion on one allele and a 4 nucleotide deletion on the second allele leading to premature stop codons in both cases (figure 4.20 E). This Rac2-deficient DG75 sub-line was used as model system for further investigations.

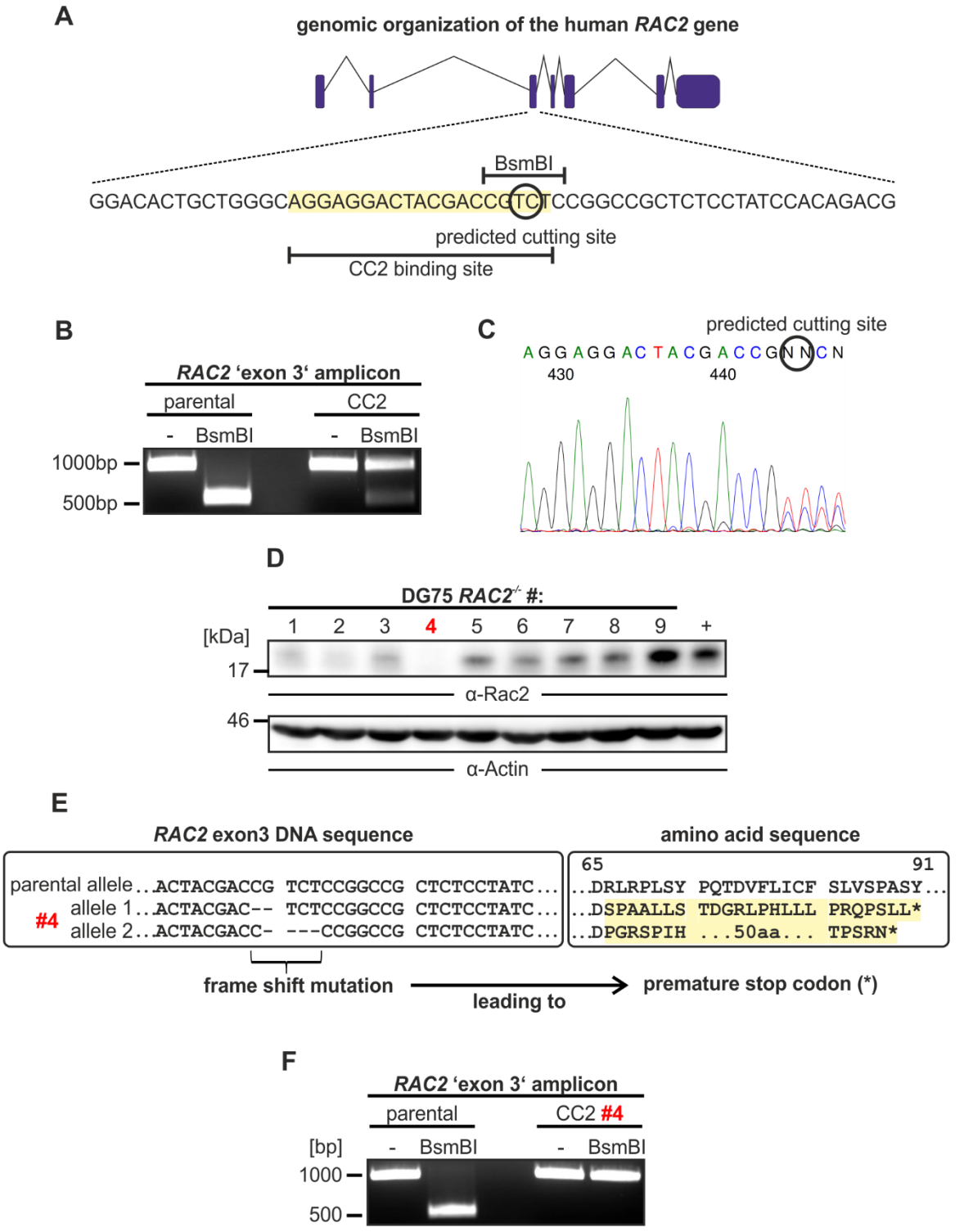

Figure 4.20: Generation of a Rac2-deficient DG75 sub-line. A) Schematic drawing of the *RAC2* genomic organization indicating the CRISPR/Cas target region. **B)** To test the activity of the CRISPR/Cas construct 2 (CC2), the targeted *RAC2* 'exon 3' was amplified by PCR from CC2-treated DG75 cells. The PCR product was cleaved with the restriction enzyme BsmBI, whose binding site overlaps with the CC2 target site and therefore can be used for CC2 activity testing. **C)** Sequencing result of the *RAC2* 'exon 3' amplicon. The targeting site of the CC2 construct is indicated. **D)** Screening of DG75 cell clones for Rac2 deficiency was done using western blot analysis. Cleared cellular lysates of $1x10^6$ DG75 cells were loaded per lane and separated by SDS-PAGE. Immunoblots were probed with anti-Rac2 and anti-Actin antibodies as indicated below individual blots.

Cleared cellular lysates of DG75 cells served as positive control (+). The molecular weight of marker proteins (in kDa) is indicated on the left. **E)** Characterization of the Rac2-deficient DG75 clone #4 was done by cloning the *RAC2* 'exon 3' amplicon into the pCR2.1 vector followed by sequencing of individual alleles. The result is representative for 10 sequencing reactions. **F)** Genomic control of DG75 *RAC2*$^{-/-}$ #4 by activity test as described in B), since one sequencing reaction showed wild-type sequence.

4.4.5 Rac2-deficient DG75 cells are capable to mobilize Ca^{2+} upon BCR stimulation

The Rac2-deficient DG75 cells were used to analyze BCR-induced Ca^{2+}-mobilization. The results show that the Rac2-deficient DG75 cell clones #1 and #4 were still able to mobilize Ca^{2+} upon BCR stimulation similar to parental cells with only a marginal reduction (figure 4.21 A), indicating that Rac2 is either not involved in BCR-induced Ca^{2+}-mobilization or has redundant functions with other small G-proteins of the Rho family. Hence, up to now the definite role of Rac proteins in BCR-induced Ca^{2+}-signaling remains unclear.

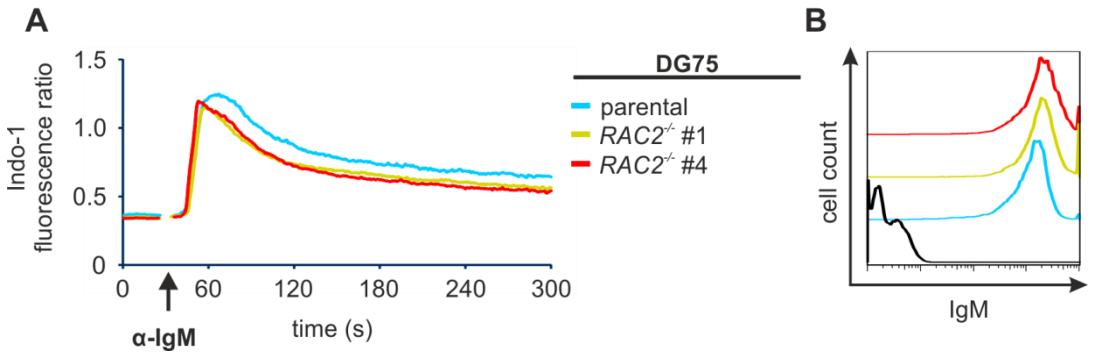

Figure 4.21: Human Rac2 in Ca^{2+}-mobilization upon BCR stimulation. A) Parental DG75 as well as Rac2-deficient cell clones #1 and #4 were analyzed for Ca^{2+}-mobilization upon BCR stimulation as before. The data show one representative example of three independent experiments. **B)** Expression levels of BCRs were measured by flow cytometry. Surface staining was done using anti-human IgM-APC. Unstained cells are depicted in black. Samples have the same color code as in A).

4.5 Analysis of the Vav1 CH-domain

4.5.1 The Vav1 CH-domain is critical for BCR-induced Ca^{2+}-signaling

In the previous chapter, I focused on the Vav1-Rac signaling axis as possible signaling knot in the context of BCR-induced Ca^{2+}-mobilization. Here, I have already described different Vav1 regions that influence Vav1 GEF activity and structural integrity of the DH-domain. Nevertheless, the N-terminally located type 3 CH-domain has been described to affect Vav1 GEF activity, too (Zugaza et al., 2002). Five different types of CH-domains exist. Type 1 and 2 CH-domains are often found in a tandem arrangement in which they

mediate binding to the Actin cytoskeleton (Gimona et al., 2002). In contrast, functions of type 3, 4 and 5 CH-domains are poorly characterized and seem to depend on the individual protein context. In Vav1, the type 3 CH-domain influences the GEF activity by forming an inhibitory loop with the centrally located DH-PH-ZF-domain unit (Zugaza et al., 2002; Chrencik et al., 2008). Deletion of the CH-domain leads to an increased GEF activity, which indicates an inhibitory role that is comparable to the already described acidic region between CH- and DH-domain (chapter 4.4.3). Deletion of the inhibitory acidic region enhances Ca^{2+}-mobilization upon BCR stimulation. However, the role of the Vav1 CH-domain in BCR-induced Ca^{2+}-signaling has not been described so far.

To test the influence of the CH-domain on BCR-induced Ca^{2+}-mobilization, I expressed a Vav1 variant carrying a deletion of the complete CH-domain (ΔCH Vav1) in Vav1-deficient DG75 cells and measured BCR-induced Ca^{2+}-mobilization (figure 4.22 A, B). This ΔCH Vav1 variant of Vav1 shows a massively reduced Ca^{2+}-mobilization compared to wild-type Vav1 indicating that the CH-domain has two different tasks. On the one hand, it serves as inhibitory unit for the GEF activity and on the other hand, it fulfills a pivotal function in BCR-induced Ca^{2+}-mobilization.

To characterize the CH-domain in more detail, I generated Vav1 variants carrying single substitutions of conserved amino acids within the CH-domain in an attempt to inactivate the domain. Substitution positions were selected by alignment of typical type 3 CH-domains and screening for conserved regions. Here, amino acids tryptophan 10 (W10), aspartate 39 (D39) and aspartate 98 (D98) displayed a high degree of conservation and were all individually substituted with alanine. The mutant Vav1 variants were expressed in Vav1-deficient DG75 cells and Ca^{2+}-mobilization was measured. The results show that cells expressing the W10A and D39A variants have a Ca^{2+}-kinetic similar to that of Vav1-deficient cells (figure 4.22 D). However, expression of these variants was low compared to wild-type Vav1, so that it is unclear, if the Ca^{2+}-mobilization phenotype depends on signaling defects or the low expression levels of the individual CH-domain mutants. In contrast, the D98A Vav1 variant shows an almost normal BCR-induced Ca^{2+}-mobilization (figure 4.22 D). Collectively, the Vav1 CH-domain is pivotal for BCR-induced Ca^{2+}-signaling, since single amino acid substitutions or deletion of the complete CH-domain resulted in dramatically decreased Ca^{2+}-mobilization.

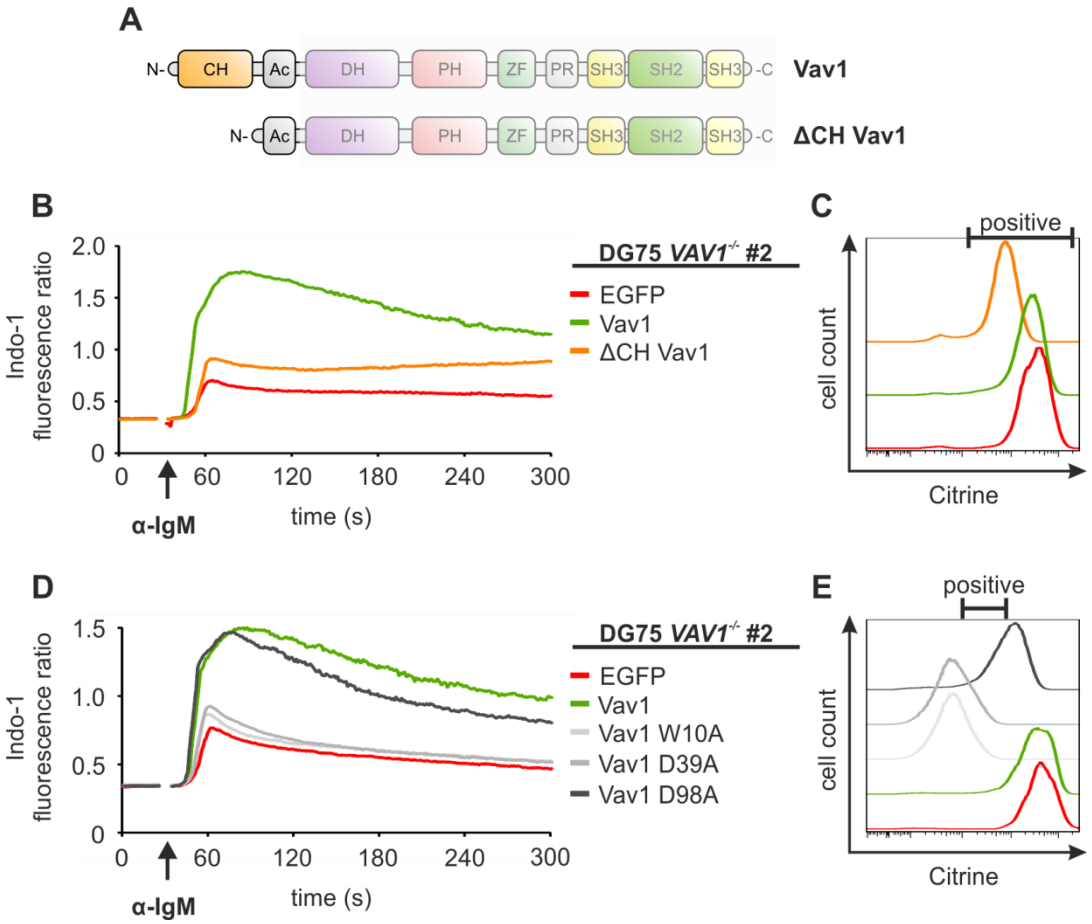

Figure 4.22: The CH-domain of Vav1 is critical for BCR-induced Ca^{2+}-mobilization. A) Schematic architecture of wild-type Vav1 and the ΔCH Vav1 variant. **B, D)** Vav1-deficient DG75 cells expressing Citrine-tagged wild-type Vav1, ΔCH Vav1, Vav1 W10A, Vav1 D39A, Vav1 D98A or EGFP were analyzed for Ca^{2+}-mobilization upon BCR stimulation as before. The graph shows Ca^{2+}-mobilization of gated cells (positive gate (C, E)). Data show one representative example of three independent experiments. **C, E)** Expression levels of analyzed proteins were determined by flow cytometry.

4.5.2 Actin-binding CH-domains cannot functionally replace the Vav1 CH-domain

Having shown that the Vav1 CH-domain is critical for Ca^{2+}-mobilization upon BCR stimulation, I further focused on the functional principle of the CH-domain. As mentioned in chapter 4.5.1, type 1 and 2 CH-domains are described to bind the Actin cytoskeleton. Yet, there is no direct proof that the Vav1 type 3 CH-domain is not able to bind to the Actin cytoskeleton.

To test whether known Actin-binding CH-domains can substitute the Vav1 CH-domain in the context of BCR-induced Ca^{2+}-mobilization, I generated Vav1 chimeras having the tandem type 1 and 2 CH-domains of β-Spectrin ($[CH]_2$ β-Spectrin-Vav1) or the type 3 CH-domain of IQGAP (CH IQGAP-Vav1) (Bañuelos et al., 1998; Umemoto et al., 2010)

instead of the Vav1 CH-domain. Constructs were expressed in Vav1-deficient DG75 cells and Ca^{2+}-mobilization was measured. Both chimeras showed reduced BCR-induced Ca^{2+}-mobilization (figure 4.23 B) similar to the ΔCH Vav1 variant (figure 4.22 B, see chapter 4.5.1). Since the Actin-binding type 1 and 2 CH-domains of β-Spectrin could not functionally replace the Vav1 CH-domain, an association with the Actin cytoskeleton might not be the task of the Vav1 CH-domain in BCR-induced Ca^{2+}-mobilization.

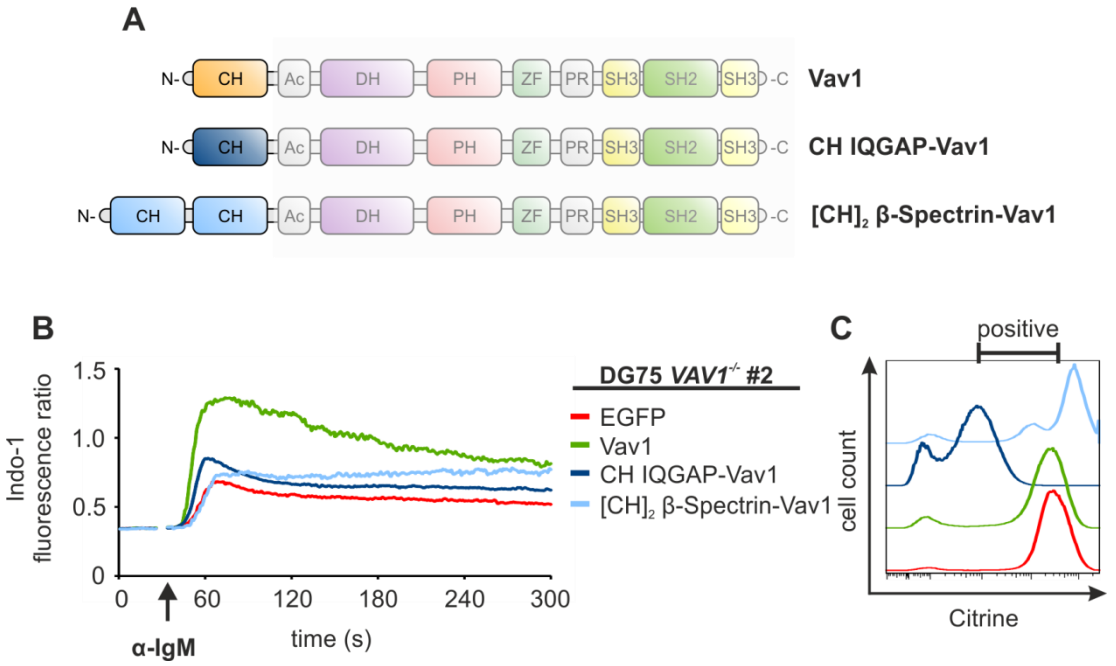

Figure 4.23: Actin-binding CH-domains cannot functionally substitute the Vav1 CH-domain in Ca^{2+}-mobilization. A) Schematic architecture of wild-type Vav1 and the chimeric CH IQGAP Vav1, $[CH]_2$ β-Spectrin-Vav1 proteins **B)** Vav1-deficient DG75 cells expressing Citrine-tagged wild-type Vav1, $[CH]_2$ β-Spectrin-Vav1, CH IQGAP-Vav1 or EGFP were analyzed for Ca^{2+}-mobilization upon BCR stimulation as before. The graph shows Ca^{2+}-mobilization of gated cells (positive gate (C)). Data show one representative example of three independent experiments. **C)** Expression levels of analyzed proteins were determined by flow cytometry.

4.5.3 The CH-domain of Vav1 functions independently of its intramolecular localization

Structural studies of the group from Xose Bustelo revealed that the CH-domain has the ability to contact the ZF-domain and thereby regulating the GEF activity of Vav1 (Zugaza et al., 2002), so that it seemed possible that the CH-domain provides structural support for the DH-PH-ZF-domain unit. To test whether the CH-domain mediates its critical role in BCR-induced Ca^{2+}-mobilization independently of the DH-PH-ZF-domain unit, I generated a Vav1 variant containing the CH-domain at the C-terminus instead of the N-terminus (Vav1 CH_{CT}), thus moving the CH-domain from its natural position in the Vav1 protein

backbone (figure 4.24 A). BCR-induced Ca^{2+}-mobilization in cells expressing the Vav1 CH_{CT} variant was similar to that of cells expressing wild-type Vav1 (figure 4.24 B). This indicates that the CH-domain might work independently of the other Vav1 domains, since the structural displacement of the CH-domain has no functional consequences for Ca^{2+}-mobilization.

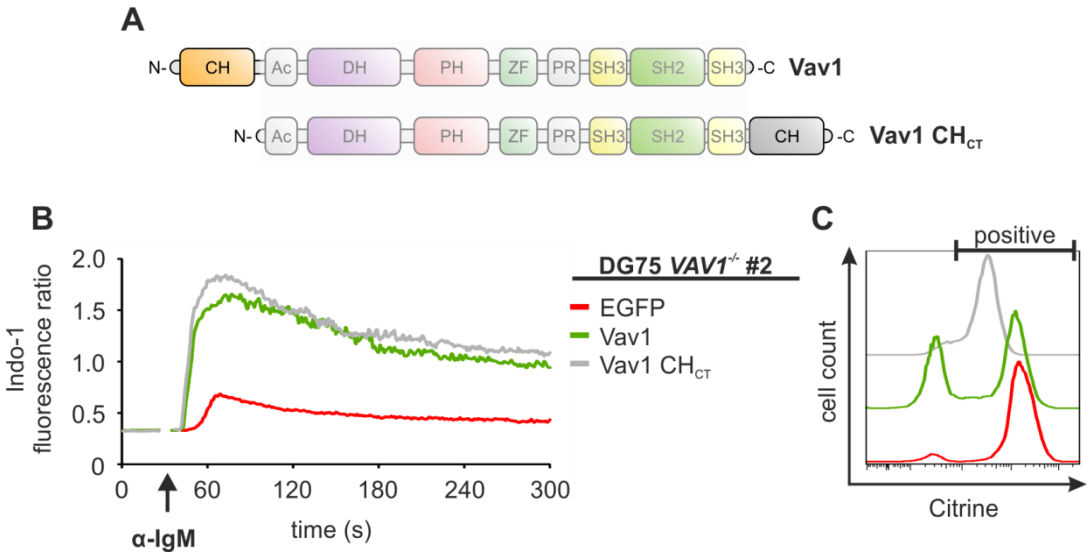

Figure 4.24: The CH-domain of Vav1 functions also at Vav1's C-terminus. A) Schematic architecture of wild-type Vav1 and the Vav1 CH_{CT} variant **B)** Vav1-deficient DG75 cells expressing Citrine-tagged wild-type Vav1, Vav1 CH_{CT} or EGFP were analyzed for Ca^{2+}-mobilization upon BCR stimulation as before. The graph shows Ca^{2+}-mobilization of gated cells (positive gate (C)). Data show one representative example of three independent experiments. **C)** Expression levels of analyzed proteins were determined by flow cytometry.

4.5.4 The CH-domain of Vav1 is not involved in plasma membrane recruitment

The results of the previous chapters point out, that the Vav1 CH-domain fulfills a specific function and acts independently of the DH-PH-ZF-domain unit. However, the functional mechanism of the CH-domain in the context of BCR-induced Ca^{2+}-mobilization is still unclear. A possible function could be the recruitment of Vav1 to the plasma membrane where BCR-signaling complexes are located.

To test this hypothesis, I generated a Vav1 chimera in which I replaced the CH-domain with the first 23 amino acids of the Lyn tyrosine kinase containing a signal for plasma membrane attachment (Lyn_{myr}-ΔCH Vav1) (Kovářová et al., 2001). This chimera was expressed in Vav1-deficient DG75 cells and its subcellular localization was analyzed by confocal microscopy. The results show that the Lyn_{myr}-ΔCH Vav1 chimera was constitutively localized at the plasma membrane, which indicates that the myristoylation

sequence was functional in Vav1 (figure 4.25 A). However, this constitutively membrane-bound variant of ΔCH Vav1 was a poor activator of BCR-induced Ca^{2+}-signaling (figure 4.25 C).

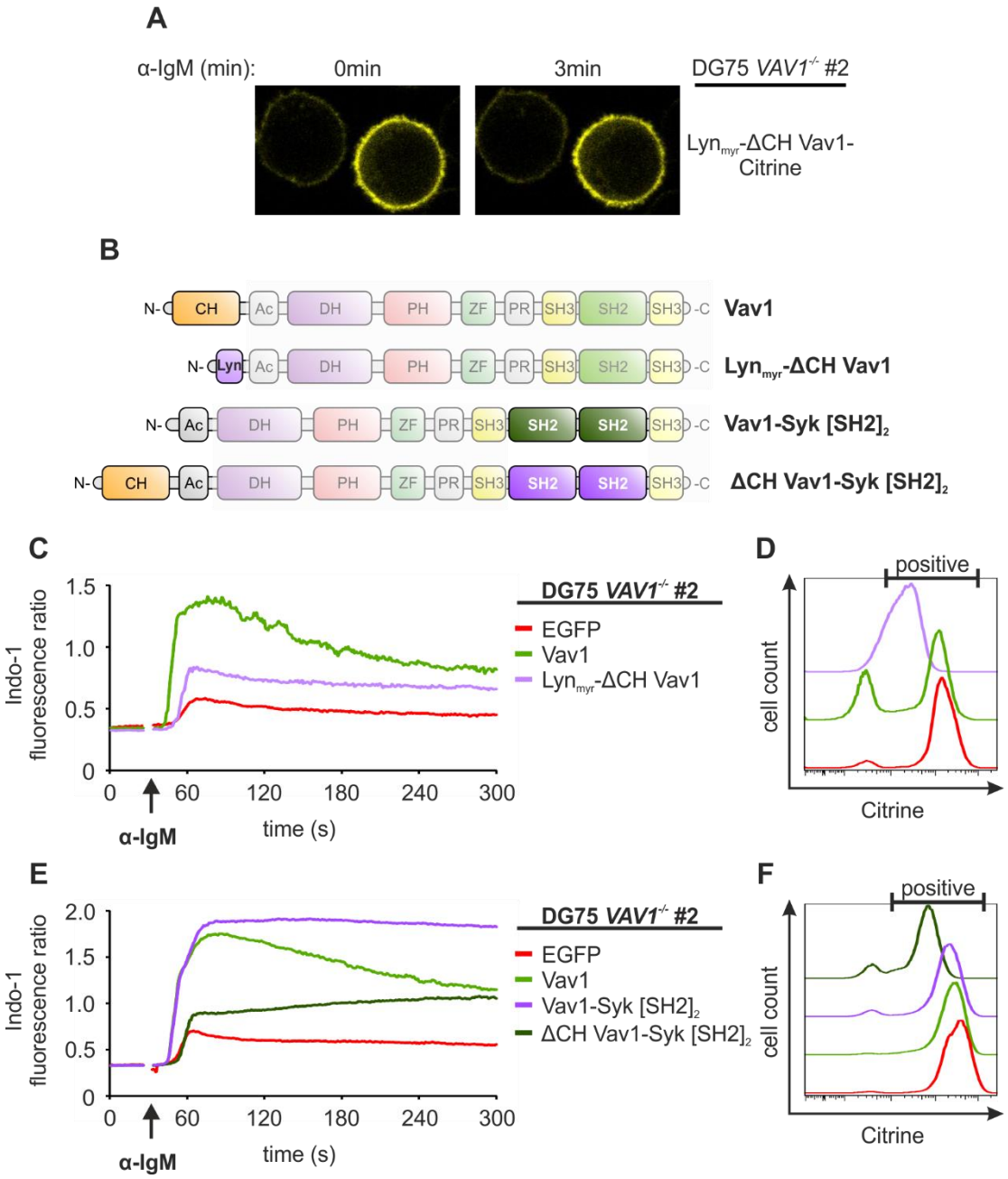

Figure 4.25: The CH-domain is not a membrane-targeting device. A) Confocal microscopy of Vav1-deficient DG75 cells expressing Lyn_{myr}-ΔCH Vav1 C-terminally tagged with Citrine. Images were taken before and 3 min after stimulation with 20 µg/ml α-IgM F(ab')$_2$ fragments. Data show one representative example of three independent experiments. **B)** Schematic architecture of wild-type Vav1 and the used Vav1 variants. **C, E)** Vav1-deficient DG75 cells expressing Citrine-tagged wild-type Vav1, Lyn_{myr}-ΔCH Vav1, ΔCH Vav1-Syk $[SH2]_2$, Vav1-Syk $[SH2]_2$ or EGFP were analyzed for Ca^{2+}-mobilization upon BCR stimulation as before. The graph shows Ca^{2+}-mobilization of gated cells (positive gate (D, F)). Data show one representative example of three independent experiments. **D, F)** Expression levels of analyzed proteins were determined by flow cytometry.

Moreover, I tested whether the tandem SH2 domains of Syk, which were previously shown to have an amplifying effect on Ca^{2+}-mobilization, can restore the Ca^{2+}-mobilization defect of the ΔCH Vav1 variant. Figure 4.25 E shows that the positive effect of the tandem SH2-domains of Syk on Ca^{2+}-mobilization (see figure 4.10) was abolished by the deletion of the Vav1 CH-domain(ΔCH Vav1-Syk $[SH2]_2$). The results show that the Vav1 CH-domain is not involved in targeting Vav1 to the BCR, but rather is involved in another yet to be identified function.

This unknown function of the CH-domain could involve protein-protein interactions. Hence, I focused on the identification of putative protein interaction partners. Therefore, I generated a GST-fusion protein containing the CH-domain of Vav1, which I used for affinity purification of interaction partners from lysates of SILAC (stable isotope labeling by/with amino acids in cell culture) labeled DG75 cells. The purified proteins were identified by mass spectrometry (Proteomics Service Facility, UMG), but the obtained results were not conclusive and hence did not reveal promising binding partner candidates (data not shown).

4.6 Phosphatidyl-inositol-4-phosphate 5-kinase in BCR-induced Ca^{2+}-mobilization

I described in the previous chapters that Vav1 is essential for BCR-induced Ca^{2+}-mobilization without affecting the formation of the Ca^{2+}-initiation complex. How Vav1 controls the activity of PLCγ2 and subsequent Ca^{2+}-mobilization remains unclear. The substrate of PLCγ2 is phosphatidyl-inositol-4,5-bisphosphate (PIP_2). The Production of PIP_2 is mainly executed by the phosphatidyl-inositol-4-phosphate 5-kinase (PIP5K) (van den Bout and Divecha, 2009). Notably, the small G-protein Rac1 was shown to interact with PIP5K (Halstead et al., 2010). Thus, Vav1, being an activator of Rac1, could be a potential regulator of PIP5K function and of cellular PIP_2 levels.

To test the influence of PIP5-kinases on Ca^{2+}-mobilization upon BCR stimulation, I ectopically expressed the PIP5K member PIP5K1a in DG75 cells. The results in figure 4.26 A show that expression of PIP5K1a in DG75 cells amplified Ca^{2+}-mobilization compared to parental DG75 cells indicating a supporting function of PIP5K1a in BCR-induced Ca^{2+}-signaling.

Next, I tested whether additional expression of PIP5K1a could substitute the lack of Vav1 in BCR-induced Ca^{2+}-mobilization. To this end, the PIP5K1a construct was expressed in Vav1-deficient DG75 cells and Ca^{2+}-mobilization was measured. The results show that

additional expression of PIP5K1a caused only a marginal increase of Ca^{2+}-mobilization in Vav1-deficient cells (figure 4.26 C). Therefore, overexpression of PIP5K1a cannot compensate the lack of Vav1. Furthermore, the much weaker Ca^{2+}-amplification by overexpression of PIP5K1a in Vav1-deficient cells compared to parental DG75 cells might indicate that PIP5K1a needs Vav1 in order to fulfill its function in BCR-induced Ca^{2+}-mobilization.

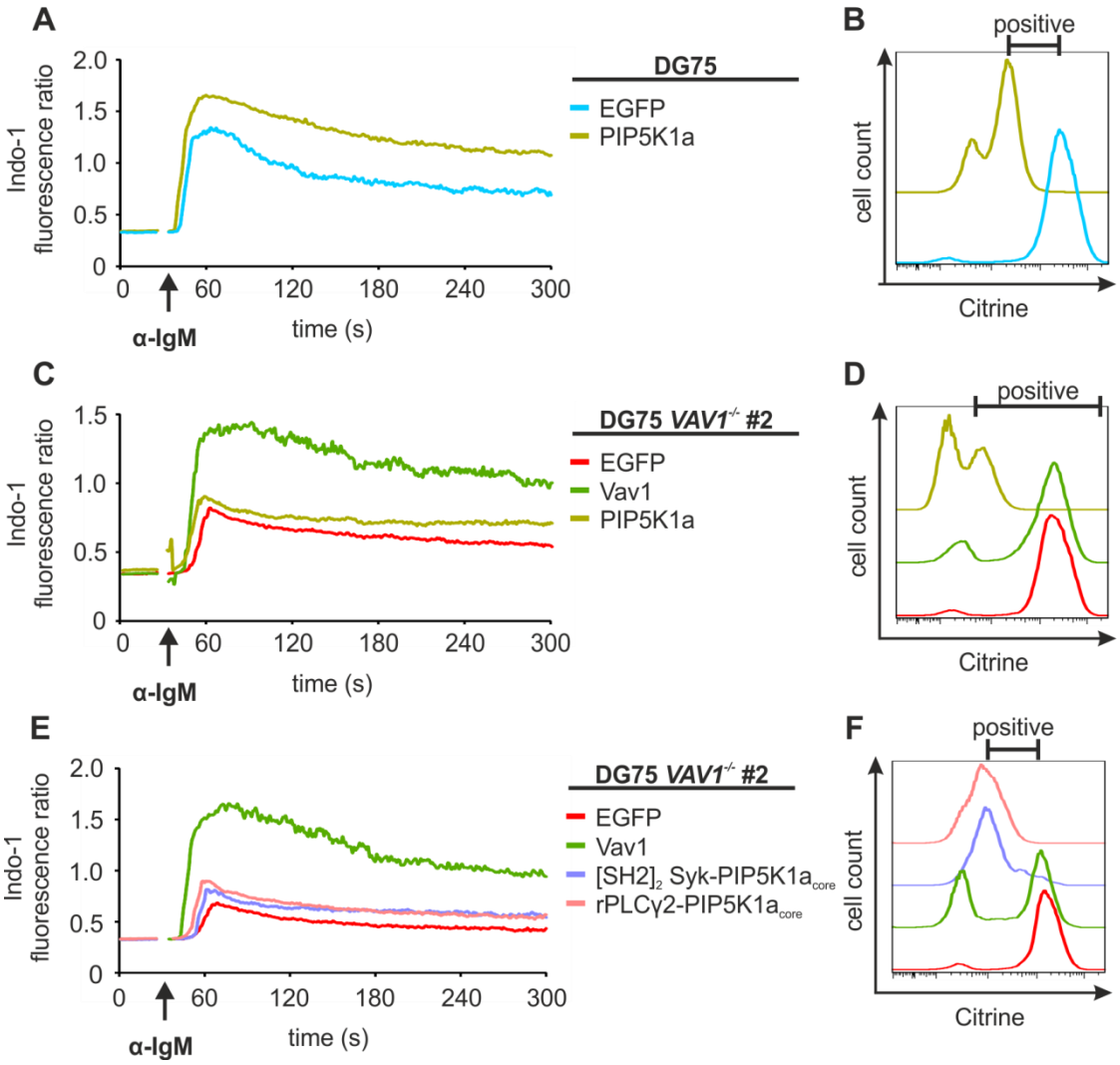

Figure 4.26: PIP5K1a influences Ca^{2+}-mobilzation, but cannot restore Vav1 function in human DG75 B cells. A, C, E) Parental DG75 cells or Vav1-deficient DG75 cells expressing Citrine- or EGFP-tagged wild-type Vav1, PIP5K1a, Syk $[SH2]_2$-PIP5K1a$_{core}$, rPLCγ2-PIP5K1a$_{core}$ or EGFP were analyzed for Ca^{2+}-mobilization upon BCR stimulation as before. The graph shows Ca^{2+}-mobilization of gated cells (positive gate (B, D, F)). Data show one representative example of three independent experiments. **B, D, F)** Proteins were N-terminally ($[SH2]_2$ Syk-PIP5K1a$_{core}$), C-terminally (Vav1, PIP5K1a) tagged with Citrine or N-terminally tagged with EGFP in the case of rPLCγ2-PIP5K1a$_{core}$ allowing flow cytometric determination of the expression levels.

To test whether the dramatically reduced Ca^{2+}-mobilization in Vav1-deficient DG75 cells is due to defective PIP5K1a positioning, I generated chimeric PIP5K1a variants that were N-terminally tagged with either the tandem SH2-domains of Syk (Syk $[SH2]_2$-PIP5K1a_{core}) or full length rat PLCγ2 (rPLCγ2-PIP5K1a_{core}). This approach was intended to target PIP5K1a either directly to the BCR via the tandem SH2-domains of Syk or to couple to it directly to its product consumer PLCγ2. Here, I used the isolated PIP5K1a kinase core domain, which was described to be the minimal unit for kinase activity (Nelson et al., 2008). The constructs were expressed in Vav1-deficient DG75 cells and Ca^{2+}-mobilization was measured. Figure 4.26 E shows only a marginal increase of BCR-induced Ca^{2+}-mobilization in cells expressing either Syk $[SH2]_2$-PIP5K1a_{core} or the rPLCγ2-PIP5K1a_{core} chimera compared to Vav1-deficient cells. This indicates that incorrect positioning of PIP5K1a might not be the reason for the Ca^{2+}-mobilization defect in Vav1-deficient DG75 cells. Collectively, PIP5K1a activity might depend on the presence of a functional Vav1, since PIP5K1a loses its Ca^{2+}-promoting function in the absence of Vav1.

5 Discussion

Engagement of the B cell antigen receptor (BCR) initiates the generation of membrane lipid-derived second messengers followed by an increase of the cytosolic Ca^{2+}-concentration, which is a hallmark of B cell activation. However, the underlying molecular signaling pathway is not completely understood. Genetic mouse models indicated a paramount role of Vav guanine nucleotide exchange factors in this context, yet they did not explain its operating principle. Therefore, the aim of this study was to analyze the role of Vav family members in BCR-induced Ca^{2+}-mobilization in human B cells. In my PhD project, I identified the Vav protein family as an essential signaling knot in BCR-induced Ca^{2+}-mobilization. Focusing on the hematopoietically expressed Vav1 family member, I investigated the importance of individual protein domains and their respective molecular mechanisms in connection to BCR-induced Ca^{2+}-mobilization. The main achievements of my PhD project are outlined below:

1. Generation of genetic model systems to study BCR-induced Ca^{2+}-signaling in human B cells.

2. Identification of Vav family proteins as crucial factors in BCR-proximal Ca^{2+}-signaling.

3. Identification of essential Vav1 protein domains for BCR-induced Ca^{2+}-mobilization.

4. Identification of key interaction partners of the SH2-domain of Vav1.

5. Identification of the Vav1 DH-PH-ZF-domain unit integrity as a prerequisite for BCR-proximal Ca^{2+}-signaling, which strongly indicates Rho family G-proteins as essential factors in that context.

5.1 Vav proteins constitute a major signaling knot in BCR-induced Ca^{2+}-mobilization

In the beginning of my PhD project, I established the TALEN gene targeting method in our laboratory to generate new genetic model systems for the investigation of human BCR signaling. Previously, efficient genetic manipulation was almost exclusively restricted to mouse models or the chicken DT40 B cell line. Human B cell lines, however, revealed technical obstacles in the context of efficient gene targeting. Based on the new gene targeting methods making use of site-specific engineered endonucleases, genetic manipulations are now technically feasible in human B cell lines, which improves the comparability with data from primary human B cells.

To investigate the role of Vav proteins in BCR-induced Ca^{2+}-mobilization, I generated a sub-line of the human DG75 B cell line deficient for the hematopoietically expressed family member Vav1. The characterization of this Vav1-deficient cell line revealed that Vav1 is a critical signaling factor in BCR-induced Ca^{2+}-signaling in DG75 cells. In addition, I showed that Vav1 is the predominant Vav family member expressed in DG75 cells, explaining the dramatic effect of the loss of Vav1 in the context of Ca^{2+}-mobilization. Nevertheless, Vav2 and Vav3 are also expressed, but to a lower extent. In primary B cells, the situation appears slightly different. Here, Vav2 and Vav3 are the predominantly expressed Vav family members indicating a more prominent role of these proteins in primary B cells.

The process of BCR-induced Ca^{2+}-mobilization requires the formation of the so-called Ca^{2+}-initiation complex resulting in the phosphorylation and activation of PLCγ2 (Engelke et al., 2007). However, Ca^{2+}-initiation complex formation is not altered in Vav1-deficient DG75 cells, since I could show that SLP-65 phosphorylation and plasma membrane recruitment as well as PLCγ2 phosphorylation are normal. In conclusion, Vav1 controls BCR-induced Ca^{2+}-mobilization downstream or independent of the canonical Ca^{2+}-initiation complex formation. These findings are in agreement with results achieved from the group of Klaus-Dieter Fischer showing that Vav1/Vav2 double-deficient mouse B cells have reduced BCR-induced Ca^{2+}-mobilization, but unaltered phosphorylation kinetics of SLP-65 and PLCγ2 (Tedford et al., 2001). However, it should be noted that in mice an isolated deficiency of Vav1 has no influence on BCR-induced Ca^{2+}-signaling (Tedford et al., 2001), which is indicative for redundant roles of Vav family members in murine B cells. This is supported by the signaling phenotype of B cells from mice lacking all three Vav proteins that show an even stronger signaling defect than Vav1/Vav2 double-deficient B cells (Fujikawa et al., 2003). In contrast to that, I showed that ectopic expression of Vav3,

but not Vav2, could restore BCR-induced Ca^{2+}-mobilization in Vav1-deficient DG75 cells. Thus Vav1 and Vav3 have redundant functions in terms of Ca^{2+}-signaling in human B cells. In agreement with this finding, Vav3 was demonstrated to be an important factor of BCR-induced Ca^{2+}-signaling in the chicken B cell line DT40 (Inabe et al., 2002). However, Vav3-deficiency in DT40 cells led to a decreased phosphorylation of PLCγ2, which is not consistent with the results gained in Vav1/Vav2 double-deficient mouse (Tedford et al., 2001) and my Vav1-deficient human model system.

Collectively, the available data show that Vav proteins fulfill an indispensable function in BCR-induced Ca^{2+}-mobilization. Nevertheless, discrepancies exist for the requirement of Vav family members, especially Vav2, in B cells from different species. This indicates an evolutionary divergent development of Vav family members. To test potential differences between human and murine Vav family members, I expressed murine Vav proteins in Vav1-deficient DG75 cells and analyzed their functionality in BCR-induced Ca^{2+}-mobilization. Like their human counterparts, only murine Vav1 and Vav3, but not Vav2, were able to support Ca^{2+}-mobilization in DG75 cells. In conclusion, the differential ability of mouse Vav2 to support Ca^{2+}-signaling might not depend on the Vav protein itself, but rather on its proximal interaction network that might differ between species.

5.2 BCR-proximal localization of Vav1 enables efficient Ca^{2+}-mobilization

BCR engagement drives the recruitment of first-line kinases like SFKs and Syk building up the first signaling complex proximal to the BCR (Reth and Wienands, 1997). In turn, a second assembly takes place mediated by the key adaptor protein SLP-65, forming the Ca^{2+}-initiation complex (Engelke et al., 2007; Scharenberg et al., 2007), followed by second messenger-induced Ca^{2+}-mobilization. The BCR-induced translocalization process of Vav1, however, is basically unknown in that context. Nevertheless, investigations focusing on Vav3 in the chicken B cell line DT40 suggest an involvement of the adaptor proteins SLP-65 and Grb2 in Vav3 recruitment to membrane rafts (Johmura et al., 2003). In agreement with this, Vav3 was found to be a component of BCR-induced micro-signalosomes (Weber et al., 2008). To elucidate the positioning of Vav1 upon BCR stimulation, I used a Citrine-tagged Vav1 variant to detect its localization by live cell imaging. Even though Citrine-tagged Vav1 was expressed and localized in the cytoplasm, no BCR-induced re-localization processes were observed indicating that the experimental set up might not be feasible for this purpose (data not shown). Therefore, I focused my research on potential Vav1 interaction partners in connection to BCR-induced Ca^{2+}-

mobilization using genetic and biochemical approaches. Many Vav1 interactions are mediated by its C-terminal adaptor part, which consists of an SH3-SH2-SH3-domain arrangement. Here, the SH2-domain is of particular importance, since it has the competence to guide Vav1 to active signaling spots. By inactivating the Vav1 SH2-domain, I could show that it is pivotal for Vav1-mediated Ca^{2+}-mobilization. To identify B cell-specific SH2-domain interaction partners, I performed affinity purifications using the Vav1 SH2-domain, which revealed a complex pattern of binding partners including the previously reported interaction partners SLP-65 and Syk (Deckert et al., 1996; Wienands et al., 1998; Chiu et al., 2002). Most remarkably, however, I showed a so far undescribed interaction between the Vav1 SH2-domain and the Igα/Igβ heterodimer of the BCR. Since Igα/Igβ contain ITAM and non-ITAM phosphorylation motifs, I further characterized this interaction and identified the ITAM sequence as Vav1 docking site.

As mentioned above, affinity purification experiments using the Vav1 SH2-domain confirmed the previously reported interaction with SLP-65 (Wienands et al., 1998). The group of Andrew Chan identified the tyrosine 91 (Y91) in chicken SLP-65 as exclusive binding site of Vav1 (Chiu et al., 2002). To check whether the equivalent tyrosine residue in human SLP-65 (Y72) serves as docking site for Vav1, I generated a SLP-65 deficient DG75 sub-line, reconstituted these cells with a SLP-65 tyrosine 72-to-phenylalanine (Y72F) variant and tested the association of the Vav1 SH2-domain with this SLP-65 mutant. Even though binding between Vav1 and SLP-65 was reduced, it was not absent. Additionally, I also tested the Y72 proximally located tyrosine 84 (Y84) and tyrosine 119 (Y119) for Vav1 binding, which are described together with tyrosine 178 (Y178) and tyrosine 189 (Y189) as PLCγ2 binding sites (Chiu et al., 2002; Engelke et al., 2013). Since Y84 and Y119 could also be identified as possible Vav1 docking sites and even the Y72/84F and Y72/119F double SLP-65 variants still interacted with Vav1, it must be assumed that Vav1 has multiple SLP-65 interaction points. This contradicts the previous results of Chiu et al. and leads to a less restricted mode of interaction in which Vav1 can bind to different SLP-65 tyrosines depending on available positions similar to what has been described for the PLCγ2-SLP-65 interaction (Chiu et al., 2002). Based on these results, SLP-65 constitutes a central building block on which effector proteins might be arranged in different ways, what might cause diverse signaling outcomes. Consequently, the data of the used genetic and biochemical approaches illustrate a conceivable recruiting mechanism involving a direct Vav1 BCR-recruitment and a Vav1-SLP-65 interaction in the context of BCR-induced signaling.

To test which interaction partner of the Vav1 SH2-domain, Igα/β or SLP-65, has a functional relevance in BCR-induced Ca^{2+}-mobilization, I analyzed Vav1 chimeras

containing either BCR- or SLP-65-binding SH2-domains to decipher the importance of the two recruiting mechanisms. In fact, both Vav1-recruiting mechanisms enabled BCR-induced Ca^{2+}-mobilization, although each to a different extent. Since recruitment to SLP-65 results in a more transient BCR-induced Ca^{2+}-mobilization, direct recruitment of Vav1 to BCR ITAMs leads to a more sustained Ca^{2+}-flux. Whether the different signaling strengths depend on different localization or on different affinities is not completely solved, however, it is clear that Vav1 localization is not restricted to a specific signaling spot, but rather to BCR-proximal areas in the context of Ca^{2+}-mobilization.

In addition to that, CD19 is described to recruit Vav1 to its cytoplasmic tail after co-ligation with the BCR, which potentiates BCR-derived signals (Weng et al., 1994; Sato et al., 1997; Fujimoto et al., 1999). However, this process seems to be not involved in BCR-induced Ca^{2+}-signaling, since CD19-negative DG75 cells show normal Ca^{2+}-mobilization upon BCR stimulation.

5.3 The structural integrity of the Vav1 DH-PH-ZF-domain unit is an essential prerequisite for BCR-signaling

Since I could show that Vav1 does not influence the formation of the Ca^{2+}-initiation complex in DG75 cells upon BCR stimulation, I focused on alternative mechanisms by which Vav1 might regulate Ca^{2+}-signaling. Functional characterizations of Vav1 in the past mainly focused on Vav1's GEF activity towards small G-proteins of the Rho-family (Bustelo, 2001; Zugaza et al., 2002). In that context, it is well established that Vav1 is a transducer of activating signals leading to cell proliferation (Tarakhovsky et al., 1995; Bonnefoy-Bérard et al., 1996). The connection between Vav1's GEF activity and BCR-induced Ca^{2+}-mobilization, however, remained unclear. To address this question, I generated two Vav1 variants containing non-functional DH-domains, one affecting the center of the catalytic DH-domain (Vav1 LK334/335AA), the other one damaging the structural integrity outside of its catalytic site (Vav1 L213Q) (Zugaza et al., 2002; Saveliev et al., 2009). Since the Vav1 LK334/335AA variant enabled normal BCR-induced Ca^{2+}-mobilization, it seems unlikely that activation of Rho family G-proteins is involved in that context. In agreement with this, TCR-induced Ca^{2+}-mobilization is not reduced in T cells from Vav1-deficient mice expressing the Vav1 LK334/335AA variant either (Saveliev et al., 2009). However, it needs to be considered that inactivation of the Vav1 LK334/335AA DH-domain was only tested in connection to Rac1 activation (Saveliev et al., 2009). Importantly, amino acid substitutions of residues involved in binding of small G-proteins can alter the activation profile of GEFs (Karnoub et al., 2001; Cheng et al., 2002; Snyder

et al., 2002; Rossman et al., 2005). Whether activation of other small G-proteins like RhoA is also impaired by the LK334/335AA mutations, remains unknown and needs to be tested in future experiments. On the other hand, I could demonstrate that the structural integrity of the DH-domain is critical for BCR-induced Ca^{2+}-mobilization. Thus, the role of the Vav1 DH-domain in BCR-induced Ca^{2+}-signaling may be to associate with critical signaling factors rather than to activate small G-proteins. Since the only known function of DH-domains is to activate small G-proteins, these proteins are the only described interaction partners. Hence, I assume that small G-proteins fulfill a critical role in BCR-induced Ca^{2+}-signaling. Vav1 activates and therefore binds the small G-proteins Rac1, Rac2 and RhoA (Movilla et al., 2001; Palmby et al., 2004; Heo et al., 2005; Rapley et al., 2008). The role of Rac1 and Rac2 in B cell biology has been demonstrated in mice deficient for either Rac1 or Rac2 or both. B cells from Rac2-deficient mice show reduced BCR-induced Ca^{2+}-mobilization (Walmsley et al., 2003). In addition, expression of a dominant-negative variant of RhoA in the murine B cell line A20 was shown to reduce BCR-induced Ca^{2+}-mobilization (Saci and Carpenter, 2005) indicating that activation of RhoA by GEFs is involved in that context. Even though RhoA can be activated by Vav1 (Movilla et al., 2001; Rapley et al., 2008), its activation might not be relevant, since I could show that the catalytically inactive Vav1 LK334/335AA variant enabled BCR-induced Ca^{2+}-mobilization.

For binding and activation of small G-proteins, Vav proteins are specially equipped with further domains. The central DH-PH complex is a conserved feature among Rho GEFs and constitutes the minimal catalytic entity (Bustelo, 2001; Zugaza et al., 2002). C-terminal of the DH-PH-domain arrangement, Vav1 contains a ZF-domain, which interacts with and thus stabilizes the DH-domain. This gives rise to the DH-PH-ZF-domain unit (Zugaza et al., 2002; Brooun et al., 2007). Results obtained from fluorescence anisotropy and NMR chemical shift mapping experiments indicate that the isolated Vav1 ZF-domain is able to directly associate with Rac1 (Heo et al., 2005). Regarding Vav2, the same group demonstrated the participation of the ZF-domain in binding as well as activation of small G-proteins like Rac1, Cdc42 and RhoA. In agreement with that, substitutions of glutamine 542 (Q542) or tyrosine 544 (Y544) with alanines within the Vav1 ZF-domain caused a dramatic reduction of Rac1 activation supporting the critical role of the ZF-domain in that context (Zugaza et al., 2002). I tested the same Vav1 ZF-domain variants and showed that an intact Vav1 ZF-domain is essential for BCR-induced Ca^{2+}-mobilization. This supports the hypothesis of G-proteins as critical factors for Vav1-mediated Ca^{2+}-signaling. Additional support is gained from experiments focusing on the acidic region of Vav1 N-terminal of the DH-PH-ZF-domain unit (Zugaza et al., 2002). This region is described to inhibit Vav1 GEF activity by forming a so-called inhibitory loop in combination with the CH-domain (Zugaza et al., 2002; Brooun et al., 2007; Yu et al., 2010). While the CH-domain is

described to intramolecularly bind the DH-PH-ZF-domain unit, the acidic region blocks the entry of the catalytically active site of the DH-domain. The latter interaction is regulated via phosphorylation of three conserved tyrosines in the acidic region, which causes release of the inhibitory loop, allowing small G-proteins to bind and get activated (Zugaza et al., 2002; Yu et al., 2010). Experimentally, substitution of these tyrosines is followed by an increased GEF activity of Vav1 (Zugaza et al., 2002). I generated a Vav1 variant carrying a deletion of the complete acidic region (ΔAR Vav1) including the three conserved tyrosine residues. This ΔAR Vav1 variant causes an elevated BCR-induced Ca^{2+}-mobilization in DG75 cells. In conclusion, an improved DH-domain accessibility for small G-proteins seems to increase Vav1's capability to promote Ca^{2+}-mobilization.

The available data suggest the concept, that small G-proteins are critical for Vav1-mediated BCR-induced Ca^{2+}-mobilization. To test directly the role of small G-proteins, I generated a Rac2-deficient DG75 sub-line. Analysis of this DG75 sub-line revealed only a marginal reduction in BCR-induced Ca^{2+}-mobilization. Given the high degree of homology between Rac2 and Rac1, this result may indicate redundant functions of these proteins. As previously mentioned, B cells of Rac2-deficient mice have only partial defects in B-cell signaling including BCR-induced Ca^{2+}-mobilization (Walmsley et al., 2003). Some of these defects are stronger in B cells of Rac1/Rac2 double-difficient mice, however, whether this applies to BCR-induced Ca^{2+}-mobilization is not known (Walmsley et al., 2003). How exactly Rac proteins may control BCR-induced Ca^{2+}-mobilization is not known either. Noteworthy, Rac2 has the capability to directly interact with PLCγ2 in chicken DT40 cells. A variant of PLCγ2 incapable of binding to Rac2 could not fully reconstitute BCR-induced Ca^{2+}-mobilization in PLCγ2-deficient DT40 cells (Walliser et al., 2015). I used the identical amino acid substitution in rat PLCγ2 and expressed this variant in a PLCγ2-deficent DG75 sub-line (kindly provided by Caren Bartsch). BCR-induced Ca^{2+}-mobilization was not completely restored in these cells either (data not shown). Whether the reduced Ca^{2+}-mobilization really depends on the loss of the PLCγ2-Rac2 interaction needs to be further characterized. Collectively, the obtained data indicate a potential signaling axis starting with the recruitment of Vav1 to the BCR and SLP-65 bringing it into close proximity of PLCγ2, where it might facilitate small G-protein-mediated PLCγ2 activation.

5.4 The Vav1 CH-domain is an indispensable regulator region of Vav1 activities

The CH-domain of Vav1 is believed to act mainly as an intramolecular inhibitor of the catalytic DH-domain. As described above, it forms an inhibitory loop together with the

acidic region by binding to intramolecular sites within the DH-PH-ZF-domain unit (Zugaza et al., 2002; Yu et al., 2010). The function of the CH-domain of Vav1 in BCR-induced Ca^{2+}-mobilization is not completely clear. Deletion of the CH-domain (ΔCH Vav1) causes a dramatically reduced Ca^{2+}-mobilization in T cells upon TCR stimulation (Li et al., 2013). I could show that the same holds true for DG75 B cells as well. However, the function of type 3 CH-domains is not well defined and might depend on the individual protein context (Gimona et al., 2002). As opposed to type 1 and type 2 CH-domains, it is not known whether the type 3 CH-domain of Vav1 can bind to the Actin cytoskeleton. Actin cytoskeleton rearrangements are discussed to be involved in the regulation of early events of B cell activation (Batista et al., 2010). To test if Actin-binding is involved in Vav1-mediated Ca^{2+}-mobilization, I substituted the Vav1 CH-domain with the Actin-binding CH-domains of β-Spectrin or IQGAP, respectively (Bañuelos et al., 1998; Umemoto et al., 2010). However, these Vav1 variants were not able to restore Ca^{2+}-mobilization upon BCR stimulation indicating that an association of Vav1 with Actin is not crucial in this process.

BCR-proximal signaling including formation of the Ca^{2+}-initiation complex takes place at the plasma membrane (Engelke et al., 2007; Scharenberg et al., 2007). As described above, Vav1's SH2-domain serves as a crucial recruitment domain via binding to the BCR and SLP-65. In addition, also the PH-domain is involved in recruitment processes as it binds different plasma membrane resident PIPs. Since these mechanisms are described to influence Vav1 activity (Han J. et al., 1998), I tested whether the CH-domain might be involved in plasma membrane recruitment. For this purpose, I substituted the CH-domain with the membrane-targeting region of the Src-kinase Lyn (Lyn_{myr}-ΔCH Vav1) (Casey, 1995; Kovářová et al., 2001). Despite efficient plasma-membrane targeting of the Lyn_{myr}-ΔCH Vav1 variant, it did not restore the Ca^{2+}-mobilization defect of cells expressing the ΔCH Vav1 variant. Thus, plasma membrane targeting is most likely not the function of the CH-domain in that context.

Considering that the CH-domain is involved in intramolecular interactions with the indispensable DH-PH-ZF-domain unit (Zugaza et al., 2002; Yu et al., 2010), the CH-domain could serve in structurally stabilizing this unit to allow for efficient Vav1-mediated Ca^{2+}-mobilization. To test this hypothesis, I removed the CH-domain from the inhibitory loop by transferring it from the N-terminus to the C-terminus. Strikingly, this positional change of the CH-domain has no functional consequences for Ca^{2+}-mobilization. Thus, the CH-domain might not structurally stabilize the DH-PH-ZF-domain unit. However, the C-terminus of Vav1 is reported to loop back to the center of Vav1 as a second inhibitory loop (Barreira et al., 2014), so that the C-terminally CH-domain might still be able to

interact with the DH-PH-ZF-domain unit. Hence, stabilization of the Vav1 3D structure by the CH-domain cannot be completely excluded as a possible function of the CH-domain.

As mentioned above, Vav2 cannot restore the BCR-induced Ca^{2+}-mobilization in Vav1-deficient DG75 cells. Yet, the simple exchange of the CH-domain of Vav2 with the CH-domain of Vav1 leads to a functional Vav2 chimera (data not shown). Vice versa, Vav1 containing the CH-domain of Vav2 also enables BCR-induced Ca^{2+}-mobilization (data not shown). In conclusion, the CH-domain of Vav2 as well as all other domains of Vav2 are in principle functional. However, in Vav2 the interplay between these domains might be impaired. In conclusion, this indicates a close cooperation between the CH-domain and other Vav domains with separate functions that are indispensable for Vav-mediated Ca^{2+}-mobilization.

5.5 Does Vav1 influence the generation of PIP_2 in BCR-induced Ca^{2+}-signaling?

Besides activation of PLCγ2 by activated Btk, supply of its substrate PIP_2 is a prerequisite for BCR-induced Ca^{2+}-mobilization. PIP_2 comprises only about 1 % of the phospholipids in the plasma membrane, so that it might be rapidly exhausted after BCR stimulation (McLaughlin and Murray, 2005). Hence, refilling of PIP_2 levels could be a critical aspect for sustained BCR-induced Ca^{2+}-mobilization. In principle, PIP_2 is generated by the family of PIP5Ks (van den Bout and Divecha, 2009). Vav1-deficient mouse B cells show a reduced PIP5K activation as well as impaired Ca^{2+}-mobilization upon CD19 and BCR co-ligation (O'Rourke et al., 1998). Since Rac1 was shown to interact with PIP5Ks (Halstead et al., 2010), a potential signaling axis including Vav1, Rac1 and PIP5K might be important for efficient BCR-induced Ca^{2+}-signaling. In accordance with this hypothesis, ectopic expression of PIP5Ks improves BCR-induced Ca^{2+}-mobilization in DG75 cells, indicating a potential function of PIP5Ks in that context. However, ectopic expression of PIP5K1a in Vav1-deficient DG75 cells could not enhance BCR-induced Ca^{2+}-mobilization, indicating that Vav1 is probably needed for PIP5K function in Ca^{2+}-mobilization. To characterize this in more detail, I fused the catalytic domain of PIP5K1a directly to rat PLCγ2 (rPLCγ2-PIP5K1a$_{core}$) to bypass a possible Vav1-mediated PIP5K recruitment. However, this chimera did not restore Ca^{2+}-mobilization in Vav1-deficient cells. Yet, it needs to be noted that PIP5K activity of the rPLCγ2-PIP5K1a$_{core}$ chimera was not tested in my experiments. Given that Vav1 was not expressed in cells expressing the rPLCγ2-PIP5K1a$_{core}$ chimera, the PIP5K1a catalytic domain might lack proper activation via the Vav1/small G-protein axis. Hence, a potential Vav1/small G-Protein/PIP5K signaling axis operating to produce

PIP_2 following BCR stimulation remains a possible scenario (figure 5.1). In that context, Rac2 is not the key G-protein, since BCR-induced Ca^{2+}-mobilization in Rac2-deficient DG75 cells is almost unaltered. Therefore, further G-proteins have to be tested for their function in BCR-induced Ca^{2+}-mobilization.

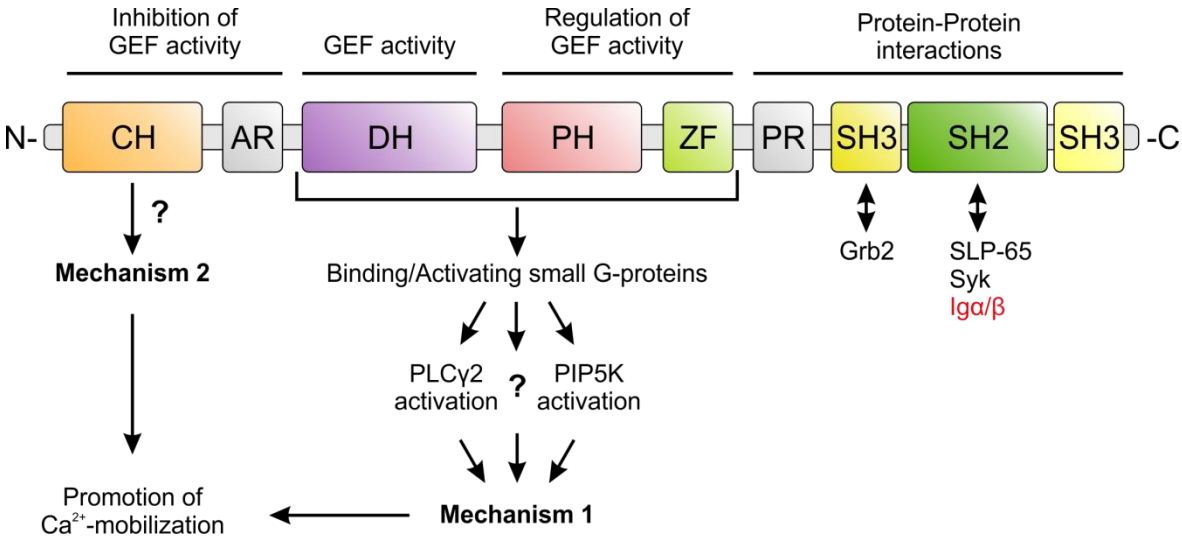

Figure 5.1: Schematic domain architecture of Vav1 indicating possible domain functions in the context of BCR-induced Ca^{2+}-mobilization. The DH-PH-ZF-domain unit (mechanism 1) and the CH-domain (mechanism 2) of Vav1 seem to cooperate for a completely functional Vav1 protein in BCR-induced Ca^{2+}-mobilization. In that context, the DH-PH-ZF-domain unit is interacting with small G-proteins that are reported to orchestrate the activity of several downstream factors including PLCγ2 and PIP5K, which have described functions in Ca^{2+}-signaling (mechanism 1). The CH-domain could be identified as crucial region in the context of Ca^{2+}-mobilization (mechanism 2), however, its exact function is not completely solved. In addition, Vav1 functionality strictly depends on interactions mediated by its SH2-domain. Besides, the previously described interaction partner SLP-65, I identified an interaction between Vav1 and the Igα/Igβ heterodimer (marked in red) and showed that this interaction enables BCR-induced Ca^{2+}-mobilization.

6 Conclusion

The results of my PhD project demonstrate an additional mechanism by which early B cell activation is controlled. So far, it was thought that the process of BCR-induced Ca^{2+}-mobilization is exclusively regulated by the phosphorylation-dependent activation of PLCγ2, which is based on the correct assembly of the Ca^{2+}-initiation complex. The absence of Vav guanine nucleotide exchange factors, however, strongly impairs the BCR-induced Ca^{2+}-mobilization, but does not affect the phosphorylation-dependent activation of PLCγ2. Hence, Vav proteins are not required to control the canonical PLCγ2 activation process, but rather act by an additional mechanism to promote mobilization of Ca^{2+} upon BCR stimulation (figure 6.1). Based on my results, the structural integrity of regions involved in binding and activation of small Rho family G-proteins is crucial for the functionality of Vav1 in that context.

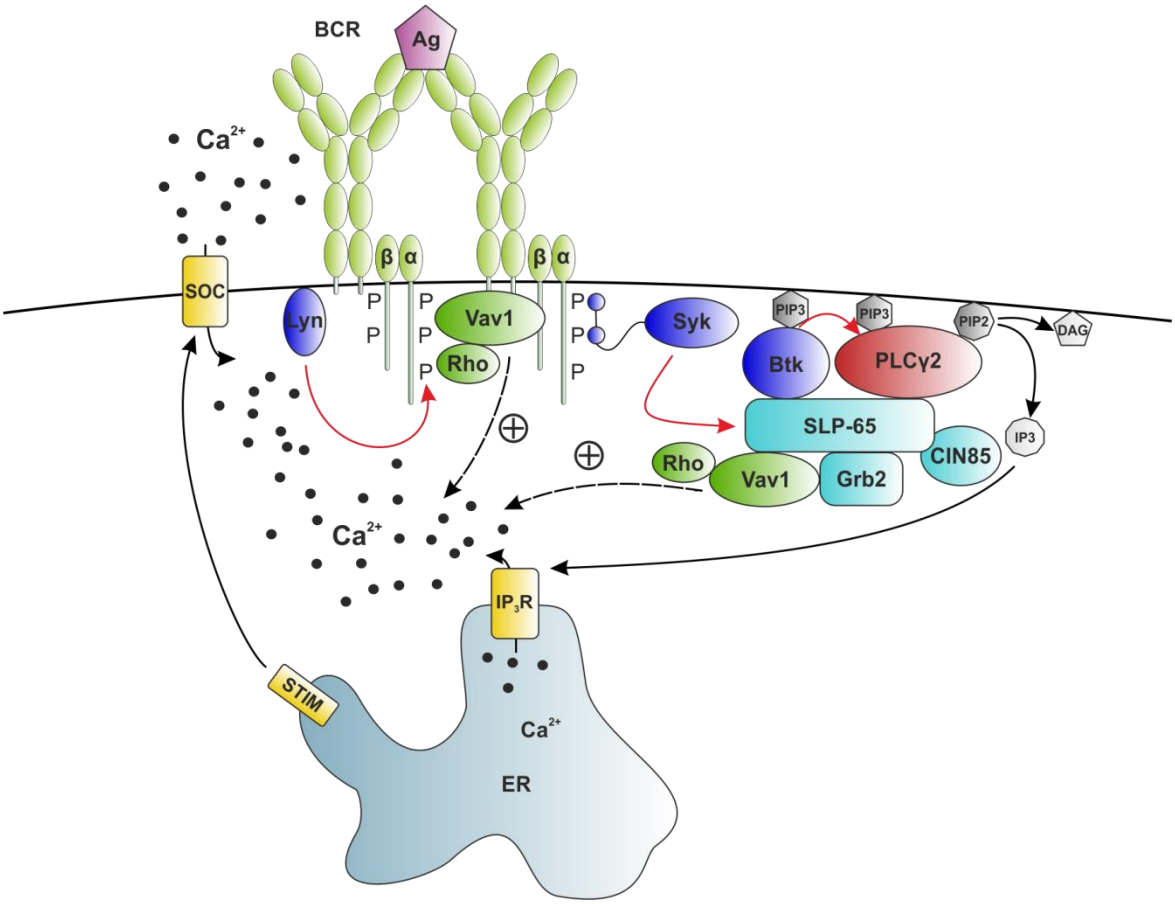

Figure 6.1: Model of Vav1 in BCR-induced Ca^{2+}-mobilization. Cross-linking of BCRs leads to phosphorylation of ITAMs in the Igα/Igβ heterodimer, followed by the recruitment of Syk, which phosphorylates SLP-65 leading to the formation of the core Ca^{2+}-initiation complex, including Btk and PLCγ2. Recruitment of Vav1 into the BCR signalosome requires the binding to SLP-65 or to the ITAM motifs of the BCR. The Ca^{2+}-promoting function of Vav1 strictly depends on the binding/activation of small G-proteins. The plus in connection with dashed lines indicate the promoting effect of Vav1 in BCR-induced Ca^{2+}-mobilization.

This emphasizes a potential role of Rho family G-proteins in the process of PLCγ2-controlled Ca^{2+}-mobilization and opens the possibility for an additional regulation pathway with regard to the generation of key second messengers that is indispensable for the activation and thus differentiation of B cells into antibody secreting plasma cells. Moreover, the data of my PhD project provide the basis for future investigations focusing on the Vav1/small G-protein signaling axis.

.

.

7 References

Abudula, A., Grabbe, A., Brechmann, M., Polaschegg, C., Herrmann, N., Goldbeck, I., Dittmann, K., and Wienands, J. (2007). SLP-65 signal transduction requires Src homology 2 domain-mediated membrane anchoring and a kinase-independent adaptor function of Syk. The Journal of biological chemistry *282*, 29059-29066.

Alexandropoulos, K., Cheng, G., and Baltimore, D. (1995). Proline-rich sequences that bind to Src homology 3 domains with individual specificities. Proc. Natl. Acad. Sci. USA *92*, 3110-3114.

Arana, E., Vehlow, A., Harwood, N.E., Vigorito, E., Henderson, R., Turner, M., Tybulewicz, V.L.J., and Batista, F.D. (2008). Activation of the small GTPase Rac2 via the B cell receptor regulates B cell adhesion and immunological-synapse formation. Immunity *28*, 88-99.

Bañuelos, S., Saraste, M., and Carugo, K.D. (1998). Structural comparisons of calponin homology domains. Structure *6*, 1419-1431.

Barreira, M., Fabbiano, S., Couceiro, J.R., Torreira, E., Martínez-Torrecuadrada, J.L., Montoya, G., Llorca, O., and Bustelo, X.R. (2014). The C-Terminal SH3 Domain Contributes to the Intramolecular Inhibition of Vav Family Proteins. Science Signaling *7*, ra35.

Batista, F.D., Treanor, B., and Harwood, N.E. (2010). Visualizing a role for the actin cytoskeleton in the regulation of B-cell activation. Immunological Reviews *237*, 191-204.

Ben-Bassat, H., Goldblum, N., Mitrani, S., Goldblum, T., Yoffey, J.M., Cohen, M.M., Bentwich, Z., Ramot, B., Klein, E., and Klein, G. (1977). Establishment in continuous culture of a new type of lymphocyte from a "Burkitt like" malignant lymphoma (line D.G.-75). Int J Cancer *19*, 27-33.

Birge, R.B., Knudsen, B.S., Besser, D., and Hanafusa, H. (1996). SH2 and SH3-containing adaptor proteins: redundant or independent mediators of intracellular signal transduction. Genes to Cells *1*, 595-613.

Bonnefoy-Bérard, N., Munshi, A., Yron, I., Wu, S., Collins, T.L., Deckert, M., Shalom-Barak, T., Giampa, L., Herbert, E., and Hernandez, J., et al. (1996). Vav: Function and Regulation in Hematopoietic Cell Signaling. STEM CELLS *14*, 250-268.

Brezski, R.J., and Monroe, J.G. (2007). B Cell Antigen Receptor-Induced Rac1 Activation and Rac1-Dependent Spreading Are Impaired in Transitional Immature B Cells Due to Levels of Membrane Cholesterol. The Journal of Immunology *179*, 4464-4472.

Brooun, A., Foster, S.A., Chrencik, J.E., Chien, E.Y.T., Kolatkar, A.R., Streiff, M., Ramage, P., Widmer, H., Weckbecker, G., and Kuhn, P. (2007). Remedial strategies in structural proteomics: expression, purification, and crystallization of the Vav1/Rac1 complex. Protein expression and purification *53*, 51-62.

Bustelo, X.R. (2001). Vav proteins, adaptors and cell signaling. Oncogene *20*, 6372-6381.

Cahalan, M.D. (2009). STIMulating store-operated Ca^{2+} entry. Nature cell biology *11*, 669-677.

Campbell, M.-A., and Sefton, B.M. (1992). Association between B-lymphocyte membrane immunoglobulin and multiple members of the Src family of protein tyrosine kinases. Molecular and Cellular Biology *12*, 2315-2321.

Casey, P.J. (1995). Protein Lipidation in Cell signaling. Science *268*, 221-225.

Cermak, T., Doyle, E.L., Christian, M., Wang, L., Zhang, Y., Schmidt, C., Baller, J.A., Somia, N.V., Bogdanove, A.J., and Voytas, D.F. (2011). Efficient design and assembly of custom TALEN and other TAL effector-based constructs for DNA targeting. Nucleic Acids Research *39*, e82-e82.

Cheng, L., Rossman, K.L., Mahon, G.M., Worthylake, D.K., Korus, M., Sondek, J., and Whitehead, I.P. (2002). RhoGEF specificity mutants implicate RhoA as a target for Dbs transforming activity. Molecular and Cellular Biology *22*, 6895-6905.

Cheng, P.C., Dykstra, M.L., Mitchell, R.N., and Pierce, S.K. (1999). A Role for Lipid Rafts in B Cell Antigen Receptor Signaling and Antigen Targeting. J. Exp. Med. *190*, 1549-1560.

Chiu, C.W., Dalton, M., Ishiai, M., Kurosaki, T., and and Chan, A.C. (2002). BLNK. Molecular scaffolding through 'cis'-mediated organization of signaling proteins. EMBO J. *21*, 6461-6472.

Chrencik, J.E., Brooun, A., Zhang, H., Mathews, I.I., Hura, G.L., Foster, S.A., Perry, J.J.P., Streiff, M., Ramage, P., and Widmer, H., et al. (2008). Structural basis of guanine nucleotide exchange mediated by the T-cell essential Vav1. Journal of molecular biology *380*, 828-843.

Cooper, M.D. (2015). The early history of B cells. Nature reviews. Immunology *15*, 191-197.

Crabtree, G.R., and Olson, E.N. (2002). NFAT signaling: choreographing the social lives of cells. Cell *109*, 67-79.

Das, B., Shu, X., Day, G.J., Han, J., Krishna, U.M., Falck, J.R., and Broek, D. (2000). Control of intramolecular interactions between the pleckstrin homology and Dbl homology

domains of Vav and Sos1 regulates Rac binding. The Journal of biological chemistry *275*, 15074-15081.

Deckert, M., Tartare-Deckert, S., Couture, C., Mustelin, T., and Altman, A. (1996). Functional and Physical Interactions of Syk Family Kinases with the Vav Proto-Oncogene Product. Immunity *5*, 591-604.

Engelke, M., Engels, N., Dittmann, K., Stork, B., and Wienands, J. (2007). Ca^{2+} signaling in antigen receptor-activated B lymphocytes. Immunological Reviews, 235-246.

Engelke, M., Oellerich, T., Dittmann, K., Hsiao, H.-H., Urlaub, H., Serve, H., Griesinger, C., and Wienands, J. (2013). Cutting edge: feed-forward activation of phospholipase Cγ2 via C2 domain-mediated binding to SLP65. The Journal of Immunology *191*, 5354-5358.

Engels, N., König, L.M., Heemann, C., Lutz, J., Tsubata, T., Griep, S., Schrader, V., and Wienands, J. (2009). Recruitment of the cytoplasmic adaptor Grb2 to surface IgG and IgE provides antigen receptor-intrinsic costimulation to class-switched B cells. Nature Immunology *10*, 1018-1025.

Engels, N., Wollscheid, B., and Wienands, J. (2001). Association of SLP-65/BLNK with the B cell antigen receptor through a non-ITAM tyrosine of Ig-alpha. Eur. J. Immunol. *31*, 2126-2134.

Erlich, H.A., Gelfandand, D.H., and Saiki, R.K. (1988). Specific DNA amplification. Nature *331*, 461-462.

Falasca, M., Logan, S.K., Lehto, V.P., Baccante, G., Lemmon, M.A., and Schlessinger, J. (1998). Activation of phospholipase C gamma by PI 3-kinase-induced PH domain-mediated membrane targeting. EMBO J. *17*, 414-422.

Flajnik, M.F., and Kasahara, M. (2010). Origin and evolution of the adaptive immune system: genetic events and selective pressures. Nature reviews. Genetics *11*, 47-59.

Fu, C., Turck, C.W., Kurosaki, T., and and Chan, A.C. (1998). BLNK a central linker protein in B cell activation. Immunity *9*, 93-103.

Fujikawa, K., Miletic, A.V., Alt, F.W., Faccio, R., Brown, T., Hoog, J., Fredericks, J., Nishi, S., Mildiner, S., and Moores, S.L., et al. (2003). Vav1/2/3-null mice define an essential role for Vav family proteins in lymphocyte development and activation but a differential requirement in MAPK signaling in T and B cells. J. Exp. Med. *198*, 1595-1608.

Fujimoto, M., Poe, J.C., Jansen, P.J., Sato, S., and Tedder, T.F. (1999). CD19 Amplifies B Lymphocyte Signal Protein Tyrosine Kinase Activation Transduction by Regulating Src-Family. The Journal of Immunology *162*, 7088-7094.

Fütterer, K., Wong, J., Grucza, R.A., and Chan, A.C. (1998). Structural Basis for Syk Tyrosine Kinase Ubiquity in Signal Transduction Pathways Revealed by the Crystal Structure of its Regulatory SH2 Domains Bound to a Dually Phosphorylated ITAM Peptide. Journal of molecular biology *281*, 523-537.

Gimona, M., Djinovic-Carugo, K., Kranewitter, W.J., and Winder, S.J. (2002). Functional plasticity of CH domains. FEBS Letters *513*, 98-106.

Goitsuka, R., Fujimura, Y.-I., Mamada, H., Umeda, A., Morimura, T., Uetsuka, K., Doi, K., Tsuji, S., and Kitamura, D. (1998). BASH, a novel signaling molecule preferentially expressed in B cells of the bursa of Fabricius. The Journal of Immunology *161*, 5804-5808.

Grabbe, A., and Wienands, J. (2006). Human SLP-65 isoforms contribute differently to activation and apoptosis of B lymphocytes. Blood *108*, 3761-3768.

Groysman, M., Russek, C.S.N., and Katzav, S. (2000). Vav, a GDP/GTP nucleotide exchange factor, interacts with GDIs, proteins that inhibit GDP/GTP dissociation. FEBS Letters *467*, 75-80.

Grynkiewicz, G., Poenie, M., and Tsien, R.Y. (1985). A new generation of Ca^{2+} indicators with greatly improved fluorescence properties. The Journal of biological chemistry *260*, 3440-3450.

Guo, B., Su, T.T., and Rawlings, D.J. (2004). Protein kinase C family functions in B-cell activation. Current Opinion in Immunology *16*, 367-373.

Guo, J., Gaj, T., and Barbas, C.F. (2010). Directed Evolution of an Enhanced and Highly Efficient FokI Cleavage Domain for Zinc Finger Nucleases. Journal of molecular biology *400*, 96-107.

Halstead, J.R., Savaskan, N.E., van den Bout, I., van Horck, F., Hajdo-Milasinovic, A., Snell, M., Keune, W.-J., Klooster, J.-P. ten, Hordijk, P.L., and Divecha, N. (2010). Rac controls PIP5K localisation and PtdIns(4,5)P_2 synthesis, which modulates vinculin localisation and neurite dynamics. Journal of cell science *123*, 3535-3546.

Han J., Luby-Phelps K., Das B., Shu X., Xia Y., Mosteller R.D., Krishna U.M., Falck J.R., White M.A., and Broek D. (1998). Role of Substrates and Products of PI 3-kinase in Regulating Activation of Rac-Related Guanosine Triphosphatases by Vav. Science *279*, 558-560.

Harwood, N.E., and Batista, F.D. (2010). Early events in B cell activation. Annual review of immunology *28*, 185-210.

Hashimoto, S., Iwamatsu, A., Ishiai, M., Okawa, K., Yamadori, T., Matsushita, M., Baba, Y., Kishimoto, T., Kurosaki, T., and Tsukada, S. (1999). Identification of the SH2 Domain Binding Protein of Bruton's Tyrosine Kinase as BLNK—Functional Significance of Btk-SH2 Domain in B-Cell Antigen Receptor-Coupled Calcium Signaling. Blood *94*, 2357-2364.

Henske, E.P., Short, M.P., Jozwiak, S., Bovey, C.M., Ramlakhan, S., Haines, J., and Kwiatkowski, D.J. (1995). Identification of VAV2 on 9q34 and its exclusion as the tuberous sclerosis gene TSC1. Ann Hum Genet. *59*, 25-37.

Heo, J., Thapar, R., and Campbell, S.L. (2005). Recognition and activation of Rho GTPases by Vav1 and Vav2 guanine nucleotide exchange factors. Biochemistry *44*, 6573-6585.

Herrmann, N. (2009). Kooperation funktioneller Domänen des Adapterproteins SLP-65 für die Ca^{2+}-Antwort in B-Lymphocyten.

Hersa, I., Vincent, E.E., and Tavaré, J.M. (2011). Akt signalling in health and disease. Cellular Signalling *23*, 1515-1527.

Hobert, O., Schilling, J.W., Beckerle, M.C., Ullrich, A., and Jallal, B. (1996). SH3 domain-dependent interaction of the proto-oncogene product Vav with the focal contact protein zyxin. Oncogene *12*, 1577-1581.

Hoffman, G.R., and Cerione, R.A. (2002). Signaling to the Rho GTPases: networking with the DH domain. FEBS Letters *513*, 85-91.

Humphrey, M.B., Lanier, L.L., and Nakamura, M.C. (2005). Role of ITAM-containing adapter proteins and their receptors in the immune system and bone. Immunological Reviews *208*, 50-65.

Inabe, K., Ishiai, M., Scharenberg, A.M., Freshney, N., Downward, J., and Kurosaki, T. (2002). Vav3 Modulates B Cell Receptor Responses by Regulating Phosphoinositide 3-Kinase Activation. J. Exp. Med. *195*, 189-200.

Iwasaki, A., and Medzhitov, R. (2015). Control of adaptive immunity by the innate immune system. Nature Immunology *16*, 343-353.

Janeway, C.A., and Medzhitov, R. (2002). Innate immune recognition. Annual review of immunology *20*, 197-216.

Jang, I.K., Zhang, J., and Gu, H. (2009). Grb2, a simple adapter with complex roles in lymphocyte development, function, and signaling. Immunological Reviews *232*, 150-159.

Johmura, S., Oh-hora, M., Inabe, K., Nishikawa, Y., Hayashi, K., Vigorito, E., Kitamura, D., Turner, M., Shingu, K., and Hikida, M., et al. (2003). Regulation of Vav Localization in Membrane Rafts by Adaptor Molecules Grb2 and BLNK. Immunity *18*, 777-787.

Jumaa, H., Wollscheid, B., Mitterer, M., Wienands, J., Reth, M., and Nielsen, P.J. (1999). Abnormal Development and Function of B Lymphocytes in Mice Deficient for the Signaling Adaptor Protein SLP-65. Immunity *11*, 547-554.

Karnoub, A.E., Worthylake, D.K., Rossman, K.L., Pruitt, W.M., Campbell, S.L., Sondek, J., and Der, C.J. (2001). Molecular basis for Rac1 recognition by guanine nucleotide exchange factors. Nature structural biology *8*, 1037-1041.

Katzav, S., Cleveland, J.L., Heslop, H.E., and Pulido, D. (1991). Loss of the Amino-Terminal Helix-Loop-Helix Domain of the vav Proto-Oncogene Activates Its Transforming Potential. Molecular and Cellular Biology *22308*, 1912-1920.

Katzav, S., Martin-Zanca, D., and and Barbacid, M. (1989). vav, a novel human oncogene derived from a locus ubiquitously expressed in hematopoietic cells. EMBO J. *8*, 2283-2290.

Kawasaki, H., Nakayama, S., and Kretsinger, R.H. (1998). Classification and evolution of EF-hand proteins. Biometals *11*, 277-295.

Kim, H.-H., Tharayil, M., and Rudd, C.E. (1998). Growth Factor Receptor-bound Protein 2 SH2/SH3 Domain Binding to CD28 and Its Role in Co-signaling. The Journal of biological chemistry *273*, 296-301.

Kovářová, M., Tolar, P., Arudchandran, R., Dráberová, L., Rivera, J., and Dráber, P. (2001). Structure-Function Analysis of Lyn Kinase Association with Lipid. Molecular and Cellular Biology *21*, 8318-8328.

Kraus, M., Alimzhanov, M.B., Rajewsky, N., and Rajewsky, K. (2004). Survival of resting mature B lymphocytes depends on BCR signaling via the Igalpha/beta heterodimer. Cell *117*, 787-800.

Ksionda, O., Saveliev, A., Köchl, R., Rapley, J., Faroudi, M., Smith-Garvin, J.E., Wülfing, C., Rittinger, K., Carter, T., and Tybulewicz, V.L.J. (2012). Mechanism and function of Vav1 localisation in TCR signalling. Journal of cell science *125*, 5302-5314.

Kurosaki, T. (1999). Genetic analysis of B cell antigen receptor signaling. Annual review of immunology *17*, 555-592.

Kurosaki, T., Johnson, S.A., Pao, L., Sada, K., Yamamura, H., and Cambier, J.C. (1995). Role of the Syk autophosphorylation site and SH2 domains in B cell antigen receptor signaling. J. Exp. Med. *182*, 1815-1823.

Kurosaki, T., Kometani, K., and Ise, W. (2015). Memory B cells. Nature reviews. Immunology *15*, 149-159.

Kurosaki, T., Shinohara, H., and Baba, Y. (2010). B cell signaling and fate decision. Annual review of immunology *28*, 21-55.

LeBien, T.W., and Tedder, T.F. (2008). B lymphocytes: how they develop and function. Blood *112*, 1570-1580.

Li, S.-Y., Du, M.-J., Wan, Y.-J., Lan, B., Liu, Y.-H., Yang, Y., Zhang, C.-Z., and Cao, Y. (2013). The N-terminal 20-amino acid region of guanine nucleotide exchange factor Vav1 plays a distinguished role in T cell receptor-mediated calcium signaling. The Journal of biological chemistry *288*, 3777-3785.

Lopez-Lago, M., Lee, H., Cruz, C., Movilla, N., and Bustelo, X.R. (2000). Tyrosine Phosphorylation Mediates Both Activation and Downmodulation of the Biological Activity of Vav. Molecular and Cellular Biology *20*, 1678-1691.

Malhotra, S., Kovats, S., Zhang, W., and Coggeshall, K.M. (2009). Vav and Rac activation in B cell antigen receptor endocytosis involves Vav recruitment to the adapter protein LAB. The Journal of biological chemistry *284*, 36202-36212.

Marshall, A.J., Niiro, H., Yun T.J., and Clark, E.A. (2000). Regulation of B cell activation and differentiation by the phosphatidylinositol 3kinase and phospholipase C pathways. Immunological Reviews *176*, 30-46.

McLaughlin, S., and Murray, D. (2005). Plasma membrane phosphoinositide organization by protein electrostatics. Nature *438*, 605-611.

Medzhitov, R., and Janeway Jr., C.A. (1997). Innate Immunity: The Virtues of a Nonclonal System of Recognition. Cell *91*, 295-298.

Mee, P.J., Skidan, I., Yang, J., Lugovskoy, A., Reibarkh, M., Long, K., Brazell, T., Durugkar, K.A., Maki, J., and Ramana, C.V., et al. (2010). Small molecule inhibition of phosphatidylinositol-3,4,5-triphosphate (PIP3) binding to pleckstrin homology domains. Proc. Natl. Acad. Sci. USA *107*, 20126-20131.

Miller, J.C., Tan, S., Qiao, G., Barlow, K.A., Wang, J., Xia, D.F., Meng, X., Paschon, D.E., Leung, E., and Hinkley, S.J., et al. (2011). A TALE nuclease architecture for efficient genome editing. Nature biotechnology *29*, 143-148.

Morita, S., Kojima, T., and Kitamura, T. (2000). Plat-E: an efficient and stable system for transient packaging of retroviruses. Gene therapy *7*, 1063-1066.

Movilla, N., and Bustelo, X.R. (1999). Biological and Regulatory Properties of Vav-3, a New Member of the Vav Family of Oncoproteins. Molecular and Cellular Biology *19*, 7870-7885.

Movilla, N., Dosil, M., Zheng, Y., and Bustelo, X.R. (2001). How Vav proteins discriminate the GTPases Rac1 and RhoA from Cdc42. Oncogene *20*, 8057-8065.

Nelson, C.D., Kovacs, J.J., Nobles, K.N., Whalen, E.J., and Lefkowitz, R.J. (2008). Beta-arrestin scaffolding of phosphatidylinositol 4-phosphate 5-kinase Ialpha promotes agonist-stimulated sequestration of the beta2-adrenergic receptor. The Journal of biological chemistry *283*, 21093-21101.

Niiro, H., and Clark, E.A. (2002). Regulation of B-cell fate by antigen-receptor signals. Nature reviews. Immunology *2*, 945-956.

Nishida, M., Nagata, K., Hachimori, Y., Horiuchi, M., Ogura, K., Mandiyan, V., Schlessinger, J., and Inagaki, F. (2001). Novel recognition mode between Vav and Grb2 SH3 domains. EMBO J. *20*, 2995-3007.

O'Rourke, L.M., Tooze, R., Turner, M., Sandoval, D.M., Carter, R.H., Tybulewicz, V.L.J., and Fearon, D.T. (1998). CD19 as a Membrane-Anchored Adaptor Protein of B Lymphocytes: Costimulation of Lipid and Protein Kinases by Recruitment of Vav. Immunity *8*, 635-645.

Odegard, V.H., and Schatz, D.G. (2006). Targeting of somatic hypermutation. Nature reviews. Immunology *6*, 573-583.

Oellerich, T., Bremes, V., Neumann, K., Bohnenberger, H., Dittmann, K., Hsiao, H.-H., Engelke, M., Schnyder, T., Batista, F.D., and Urlaub, H., et al. (2011). The B-cell antigen receptor signals through a preformed transducer module of SLP65 and CIN85. EMBO J. *30*, 3620-3634.

Oellerich, T., Grønborg, M., Neumann, K., Hsiao, H.-H., Urlaub, H., and Wienands, J. (2009). SLP-65 Phosphorylation Dynamics Reveals a Functional Basis for Signal Integration by Receptor-proximal Adaptor proteins. Molecular & Cellular Proteomics.

Ogilvy, S., Elefanty, A.G., Visvader, J., Bath, M.L., Alan W. Harris, and Adams, J.M. (1998). Transcriptional Regulation of vav, a Gene Expressed Throughout the Hematopoietic Compartment. Blood *91*, pp 419-430.

Oh-hora, M., Johmura, S., Hashimoto, A., Hikida, M., and Kurosaki, T. (2003). Requirement for Ras guanine nucleotide releasing protein 3 in coupling phospholipase C-gamma2 to Ras in B cell receptor signaling. J. Exp. Med. *198*, 1841-1851.

Okkenhaug, K., and Vanhaesebroeck, B. (2003). PI3K in lymphocyte development, differentiation and activation. Nature reviews. Immunology *3*, 317-330.

Palmby, T.R., Abe, K., Karnoub, A.E., and Der, C.J. (2004). Vav Transformation Requires Activation of Multiple GTPases and Regulation of Gene Expression. Mol Cancer Res *12*, 702-711.

Park, C.Y., Hoover, P.J., Mullins, F.M., Bachhawat, P., Covington, E.D., Raunser, S., Walz, T., Garcia, K.C., Dolmetsch, R.E., and Lewis, R.S. (2009). STIM1 clusters and activates CRAC channels via direct binding of a cytosolic domain to Orai1. Cell *136*, 876-890.

Parkin, J., and Cohen, B. (2001). An overview of the immune system. The Lancet *357*, 1777-1789.

Pertea, M., and Salzberg, S.L. (2010). Between a chicken and a grape estimating the number of human genes. Genome Biology *11*.

Pierce, S.K., and Liu, W. (2010). The tipping points in the initiation of B cell signalling: how small changes make big differences. Nature reviews. Immunology *10*, 767-777.

Pirkuliyeva, S. (2015). Structural and functional elucidation of the primary transducer module of the B cell antigen receptor.

Pleiman, C.M., D'Ambrosio, D., and and Cambier, J.C. (1994). The B-cell antigen receptor complex: structure and signal transduction. Immunology today *15*, 393-398.

Ran, F.A., Hsu, P.D., Wright, J., Agarwala, V., Scott, D.A., and Zhang, F. (2013). Genome engineering using the CRISPR-Cas9 system. Nature protocols *8*, 2281-2308.

Rapley, J., Tybulewicz, V.L.J., and Rittinger, K. (2008). Crucial structural role for the PH and C1 domains of the Vav1 exchange factor. EMBO reports *9*, 655-661.

Reth, M. (1989). Antigen receptor tail clue. Nature *338*, 383-384.

Reth, M., and Wienands, J. (1997). Initiation and processing of signals from the B cell antigen receptor. Annual review of immunology *15*, 453-479.

Roberts, P.J., Mitin, N., Keller, P.J., Chenette, E.J., Madigan, J.P., Currin, R.O., Cox, A.D., Wilson, O., Kirschmeier, P., and Der, C.J. (2008). Rho Family GTPase modification and dependence on CAAX motif-signaled posttranslational modification. The Journal of biological chemistry *283*, 25150-25163.

Rolli, V., Gallwitz, M., Wossning, T., Flemming, A., Schamel, W.W.A., Zürn, C., and Reth, M. (2002). Amplification of B Cell Antigen Receptor Signaling by a Syk/ITAM Positive Feedback Loop. Molecular Cell *10*, 1057-1069.

Romero, D.C., Pozo F., Reeves W.H., Camonis J., Gisselbrecht S., and Fischer S. (1996). p95vav Associates with the Nuclear Protein Ku-70. Molecular and Cellular Biology *16*, 37-44.

Romero, F., Germani, A., Puvion, E., Camonis, J., Varin-Blank, N., Gisselbrecht, S., and Fischer, S. (1998). Vav Binding to Heterogeneous Nuclear Ribonucleoprotein (hnRNP) C. EVIDENCE FOR Vav-hnRNP INTERACTIONS IN AN RNA-DEPENDENT MANNER. The Journal of biological chemistry *273*, 5923-5931.

Rossman, K.L., Der, C.J., and Sondek, J. (2005). GEF means go: turning on RHO GTPases with guanine nucleotide-exchange factors. Nature reviews. Molecular cell biology *6*, 167-180.

Saci, A., and Carpenter, C.L. (2005). RhoA GTPase regulates B cell receptor signaling. Molecular Cell *17*, 205-214.

Salim, K., Bottomley, M.J., Querfurth, E., Zvelebil, M.J., Gout, I., Scaife, R., Margolis, R.L., Gigg, R., Smith, C.I., and Driscoll, P.C., et al. (1996). Distinct specificity in the recognition of phosphoinositides by the pleckstrin homology domains of dynamin and Bruton's tyrosine kinase. EMBO J. *15*, 6241-6250.

Salojin, K.V. (2000). ZAP-70 Is Essential for the T Cell Antigen Receptor-induced Plasma Membrane Targeting of SOS and Vav in T Cells. The Journal of biological chemistry *275*, 5966-5975.

Sanchez, M., Misulovin, Z., Burkhardt, A.L., Mahajan, S., Costa, T., Franke, R., Bolen, J.B., and Nussenzweig, M. (1993). Signal transduction by immunoglobulin is mediated through Ig alpha and Ig beta. J. Exp. Med. *178*, 1049-1055.

Sanjana, N.E., Le Cong, Zhou, Y., Cunniff, M.M., Feng, G., and Zhang, F. (2012). A transcription activator-like effector toolbox for genome engineering. Nature protocols *7*, 171-192.

Sato, S., Jansen, P.J., and Tedder, T.F. (1997). CD19 and CD22 expression reciprocally regulates tyrosine phosphorylation of Vav protein during B lymphocyte signaling. Proc. Natl. Acad. Sci. USA *94*, 13158-13162.

Satterthwaite, A.B., Li, Z., and Witte, O.N. (1998). Btk function in B cell development and response. Seminars in immunology *10*, 309-316.

Saveliev, A., Vanes, L., Ksionda, O., Jonathan Rapley, J., Smerdon, S.J., Rittinger, K., and Tybulewicz, V.L.J. (2009). Function of the Nucleotide Exchange Activity of Vav1 in T Cell Development and Activation. Science Signaling *2*, ra83.

Scharenberg, A.M., Humphries, L.A., and Rawlings, D.J. (2007). Calcium signalling and cell-fate choice in B cells. Nature reviews. Immunology *7*, 778-789.

Schatz, D.G., and Ji, Y. (2011). Recombination centres and the orchestration of V(D)J recombination. Nature reviews. Immunology *11*, 251-263.

Schroeder, H.W., and Cavacini, L. (2010). Structure and function of immunoglobulins. The Journal of allergy and clinical immunology *125*, S41-52.

Schuebel, K.E., Bustelo, X.R., Nielsen, D.A., Song, B.J., Barbacid, M., Goldman, D., and Lee I.J. (1996). Isolation and characterization of murine vav2, a member of the vav family of proto-oncogenes. Oncogene *13*, 363-371.

Sen, R. (2006). Control of B lymphocyte apoptosis by the transcription factor NF-kappaB. Immunity *25*, 871-883.

Siegers, G.M., Yang, J., Duerr, C.U., Nielsen, P.J., Reth, M., and Schamel, W.W.A. (2006). Identification of disulfide bonds in the Ig-alpha/Ig-beta component of the B cell antigen receptor using the Drosophila S2 cell reconstitution system. International immunology *18*, 1385-1396.

Snyder, J.T., Worthylake, D.K., Rossman, K.L., Betts, L., Pruitt, W.M., Siderovski, D.P., Der, C.J., and Sondek, J. (2002). Structural basis for the selective activation of Rho GTPases by Dbl exchange factors. Nature structural biology *9*, 468-475.

Songyang, Z., Shoelson, S.E., McGlade, J., Olivier, P., Pawson, T., Bustelo, X.R., Barbacid, M., Sabe, H., Hanafusa, H., and Yi, R., et al. (1994). Specific motifs recognized by the SH2 domains of Csk, 3BP2, fps/fes, GRB-2, HCP, SHC, Syk, and Vav. Molecular and Cellular Biology *14*, 2777-2785.

Stavnezer, J., Guikema, J.E.J., and Schrader, C.E. (2008). Mechanism and regulation of class switch recombination. Annual review of immunology *26*, 261-292.

Su, Y.-W., Zhang, Y., Schweikert, J., Koretzky, G.A., Reth, M., and Wienands, J. (1999). Interaction of SLP adaptors with the SH2 domain of Tec family kinases. Eur. J. Immunol. *29*, 3702-3711.

Sylvain, N.R., Nguyen, K., and Bunnell, S.C. (2011). Vav1-Mediated Scaffolding Interactions Stabilize SLP-76 Microclusters and Contribute to Antigen-Dependent T Cell Responses. Science Signaling, ra14.

Takai, Y., Kishimoto, A., Iwasa, Y., Kawahara, Y., Mori, T., and Nishizuka, Y. (1979). Calcium-dependent activation of a multifunctional protein kinase by membrane phospholipids.ll. The Journal of biological chemistry *254*, 3692-3695.

Tarakhovsky, A., Turner, M., Schaal, S., Mee, P.J., Duddy, L.P., Rajewsky, K., and Tybulewicz, V.L.J. (1995). Defective antigen receptor mediated proliferation of B cells and T cells in the absence of Vav. Nature *374*, 467-470.

Tedford, K., Nitschke, L., Girkontaite, I., Charlesworth, A., Chan, G., Sakk, V., Barbacid, M., and Fischer, K.D. (2001). Compensation between Vav-1 and Vav-2 in B cell development and antigen receptor signaling. Nature Immunology *2*, 548-55.

Towbin, H., Staehelin, T., and Gordon, J. (1979). Electrophoretic transfer of proteins from polyacrylamide gels to nitrocellulose sheets procedure and some applications. Proc. Natl. Acad. Sci. USA *76*, 4350-4354.

Tybulewicz, V.L.J. (2005). Vav-family proteins in T-cell signalling. Current Opinion in Immunology *17*, 267-274.

Tybulewicz, V.L.J., and Henderson, R.B. (2009). Rho family GTPases and their regulators in lymphocytes. Nature reviews. Immunology *9*, 630-644.

Umemoto, R., Nishida, N., Ogino, S., and Shimada, I. (2010). NMR structure of the calponin homology domain of human IQGAP1 and its implications for the actin recognition mode. Journal of biomolecular NMR *48*, 59-64.

van den Bout, I., and Divecha, N. (2009). PIP5K-driven PtdIns(4,5)P2 synthesis: regulation and cellular functions. Journal of cell science *122*, 3837-3850.

Walliser, C., Tron, K., Clauss, K., Gutman, O., Kobitski, A.Y., Retlich, M., Schade, A., Röcker, C., Henis, Y.I., and Nienhaus, G.U., et al. (2015). Rac-mediated Stimulation of Phospholipase Cγ2 Amplifies B Cell Receptor-induced Calcium Signaling. The Journal of biological chemistry *290*, 17056-17072.

Walmsley, M.J., Ooi, S.K.T., Reynolds, L.F., Smith, S.H., Ruf, S., Mathiot, A., Vanes, L., Williams, D.A., Cancro, M.P., and Tybulewicz, V.T.J. (2003). Critical Roles for Rac1 and Rac2 GTPases in B Cell Development and Signaling. Science *302*, 459-462.

Weber, K., and Osborn, M. (1969). The reliability of molecular weight determinations by dodecyl sulfate-polyacrylamide gel electrophoresis. The Journal of biological chemistry *244*, 4406-4412.

Weber, M., Treanor, B., Depoil, D., Shinohara, H., Harwood, N.E., Hikida, M., Kurosaki, T., and Batista, F.D. (2008). Phospholipase C-gamma2 and Vav cooperate within signaling microclusters to propagate B cell spreading in response to membrane-bound antigen. The Journal of experimental medicine *205*, 853-868.

Weng, W.-K., Jarvis, L., and LeBien, T.W. (1994). Signaling through CD19 Activates Vav/Mitogen-Activated Protein Kinase Pathway and Induces Formation of a

CD19/Vav/Phosphatidylinositol 3-Kinase Complex in Human B Cell Precursors. The Journal of biological chemistry *269*, 32514-32521.

Wienands, J., Schweikert, J., Wollscheid, B., Jumaa, H., Nielsen, P.J., and Reth, M. (1998). SLP-65 A New Signaling Component in B Lymphocytes which Requires Expression of the Antigen Receptor for Phosphorylation. J. Exp. Med. *188*, 791-795.

Wu J., Motto D.G., Koretzky G.A., and Weiss A. (1996). Vav and SLP-76 Interact and Functionally Cooperate in IL-2 Gene Activation. Immunity *4*, 593-602.

Wu J., Zhao Q., Kurosaki T., and Weiss A. (1997). The Vav binding site (Y315) in ZAP-70 is critical for antigen receptor-mediated signal transduction. J. Exp. Med. *185*, 1877-1882.

Xu, Z., Zan, H., Pone, E.J., Mai, T., and Casali, P. (2012). Immunoglobulin class-switch DNA recombination: induction, targeting and beyond. Nature reviews. Immunology *12*, 517-531.

Yamanashi, Y., Fukui, Y., Wongsasant, B., Kinoshita, Y., Ichimori, Y., Toyoshima, K., and Yamamoto, T. (1992). Activation of Src-like protein-tyrosine kinase Lyn and its association with phosphatidylinositol 3-kinase upon B-cell antigen receptor-mediated signaling. Proc. Natl. Acad. Sci. USA *89*, 1118-1122.

Yang, J., and Reth, M. (2010). Oligomeric organization of the B-cell antigen receptor on resting cells. Nature *467*, 465-469.

Yu, B., Martins, I.R.S., Li, P., Amarasinghe, G.K., Umetani, J., Fernandez-Zapico, M.E., Billadeau, D.D., Machius, M., Tomchick, D.R., and Rosen, M.K. (2010). Structural and energetic mechanisms of cooperative autoinhibition and activation of Vav1. Cell *140*, 246-256.

Zhang, S.L., Yu, Y., Roos, J., Kozak, J.A., Deerinck, T.J., Ellisman, M.H., Stauderman, K.A., and Cahalan, M.D. (2005). STIM1 is a Ca2+ sensor that activates CRAC channels and migrates from the Ca2+ store to the plasma membrane. Nature *437*, 902-905.

Zugaza, J.L., López-Lago, M.A., Caloca, M.J., Dosil, M., Movilla, N., and Bustelo, X.R. (2002). Structural determinants for the biological activity of Vav proteins. The Journal of biological chemistry *277*, 45377-45392.

8 Appendix

8.1 List of Figures

Figure 2.1: Schematic drawing of BCR-proximal signaling events..... 8
Figure 2.2: Domain architecture of Vav1. 10
Figure 4.1: Schematic overview of the TALEN method. 53
Figure 4.2: Generation of a Vav1-deficient DG75 sub-line. 55
Figure 4.3: Vav1 controls Ca^{2+}-mobilization upon BCR stimulation in DG75 cells. 57
Figure 4.4: Vav3, but not Vav2, can restore Ca^{2+}-mobilization in Vav1-deficient DG75 B cells. 59
Figure 4.5: The mouse Vav protein family behaves similar to their human counterparts in the context of BCR-induced Ca^{2+}-mobilization. 60
Figure 4.6: The formation of the Ca^{2+}-initiation complex is not altered in Vav1-deficient DG75 cells. 62
Figure 4.7: Vav1 positively influences the Akt signaling pathway. 63
Figure 4.8: The SH2-domain of Vav1 is essential to promote BCR-induced Ca^{2+}-mobilization. 65
Figure 4.9: Vav1 can directly bind to the ITAMs of the Igα/Igβ heterodimer of the BCR. ..67
Figure 4.10: BCR-binding SH2-domains can replace the Vav1 SH2-domain in the context of BCR-induced Ca^{2+}-mobilization. 70
Figure 4.11: Interaction of Vav1 with the BCR is sufficient for Vav1 function in Ca^{2+}-mobilization. 72
Figure 4.12: Generation of a SLP-65-deficient DG75 sub-line. 73
Figure 4.13: Human SLP-65 has a pivotal role in Ca^{2+}-mobilization upon BCR stimulation. 75
Figure 4.14: Phosphorylation of several SLP-65 tyrosines is important for BCR-induced Vav1 binding and Ca^{2+}-mobilization. 77
Figure 4.15: The interaction between Vav1 and SLP-65 enables Ca^{2+}-mobilization upon BCR stimulation. 79
Figure 4.16: CD19 is not involved in Ca^{2+}-mobilization upon BCR stimulation. 80
Figure 4.17: The structural integrity of the Vav1 DH-domain is crucial for BCR-induced Ca^{2+}-mobilization. 81
Figure 4.18: The DH-domain does not mediate the translocation of Vav1 to the plasma membrane. 83
Figure 4.19: The ZF-domain and the acidic region regulate Vav1 activity in BCR-induced Ca^{2+}-mobilization. 85
Figure 4.20: Generation of a Rac2-deficient DG75 sub-line. 87

Figure 4.21: Human Rac2 in Ca^{2+}-mobilization upon BCR stimulation. 88
Figure 4.22: The CH-domain of Vav1 is critical for BCR-induced Ca^{2+}-mobilization. 90
Figure 4.23: Actin-binding CH-domains cannot functionally substitute the Vav1 CH-domain in Ca^{2+}-mobilization. 91
Figure 4.24: The CH-domain of Vav1 functions also at Vav1's C-terminus. 92
Figure 4.25: The CH-domain is not a membrane-targeting device. 93
Figure 4.26: PIP5K1a influences Ca^{2+}-mobilzation, but cannot restore Vav1 function in human DG75 B cells. 95
Figure 5.1: Schematic domain architecture of Vav1 indicating possible domain functions in the context of BCR-induced Ca^{2+}-mobilization. 106
Figure 6.1: Model of Vav1 in BCR-induced Ca^{2+}-mobilization. 107

8.2 List of Tables

Table 3.1: Consumables used in this study. 15
Table 3.2: Enzymes used in this study. 16
Table 3.3: Reaction systems (kits) used in this study. 16
Table 3.4: Primer used in this study. 17
Table 3.5: Plasmids used for cloning and expression in this study. 25
Table 3.6: Antibodies used in this study. 28
Table 3.7: Synthetic peptides used in this study. 29
Table 3.8: Instruments used in this study. 30
Table 3.9: Software used in this study. 31
Table 3.10: Data base used in this study. 31
Table 3.11: *Escherichia coli* strains used in this study. 32
Table 3.12: Standard PCR cycle conditions. 36
Table 3.13: DG75 characteristics. 43
Table 3.14: DG75 knock out sub-lines. 43
Table 3.15: Optimization of Golden Gate Ligation kit. 49
Table 3.16: Vectors and modules used for the generation of TALEN construct 22. 49

8.3 Abbreviations

α	Anti
aa	Amino acid
AA	Acrylamide
ABD	Actin-binding domain

ABS	Actin-binding site
Ag	Antigen
AP	Affinity purification
APC	Allophycocyanin
APS	Ammonium persulphate
AR	Acidic region
ATP	Adenosine triphosphate
BASH	B cell adaptor protein containing SH2 domain
BCR	B cell antigen receptor
BLNK	B cell linker protein
bp	Base pair
BSA	Bovine serum albumin
Btk	Bruton's tyrosine kinase
C	Celsius
C2	Adaptor region of Vav1
Cas	CRISPR-associated protein
Cbl	Casitas B-lineage lymphoma
CC	CRISPR/Cas construct
CCL	Cleared cellular lysate
CD	Cluster of differentiation
cDNA	Complementary DNA
CH	Calponin-homology
C_H	Heavy chain constant domain
CIN85	Cbl-interacting protein of 85kDa
CIP	Calf intestinal phosphatase
Cit	Citrine
C_L	Heavy chain constant domain
CRAC	Ca^{2+} release-activated channel
CRISPR	Clustered Regularly Interspaced Short Palindromic Repeats
C-terminal	Carboxy-terminal
3D	Three dimensional
DAG	Diacylglycerol
DH	Dbl-homology
D_H	Heavy chain diversity gene segment
DMSO	Dimethylsulfoxide
DNA	Deoxyribonucleic acid
dNTP	2'-deoxynucleoside-5'-triphosphate

DSB	Double strand break
DSMZ	Deutsche Sammlung von Mikroorganismen und Zellkulturen
EB	EcoBlast (Ecotropic receptor, Blasticidin resistance in vector)
ECL	Enhanced chemical luminescence
E. coli	*Escherichia coli*
EGFP	Enhanced green fluorescent protein
env	Envelope, gene encoding glycoprotein 160
ER	Endoplasmic reticulum
Erk	Extracellular signal-regulated kinase
$F(ab')_2$	Bivalent antigen-binding fragment
FACS	Fluorescence activated cell sorter
Fc	Fragment crystalline
FCS	Fetal calf serum
FITC	Fluorescein isothiocyanate
g	Gram
x g	Times gravity
gag	Gene encoding p55 (core protein)
GDI	GDP-dissociation inhibitor
GDP	Guanosine diphosphate
GEF	Guanine nucleotide exchange factor
GFP	Green fluorescent protein
Grb2	Growth factor receptor-bound protein 2
GST	Glutathione S-transferase
GTP	Guanosine triphosphate
h	Hours
HA	Hemagglutinin
HEK	Human embryonic kidney
HEPES	2-[4-(2-Hydroxyethyl)-1-piperazinyl]-ethanesulfonic acid
hnRNP	Heterogeneous nuclear ribonucleoprotein
HRPO	Horseradish peroxidase
Ig	Immunoglobulin
Indo-1 AM	1H-indole-6-carboxylic acid, 2-[4-[bis[2[(acetyloxy) methoxy]-2-oxoethyl]amino]-3-[2-[2-[bis[2 [(acetyloxy) methoxy]-2oxoethyl]amino]-5methylphenoxy] ethoxy]phenyl] (acetyloxy)methyl ester
IP_3	Inositol-1,4,5,-triphosphate
IP_3R	IP_3 receptor

IPTG	Isopropyl-β-D-thiogalacto-pyranoside
IQGAP	IQ motif containing GTPase activating protein
IRES	internal ribosome entry site
ITAM	Immunoreceptor tyrosine-based activation motif
Itk	IL2-inducible T-cell kinase
J_H	Heavy chain joining gene segment
J_L	Light chain joining gene segment
JNK	c-JUN NH2-terminal kinase
L	Liter
LB	Lysogeny broth
Lyn	Lck/yes-related tyrosine kinase
kDa	Kilo Dalton
M	Mole
mA	Milliampere
MACS	Magnetic-activated cell sorting
MAPK	Mitogen activated protein kinase
mIg	Membrane-bound immunoglobulin
mg	Milligram
µg	Microgram
µl	Microliter
min	Minutes
ml	Milliliter
mM	Millimole
MMLV	Moloney Murine Leukemia Virus
mRNA	Messenger RNA
Myr	myristoylation
Nck	Non-catalytic region of tyrosine kinase
NFAT	Nuclear factor of activated T cells
NF-κB	Nuclear factor of κ light polypeptide gene enhancer in B cells
NLS	Nuclear localization signal
NP40	nonidet P40
N-terminal	Amino-terminal
OD	Optical density
PAGE	Polyacrylamide gel electrophoresis
PBS	Phosphate buffered saline
PCR	Polymerase chain reaction
PDK1	Phosphoinositide-dependent kinase-1

PE	Phycoerythrin
PH	Pleckstrin-homology
PI3K	phosphoinositide 3'-kinase
PIP	Phosphatidyl-inositol-phosphate
PIP_2	Phosphatidyl-inositol-4,5-bisphosphate
PIP_3	Phosphatidyl-inositol-3,4,5-trisphosphate
PIP5K	Phosphatidyl-inositol-4-phosphate
PKC	Protein kinase C
PKB	Protein kinase B
Plat E	Platinum E
PLCγ2	Phospholipase Cγ2
PR	Proline rich
PTPN6	Tyrosine-protein phosphatase non-receptor type 6
pTyr	Phospho-tyrosine
pY	Phospho-tyrosine
Rac	Ras-related C3 botulinum toxin substrate
Ras	Rat sarcoma
RasGRP	Ras guanine nucleotide release protein
RFP	red fluorescent protein
Rho	Ras homolog
RNA	Ribonucleic acid
RPMI	Roswell Park Memorial Institute medium
RT	Room temperature
s	Seconds
SDS	Sodium dodecyl sulfate
SFK	Src family kinase
SH2	Src homology 2 domain
SH3	Src homology 2 domain
SLP-65	SH2-domain-containing leukocyte adaptor protein of 65 kDa
SLP-76	SH2 domain-containing leukocyte phosphoprotein of 76 kDa
SOC	Store-operated Ca^{2+} channel
STIM	Stromal interaction molecule
Syk	Spleen tyrosine kinase
TAE	Tris acetate EDTA buffer
tagRFP	'tag' red fluorescent protein
TALEN	Transcription activator-like effector nuclease
TBS	Tris buffered saline

TCR	T cell receptor
TEMED	N,N,N',N'-tetramethylethylene-diamine
Tris	Tris-(hydroxymethyl)-aminomethane
Triton X-100	4-(2',2',4',4'tetramethylbutyl) phenyldecaethyleneglycolether
UV	Ultraviolet
V	Volt
V_H	Variable heavy chain segment
V_L	Variable light chain segment
VSV-G	Vesicular stomatitis virus glycoprotein
v/v	Volume/volume
w/v	Weight/volume
X-gal	(5-bromo-4-chloro-3-indolyl-beta-D-galacto-pyranoside)
Xid	X-linked immunodeficiency
XLA	X-linked agammaglobulinemia
ZAP70	70 kDa zeta-chain associated protein
ZF	Zinc-finger

Deoxyribonucleotides

Name	Code
Deoxyadenosine monophosphate	A
Deoxycytidine monophosphate	C
Deoxyguanine monophosphate	G
Deoxythymidine monophoshate	T

Amino Acids

Name	3-letter code	1-letter code
Alanine	Ala	A
Arginine	Arg	R
Asparagine	Asn	N
Aspartic Acid	Asp	D
Cysteine	Cys	C
Glutamic Acid	Glu	E
Glutamine	Gln	Q
Glycine	Gly	G
Histidine	His	H
Isoleucine	Ile	I
Leucine	Leu	L
Lysine	Lys	K
Methionine	Met	M
Phenylalanine	Phe	F
Proline	Pro	P
Serine	Ser	S
Threonine	Thr	T
Tryptophan	Trp	W
Tyrosine	Tyr	Y
Valine	Val	V

9 Curriculum Vitae